DEMOCRATIC AND POPULAR REPUBLIC OF ALGERIA

MINISTRY OF HIGHER EDUCATION AND SCIENTIFIC RESEARCH

UNIVERSITY OF KASDI MERBAH – OUARGLA

FACULTY OF MATHEMATICS AND MATERIAL SCIENCES

DEPARTMENT OF PHYSICS

Order N° : .....
Serial N° : .....

THESIS OF LMD DOCTORATE

SPECIALITY: **PHYSICS**

OPTION: **MATERIALS SPECTROSCOPY**

BY: **DJAADI SOUMAIA**

THEME

AB INTIO ELECTRONIC PROPERTIES OF PURE Ge_{n+1} AND $SnGe_n$ CLUSTERS

(n =1-17)

Defended on 04/02/2021 in front of the jury composed of:

Pr.	**Boukraa Aomar**	**Ouargla University**	**President**
Pr.	**Rehouma Ferhat**	**El-Oued University**	**Examiner**
Pr.	**Daoudi Bahmed**	**Ghardaia University**	**Examiner**
Dr.	**Achouri Abderrahim**	**Ouargla University**	**Examiner**
Dr.	**Bentouila Omar**	**Ouargla University**	**Examiner**
Pr.	**Aïadi Kamel Eddine**	**Ouargla University**	**Supervisor**

I dedicate this thesis to all my family

To all my friends

To all those who were giving me any kind of support

Table of contents

Abstract

In this work, the structures, relative stability and magnetic properties of pure Ge_{n+1}, neutral ,cationic and anionic $SnGe_n$ (n = 1-17) clusters have been investigated by using the first principal density functional theory (DFT) implemented in SIESTA packages. The absorption cross-section over the optical range of frequencies of pure germanium and tin doped germanium clusters of up to 18 atoms was calculated using time-dependent density functional theory (TDDFT). Calculations were performed using the Octopus package and used the explicit time propagation method. The wavefunctions were calculated over a real-space grid and exchange-correlation interactions were including using the local density approximation. We find through DFT calculations that with the increasing of cluster size, the Ge_{n+1} and $SnGe_n^{(0,\pm1)}$ clusters tend to adopt compact structures. It has been also found that the Sn atom occupied a peripheral position for $SnGe_n$ clusters when n<12 and occupied a core position for n>12. The structural and electronic properties such as optimized geometries, fragmentation energy, binding energy per atom, HOMO–LUMO gaps and second-order differences in energy of the pure Gen 1 and $SnGe_n$ clusters in their ground state are calculated and analyzed. All isomers of neutral SnGen clusters are generally nonmagnetic except for n=1 and 4, where the total spin magnetic moments is 2 μb. The total (DOS) and partial (PDOS) density of states of these clusters have been calculated to understand the origin of peculiar magnetic properties. The cluster size dependence of vertical ionization potentials (VIP), vertical electronic affinities (VEA), chemical hardness (η), adiabatic electron affinities (AEA) and adiabatic ionization potentials (AIP) have been calculated and discussed. In addition, we find through TDDFT calculations that when increase of the numbers of atoms, the sizes of these Germanium clusters grow, and their absorption spectra converted gradually from many peaks to broad absorption bands. In general, increasing the number of atoms can enhance the absorption intensity. A compared with pure germanium, The absorption spectra after Sn doping are characterized by the emergence of a dominant and relatively broad peak between 6 and 10 eV, accompanied by broad absorption peaks also at the same region but smaller intensities . This common feature is coupled to a blue shift of the main peak with increasing cluster size. The cluster size dependence of optical gap energies (E_{opt}) and exciton binding energies (E_x) have been calculated and discussed.

Key words: DFT calculations, Sn-Ge clusters, structural properties, electronic properties, magnetic properties, Siesta package, TDDFT calculations, Octopus package, absorption spectra.

الملخص

في هذه العمل، تمت دراسة البنى، الاستقرار النسبي و كذا الخصائص المغناطيسية لعناقيد الجيرمانيوم النقية Ge_{n+1}، والمطعمة بالقصدير في حالاتها الثلاث المحايدة و الهابطة و كذا الصاعدة $SnGe_n^{(0,\pm1)}$ (n = 1-17) باستخدام المبادئ الأولية لنظرية الكثافة التابعية (DFT) و التي تم تنفيذها بواسطة حزمة SIESTA. كما تم حساب المقطع العرضي للامتصاص على المدى البصري بدلالة الترددات لعناقيد الجرمانيوم النقية والمطعمة بالقصدير التي يصل حجمها إلى غاية 18 ذرة باستخدام نظرية الكثافة التابعية المعتمدة على الوقت (TDDFT). اجريت حسابات TDDFT باستخدام طريقة انتشار الوقت الصريح التي نفذت بحزمة Octopus. تم حساب الدوال الموجية في هذه الطريقة عبر شبكة فضاء حقيقي مع تضمين تفاعلات الارتباط التبادلي باستخدام تقريب الكثافة المحلية. توصلنا من خلال حسابات DFT أن بنى هذه العناقيد و مع زيادة حجمها تميل في هيكلتها الى البنى المدمجة. كما وجدنا أيضًا أن ذرة القصدير Sn تحتل موقعًا في سطح الهيكل لهذه العناقيد لما n <12 وفي قلب الهيكل لما 12 <n. قمنا بحساب وتحليل الخصائص البنيوية والإلكترونية مثل الأشكال الهندسية المحسنة وطاقة التجزئة وطاقة الربط لكل ذرة وفجوات الطاقة HOMO-LUMO والفرق في الطاقة من الدرجة الثانية لهذه العناقيد و هي في حالتها الأساسية. تشير أيضا حسابات DFT الى أن جميع العناقيد المحايدة $SnGe_n$ بمختلف ايزوماراتها ليس لها طابع مغناطيسي باستثناء الحالتين n = 1 و n = 4 ، حيث يكون إجمالي عزم الدوران المغناطيسي لهما مساويا لـ $2\mu_b$. قمنا بحساب ايضا كثافة الحالات الكلية (DOS) والجزئية (PDOS) لهذه العناقيد لفهم مصدر هذه الخصائص المغناطيسية المثيرة. لقد قمنا ايضا بحساب ومناقشة ،اعتمادا على حجم العناقيد، كل من كمون التأين الرأسي (VIP) ، والألفة الإلكترونية الرأسية (VEA) ، والصلادة الكيميائية (η) ، والألفة الإلكترونية الأديباتيكية (AEA) و كومون التأين الأديباتيكي (AIP). بالإضافة إلى ذلك ، وجدنا من خلال حسابات TDDFT أنه عند زيادة عدد الذرات ، تنمو أحجام هذه العناقيد، فتتحول أطياف امتصاصها تدريجياً من قمم متعددة إلى نطاقات امتصاص واسعة. فخلصنا و بشكل عام أن زيادة عدد الذرات يمكن أن يعزز شدة الامتصاص. بالمقارنة مع الجرمانيوم النقي ، تتميز أطياف الامتصاص لعناقيد الجيرمانيوم بعد التطعيم بالقصدير بظهور ذروة سائدة وواسعة نسبيًا بين 6 و 10 فولت، مصحوبة بقمم امتصاص واسعة أيضًا في نفس المنطقة ولكن بشدة أصغر. تقترن هذه الميزة المشتركة بانزياح اللون الأزرق للقمة الرئيسية مع زيادة حجم العنقود. تم حساب ومناقشة ،اعتمادا على حجم العنقود، كل من طاقات الفجوة الضوئية (Eopt) وطاقات ربط الإكسيتون (Ex).

الكلمات المفتاحية: حسابات DFT ، مجموعات Sn-Ge ، الخصائص البنيوية ، الخصائص الإلكترونية ، الخصائص المغناطيسية ، حزمة Siesta ، حسابات TDDFT ، حزمة Octopus ، اطياف الإمتصاص.

Résumé

Dans ce travail, les structures, la stabilité relative et les propriétés magnétiques des clusters de Ge_{n+1} purs et $SnGe_n$ (n = 1-17) neutres, cationiques et anioniques ont été étudiées en utilisant la première principal de la théorie fonctionnelle de la densité (DFT) implémentée dans la package SIESTA. La section efficace d'absorption sur la gamme optique de fréquences des agrégats de germanium pur Ge_{n+1} et dopés $SnGe_n$ et à l'étain jusqu'à 18 atomes a été calculée en utilisant la théorie fonctionnelle de la densité dépendante du temps (TDDFT). Les calculs ont été effectués à l'aide du package Octopus et ont utilisé la méthode de propagation temporelle explicite. Les fonctions d'onde ont été calculées sur une grille en espace réel et les interactions d'échange-corrélation ont été incluaient en utilisant l'approximation de densité locale. Nous constatons grâce aux calculs DFT qu'avec l'augmentation de la taille des clusters, les clusters Ge_{n+1} et $SnGe_n^{(0,\pm 1)}$ ont tendance à adopter des structures compactes. Il a également été constaté que l'atome Sn occupait une position périphérique pour les clusters $SnGe_n$ lorsque n <12 et occupait une position centrale pour n> 12. Les propriétés structurelles et électroniques telles que les géométries optimisées, l'énergie de fragmentation, l'énergie de liaison par atome, les gaps HOMO – LUMO et les différences d'énergie du second ordre des clusters Ge_{n+1} purs et $SnGe_n$ dans leur état fondamental sont calculées et analysées. Tous les isomères des clusters $SnGe_n$ neutres sont généralement non magnétiques sauf pour n = 1 et 4, où les moments magnétiques de spin totaux sont de 2 μb. La densité totale (DOS) et partielle (PDOS) des états de ces clusters a été calculée pour comprendre l'origine de propriétés magnétiques particulières. La dépendance de la taille des clusters des potentiels d'ionisation verticale (VIP), des affinités électroniques verticales (VEA), de la dureté chimique (η), des affinités électroniques adiabatiques (AEA) et des potentiels d'ionisation adiabatique (AIP) ont été calculées et discutées. De plus, nous constatons grâce aux calculs TDDFT que lorsque le nombre d'atomes augmente, les tailles de ces clusters de germanium augmentent et leurs spectres d'absorption sont progressivement convertis de nombreux pics à de larges bandes d'absorption. En général, l'augmentation du nombre d'atomes peut améliorer l'intensité d'absorption. A par rapport au germanium pur, les spectres d'absorption après dopage Sn sont caractérisés par l'émergence d'un pic dominant et relativement large entre 6 et 10 eV, accompagné de pics d'absorption larges également dans la même région mais d'intensités plus faibles. Cette caractéristique commune est couplée à un décalage vers le bleu du pic principal avec une taille de cluster croissante. La dépendance de la taille des agrégats des énergies gaps optique (Eopt) et des énergies de liaison à l'exciton (Ex) a été calculée et discutée.

Mots clés: Calculs DFT, clusters Sn-Ge, propriétés structurelles, propriétés électroniques, propriétés magnétiques, package Siesta, calculs TDDFT, package Octopus, spectres d'absorption

Acknowledgements

I would like to express my deepest appreciation to my supervisor, **Pr. K.E. Aïadi**, for his excellent guidance, patience, and continuous conveyed spirit of adventure in regard to research. His motivation, enthusiasm and immense knowledge were constantly pushing me to strive for excellence, and without his endless help this thesis would not be possible.

I would also like to express my sincere gratitude and appreciation to **Pr. S. Mahtout** for his guidance and support throughout my research and for sharing his wisdom, the insightful comments and suggestions, the encouragement to always look for new and innovative ideas, and to continually deepen the understanding of the problem in hand.

I am also grateful to **Pr. A. Bahayou** and I would like to express my sincere gratitude and appreciation for him because he helped me a lot in informatics and guide me to install some software .I also thank him for his quick response to all of my questions and his attempts to solve all my problems.

I would also like to acknowledge my doctoral committee, **Pr. A. Boukraa**, **Pr**. **F. Rehouma**, **Pr. B. Daoudi, Dr. O. Bentouila** and **Dr. A. Achouri** for their effort on examining the progress of my study in Materials Science. **Pr. A. Boukraa** and **Dr. O. Bentouila** generously provided valuable helps and advices in my research.

I cannot find words to express my gratitude to my family for their boundless love and support. The encouragement and motivation that I continuously received from them is the perpetual fuel that makes me always move forward. I offer my gratitude and thanks to everyone who supported me, I also give special thanks to **Dr Z. Ayat**, **A. Boussada** and **K. Guezoul** for their continued support to me. My most sincere thanks to my work mates and my friends, **Halima**, **Asma** and **Khadidja** for their spontaneous jokes, lovely discussions, and perceptive comments and putting up with me for all this time.

List of figures

List of tables

Introduction

Optoelectronic components do conversions between optical and electrical energy and are used to generate (e.g., Light Emission Diods and lasers), control (e.g., optical modulators), and detect (e.g., photodiodes) light. During the past three decade, optoelectronics have had a big in interest due to the increasing importance of optoelectronics for computing applications (reductions in component sizes within integrated circuits over time)[1].

Clusters are nothing but a collection of atoms. In the past, people had used the so-called clusters to make colored glasses, without any scientific knowledge. The number of atoms can vary from the lowest possible value of two to tens or hundreds of thousand atoms. In this regime, the physical and chemical properties of clusters are size dependent. Thus, clusters are often considered as a bridge for comprehensive understanding as to how matter evolves from atoms to bulk [2, 3]. The cluster physics field is an interesting field of investigation for understanding size effects in finite dimensional systems. Clusters made up of covalent atoms alone constitute an important part of the discipline: "cluster physics", and possess an impressive variety of forms. In particular, carbon, silicon and germanium, although having a similar basic electronic configuration, lead to homogeneous clusters with completely different geometries. Carbon tends to form empty fullerene cages, whereas silicon and germanium leads to compact three-dimensional structures. There has been tremendous progress in the scientific exploration of properties of these clusters, especially in the recent few decades [4-9]. The study of mixed doped clusters consisting of two (or more) types of atoms makes it possible to explore the properties compared to those of pure clusters. The properties of the new systems obtained, or the disturbances associated with doping, are also a subject of research quite widely addressed. Interestingly, the properties exhibited by clusters are often different from that of their bulk counterparts. Also, clusters offer a great tunability or tailoring the properties of materials, which is otherwise not possible in simple molecules. Owing to tremendous tunability of properties, clusters are favored in technological applications. A plethora of synthetic molecules can be explored to investigate science, which is otherwise difficult with normal elements. Many clusters have ability to store hydrogen molecules, thereby suggesting the possibility of solid-state hydrogen

energy storage devices [10]. Clusters are also promising candidates as catalysts [11].

Semiconductor nanostructures form, specially the clusters, a leading class of materials with a large degree of freedom to design optoelectronic properties through variations in composition, size and dimensionality. They are contributing to the development of disruptive technology, for instance in lighting and displays, telecommunication, (quantum) information processing and (quantum) sensing. The importance of germanium and its applications is well established today. In particular, its applications in electronics such as transistors or solar cells are very famous, and the greatest revolution of this century is surely largely due to the development of microchips, real brains in computers. Also studies done on germanium clusters are interesting and potentially useful. The production of clusters of semiconductor materials, particularly germanium, has become a very active area of research in recent years.

Quantum mechanical methods are based on density functional theory (DFT) for determines the ground-state electron density, followed by calculations of the optical properties based on time-dependent density functional theory (TDDFT). The theoretical study of small clusters makes it possible to interpret and understand the existing experimental results, it also makes it possible to study properties useful to know which are difficult to access to the experiment. For example, the geometric structure, which is an essential element for the interpretation and analysis of results, remains very difficult to determine experimentally, and can only be done indirectly. On the other hand, it is directly accessible to theoretical studies combining quantum chemistry methods for energy calculation and geometry optimization processes. For this reason we carried out a systematic theoretical study of the pure and tin doped germanium clusters, Ge_{n+1} and $SnGe_n$ (n=1-17), neutrals and cations, to find their most stable structures and their optical, electronic properties.

In This thesis, we were apply the DFT and TDDFT methods to pure and tin doped germanium clusters of up to 18 atoms in size. DFT calculations have been performed by using the SIESTA simulation package, and TDDFT calculations have been performed by using OCTOPUS package. Firstly, we searched for the most stable geometric structures of clusters, and we have calculated some properties that can be measured experimentally: the ionization potential energy, the electron infinity energy, the binding energy, HOMO-LUMO gap by using DFT calculations. Secondly, we obtained the photo-absorption spectra of the more stable structures of these clusters by using TDDFT calculations. It was identify trends in the optical response of the clusters as a function of the cluster size. It was also investigate the

impact of substituting germanium atom by tin atom on these photo-absorption spectra, and the calculated optical spectra will be compared to previous calculations and experimental measurements.

This thesis is comprised of four chapters. Chapter 1 will summarize previous work on germanium clusters. It will summarize a brief presentation of the current state of knowledge on these germanium clusters, which constitute the object of our study, as well as investigations into cluster structure, electronic and optical properties, using quantum mechanical methods.

The theoretical background of DFT and TDDFT, on which the calculations performed in this thesis are based, will then be described in chapter 2. This will include both the formal theory, as well as numerical methods. Also, in this chapter, a brief introduction to the various computational methods and implementation programs will present.

The results are presented and discussed over the subsequent two chapters. In chapter 3, we will present the different structures of pure and doped germanium clusters obtained from DFT calculations and we will discuss their structural and electronic properties.

Chapter 4 performs TDDFT calculations on the more stable structures of pure and doped germanium clusters, including identifying changes to the optical absorption spectra caused by the addition of tin atom in pure germanium clusters. Finally, will summaries the findings of this thesis, as well as suggesting possible avenues for future work.

FUNDAMONTALS

1. Literature Review and motivation

Introduction

In this chapter, we will present a brief review of previous works on germanium clusters. We will outline progress to date in two main areas; structural calculations, and optical calculations.

1.1. Nanorevolution; impact of nanosystems on technology

The term 'Nano', in terms of physical dimensions, refers to the order of a billionth of a meter (10^{-9} m). Due to the nanosize dimensions, the materials exhibit various interesting properties which are distinctly different from their bulk counter parts[12]. The 'Nanotechnology' is a technology that provides a way to engineer the functional systems at the molecular scale. It possess the ability to construct materials from bottom up and top down approaches and considered as one of the most important and dynamic technologies due to its abilities and numerous applications. Nanotechnology allows manipulating, assembling, synthesizing, characterizing, and manufacturing functional structures and devices with atomic, molecular and nanometer-scale dimensions. The applications of nanotechnology is not limited to the areas of electronics, optics, catalysis, environmental engineering and aerospace but also to cosmetics industry, medicine, pharmacy, engineering, human health and so on[13]. In general, nanotechnology can be understood as a technology of design, fabrication and applications of nanostructures and nanomaterials, as well as fundamental understanding of physical properties and phenomena of nanomaterials and nanostructures [14, 15].

The nanomaterials, the basic unit of nanoscience and nanotechnology, have received a great attention due to their exotic properties and versatile applications[16]. Among various nanomaterials, the semiconductor nanomaterials possess a special place due to their special properties and wide applications. Recently, the semiconductor nanomaterials are used for environmental applications which primarily include the degradation and sensing applications[17, 18].

1.2. Semiconductor nanostructures

The semiconductor nanomaterials hold significant scientific and technological importance

not only in the areas of electronics and optoelectronics but also in biomedicine, energy technologies, environment protection and health. Over the past decades the physics and chemistry of semiconductor nanomaterials have been hot topics in nanoscience and nanotechnology. The semiconductor nanomaterials are exhibiting high potential for fabricating selective, sensitive, simple, and low cast sensors for the detection of various organic pollutants because of their unique electrical, structural and optical properties.

1.2.1. Classifications of Semiconductor Nanostructures

In bulk materials, carriers can freely move in all three dimensions and the material is referred as a three dimensional (3D) system, the energy of the conduction electron equation of this system is already well defined[19, 20].

In the nanostructure materials, the electrons are confined to various regions, i.e. zero dimension, one dimension, two dimension and three dimensions. For a semiconductor, the de Broglie wavelength of free electron is around 10 nm and the nanostructures of semiconductor crystals having the z direction below this critical value (thin film, layer structure, quantum well) are defined as two- dimensional (2D) system since carriers are free to move in two dimensions and confined in one dimension.

The two spatial dimensions of a material are in nanometer range but the other one is larger than the resulting structure is referred as quantum wires and linear chain structures. It is a one-dimensional (1D) system. Here, carriers are free moving in one dimension and are confined in the other two dimensions.

Similarly, quantum dot, cluster, colloid and nanocrystal can be defined as three dimension materials are in nanometer range and it is considered to be a zero-dimensional (0D) system since carriers are confined in all three dimensions.

In generally, the term 'nanoparticle' is used in materials science to specify particles with diameter less than 100 nm, and there is no strict distinction in literature between the terms “clusters, nanoparticles and quantum dots.” However, often “clusters” are used for agglomerates of very few atoms, “nanoparticles” are used for larger agglomerates (usually of metals or carbon), and “quantum dots” are used for semiconductor particles and islands where quantum confinement of charge carriers or excitons determines their properties[21].

1.2.2. Semiconductor clusters and nanoparticles

Nanoclusters possess potentially useful attributes, such as high surface-to-volume ratios, a high degree of geometrical surface defects, and unique electronic structures. Because of the

unique properties of, and interactions between nanoclusters, materials assembled from them differ from conventional materials. Therefore, nanoclusters can be used as building blocks to design new materials exhibiting unique or improved electronic, magnetic, optical, mechanical, and chemical properties.

In recent years, the clusters of different materials have attracted a great interest and their study has become a hot topic of research in both physics and chemistry. Because of their very small size, the evolution of their physical and chemical properties became very important for many applications in different fields such as optoelectronic materials, catalyst, nanoelectronic and spintronic[22, 23]. Semiconductor clusters and nanoparticles formed by the elements of group 14 have been also extensively investigated experimentally and theoretically in view of their fundamental understanding and technological applications. When the size of semiconductor materials is reduced to nanoscale, their physical and chemical properties change drastically, resulting in unique properties due to their large surface area or quantum size effect. The conductivity of the semiconductor and its optical properties (absorption coefficient and refractive index) can be altered. Such nanoparticles have been used in many technological applications such as advanced electronic devices [24, 25], light-emitting devices [26], photodetectors [27], and solar cells [28-30]. As the size of semiconductor nanosystems can be made smaller and smaller, the influence of quantum confinement on their optical properties becomes larger. Therefore, the optical properties of semiconductor clusters as the function of the particle size have attracted much interest. For instance, the optical absorption spectra of CdSe nanocrystals can span across the entire visible light region by varying the size of the nanoparticles [31, 32]. It has also been reported that the optical properties of Si nanoparticles were affected by different crystallinity. Experiment [33] shows that amorphous Si nanoparticles have stronger optical absorption than those with higher crystallinity, especially in short wavelength region. Theoretical calculations also show that the absorption spectra of non-crystalline silicon nanoclusters exhibit a red-shift compared to those of crystalline silicon structures, and doping Phosphor and Aluminum can cause the spectrum to shift even further toward the red region[34, 35]. Furthermore, localized surface plasma resonance (LSPR) can be produced when more than 10 P atoms are doped in a Si nanocrystal of 1.8 - 4 nm [36]. In addition, reconstructed surface [37], different passivants (hydrogen, chlorine, fluoride, oxygen, sulfur, and soon)[38], different oxygen content (hydrogen, hydroxyls, one oxide shell and two oxide shells) on surface[39]. Also Wei Qin et al [40-42]

show that Silicon nanoclusters of the same size but with different structure motifs exhibit different optical absorption. Contrast to the abundant research on Si nanoparticles (either clusters or nanocrystal), study of optical properties of germanium nanoclusters is very limited although Germanium is also one of the most important semiconductor materials.

1.3. Germanium

Germanium has been a popular material of study as its properties benefit many applications. Germanium was the choice of material used in the first bipolar transistor which was invented in 1949 by Bardeen, Brattain, and Shockley; hence proving its electrical functionality [43, 44]. Due to its small energy band gap 0.66 eV, Germanium is also popularly used in optical and optoelectronic devices. Examples of optical and optoelectronic devices that uses Ge are photodetectors [44, 45], solarcells [44], and waveguides [44, 46]. However, the challenge to design a light source based on Germanium has not been solved as Germanium is known to be a poor light emitter, but the scaling of materials toward nanoscale, which will change its properties as the motion of electrons, holes, and excitons are restricted in three dimensions, has shed some ray of hope for Germanium to emit light. Germanium nanostructures have shown considerable promise for light emitting applications, as the indirect band gap of Germanium can be converted to a direct one through a combination of applying tensile strain and appropriate doping at a high level [47].

1.3.1. Germanium crystal Structure and Physical Properties

Germanium is a Period 4 element belonging to Group 14, Block P with an atomic number of 32. The electronic configuration of Germanium (Ge) is [Ar] $3d^{10}$ $4s^2$ $4p^2$. The germanium atom has a radius of 122.5 pm and a Van der Waals radius of 211 pm. Germanium is non-toxic. It is a hard, lustrous, grayish-white metalloid chemically similar to its group neighbors, tin and silicon. Germanium is mainly obtained from sphalerite but is also found in lead, silver and copper ores. Clemens Winkler discovered germanium in 1886. The name Germanium finds its origin from the latin word ‘Germania'. Like silicon, Germanium has the diamond cubic crystal structure and varies in that it has a slightly higher lattice parameter 5.66 Å. It has an indirect band gap of 0.66 eV which lies in the infrared region, and if quantum confinement is demonstrated, will widen[48].

1.4. Germanium clusters

Study of small atomic clusters is greatly beneficial to the understanding of evolution of materials from the molecular to macroscopic regimes. Small to medium sized semiconductor

clusters, such as Silicon and Germanium clusters, have received considerable attention since the 1980s, largely because of their potential relevance to and applications in the nano-electronics industry. During the last four decades, pure and doped germanium clusters have been intensively studied experimentally [49-55]and theoretically [12, 18, 20, 21, 33, 40-42, 47, 56-73]. Today, the most stable structures of small germanium clusters are known thanks to many theoretical works [57, 74-79] and have been confirmed by experimental studies [80-83]. In contrast, for larger clusters the determination of the most stable structure is an open topic despite numerous studies published recently [84-86]. The results are still very dependent on the method of calculating energy and also the algorithm for exploring the space of geometric configurations. We will now briefly present an overview of the structures knowledge, the electronic and optical properties of pure germanium clusters and then doped germanium clusters.

1.4.1. Structural and sizes

1.4.1.1. Small size clusters (2-10 atoms)

The numerous experimental and theoretical studies carried out on small germanium clusters Ge_n ($n \leq 10$) have given a fairly precise idea of their geometry and their electronic structure. As early as 1954, the Ge_n clusters containing two to eight atoms were experimentally studied for the first time by Kohl [87].The atomization energies of small Germanium clusters were first determined by Kant and Strauss [88] using Mass Spectrometry. Other studies of Ge_n clusters include Mass Spectrometry [89, 90], Raman spectra [91], Photoelectron spectroscopy [49, 51, 92-95], Photodetachment Thresholds and Infrared Spectroscopy [80-83].

Numerous theoretical calculations [57, 74-79], have been performed on small germanium clusters. One of the first theoretical studies on germanium aggregate structures is that of J. Harris et al[96] who performed the DFT (density functional theory) calculations using the local-density-functional method. Structures of very small germanium clusters up to 10 atoms have been well established [57, 74-77]. Xu and coworkers [97]did an extensive search on structures for small Ge_n and Ge_n^- (n=1-6). King and coworkers did a limited search on structures for small $Ge_n^{(0, \pm2, \pm4, \pm6)}$ (n = 5-13) clusters [98-106].

Madhu Menon is calculate ground state structures of small clusters using the tight-binding method [107]. For small germanium clusters up to n = 4 the most stable structure is flat. For

Ge_3-Ge_6 the most stable structures are structures corresponding to an isosceles triangle (Ge_3), a plane rhombus (Ge_4), a trigonal bipyramid (Ge_5), an edge-capped trigonal bipyramid (Ge_6). For Ge_7-Ge_{10} the most stable structures are pentagonal bipyramid, a distorted bicapped octahedron, a distorted tricapped trigonal prism and a tetracapped trigonal prism, respectively, and are presented in Figure1. Jinlan Wang et al. [57] as well calculated the structures, for small and medium sizes aggregates of pure germanium, Ge_n (n = 2-25), with DFT methods. The lowest energy structures are identical to those obtained by Madhu Menon [107] for $n \leq 5$. For n = 6, the most stable structure has distorted octahedron (D_{2h}) and the Ge_8 structure is a capped pentagonal bipyramid. The most stable structure for Ge_9 is a bicapped pentagonal bipyramid. In the case of the Ge_{10}, they calculations suggest that the tetracapped trigonal

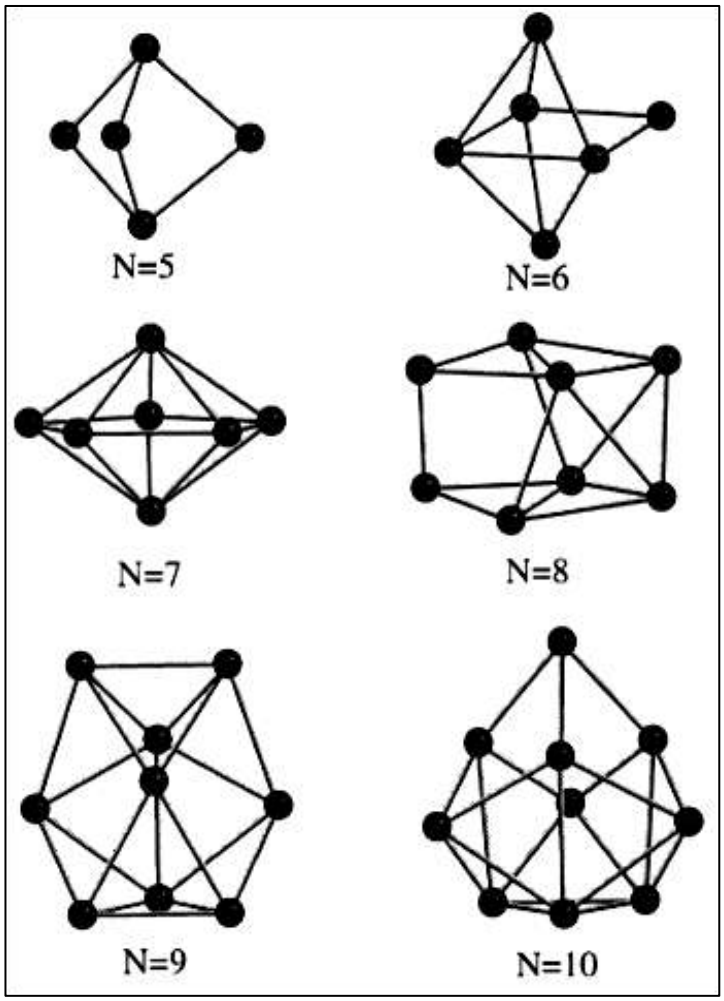

Figure.1: The most stable structures of Ge_n (n=5-10) clusters [107].

prism (C_{3v}) has favorable energy, and are consistent with previous DFT calculations [74, 75, 108].

1.4.1.2. Medium and large size clusters (>10 atoms)

The theoretical determination of the most stable structures for medium and large sized aggregates is a very complex task as full exploration of the potential surface is almost impossible. Numerous theoretical calculations have been performed on medium sizes germanium clusters. The lowest-energy geometries of Ge_n (n = 2-25) clusters have been obtained by DFT-GGA calculations combined with a genetic algorithm made by Jinlan Wang et al. [57]. They found that the germanium clusters follow a prolate growth pattern starting from n=13 and the stacked layer structures are dominant in the size range of n= 13-18. However, a near-spherical compact cage like structure appears in the cluster Ge_{19}. The competition between compact structure and stacked layer structure leads to the alternative appearance of these two types of geometries. Stacked-compact structures are predominant for larger clusters. The Figure2 showed those structures.

Li and coworkers [109]did an extensive search on medium-sized clusters Ge_n (n = 21-25) clusters and suggested that low-lying prolate clusters could be built upon stacked tricaped trigonal prism (TTP) motifs. Zeng and coworkers did a limited search on structures for medium sized Ge_n (n = 12-29) clusters[78, 79]. They suggested that most low-lying medium sized clusters consist of the six/nine and six/ten motifs. J.J. Zhao and coworkers [84] did a limited search on structures for medium Ge_n (n =30-39). Ho and coworkers [84-86] who did a limited search on structures for medium Ge_n (n = 2-44) clusters.

Hunter et al. [110] studied the mobilities of Ge_n^+ (n = 7-54) and Ge_n^{2+} (n =44-86) clusters and revealed that the structural transition to more spherical geometries begins at n = 65. They have observed an elongated growth for the Ge_n^+ cluster ions with n = 10-35 and a gradual deviation from this growth sequence for the clusters with more than 35 atoms. Through comparison with the results on the dissociation energies, they have proposed the structures of the Ge_n clusters with up to 70 atoms as weakly bound assemblies of small stable fragments such as Ge_7 and Ge_{10}. The structural transition at around 70 atoms has been ascribed to a reconstruction to a more compact bulk-like structure. Zhang and coworkers [111] investigated the mass selected laser photo-dissociation of germanium cations prepared by laser vaporization and supersonic beam expansion using tandem time-of-flight mass spectrometry. Germanium clusters up to size 40 were studied. As a general observation, the nature of the

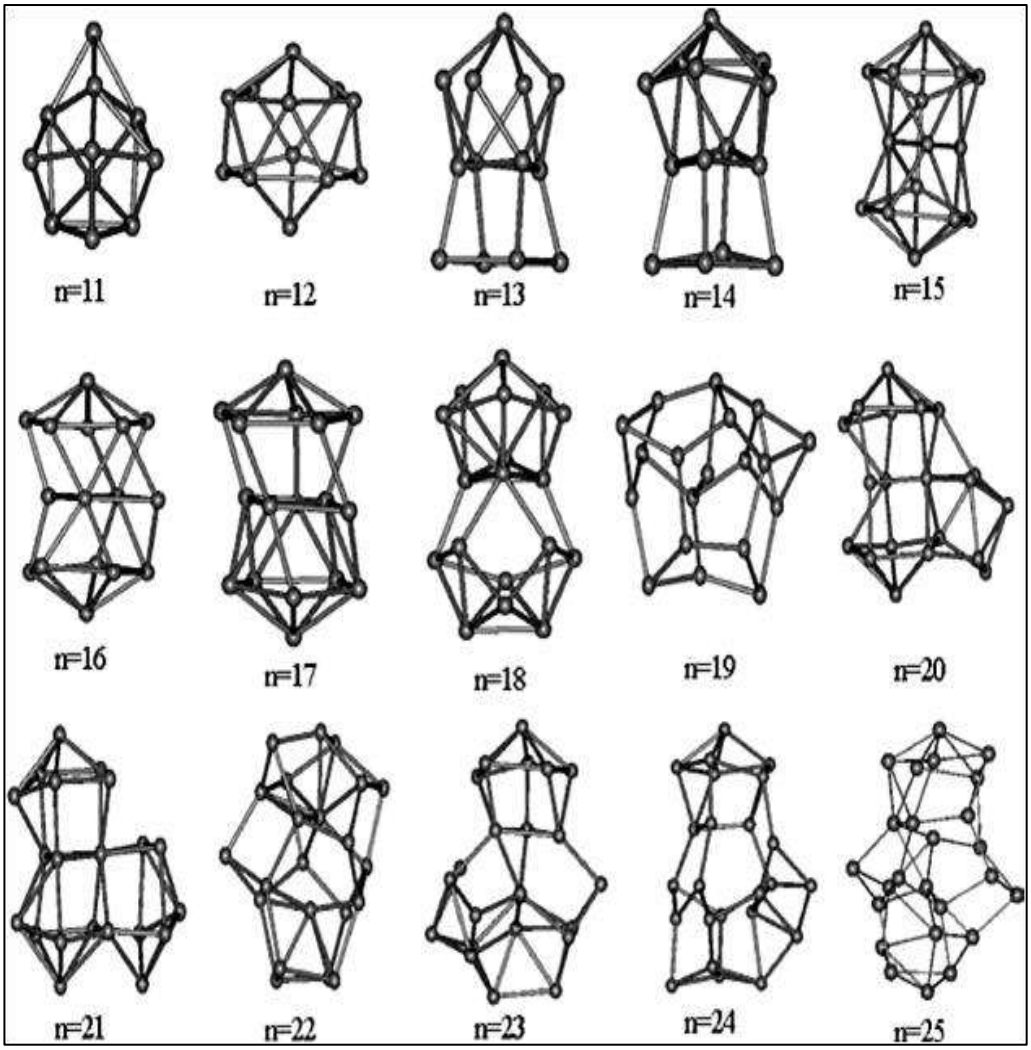

Figure.2 : Lowest energy structures of Ge_n (n=11-25) clusters**[57]**.

fragmentation patterns does not depend qualitatively upon the fragmentation laser used, although there are significant dependencies upon fragmentation laser fluence. Zhao et al [112] calculated the second order difference in energy, Δ_2E for Ge_n clusters (n = 3-32). The calculated values of Δ_2E show maxima at n = 4, 7, 10, 12, and 14. Ge_7 and Ge_{10} correspond to prominent peaks. Ge_{20}, Ge_{23}, Ge_{26} and Ge_{29} also exhibit special stability because each of these clusters contains two stable Ge_{10} subunits. These results also suggest that Ge_{10} is a very favorable building block for the growth of large germanium clusters. The cohesive energy of bulk germanium is 3.85 eV per atom, and the fragmentation energies of clusters with up to 10 atoms are comparable to the bulk cohesive energy. These small-sized clusters with large fragmentation energies are not easy to dissociate. For clusters with more than 11 atoms, the fragmentation energies drop sharply. In the fragmentation products, Ge_6, Ge_7 and Ge_{10} are obviously more abundant, this is in agreement with the experimental results.

Ion mobility measurements by Hunter et al [110] have revealed that the medium sized cations Ge_n are generally prolate in shape and the structural transition from the prolate to spherical-like shape appears at n =65 were different isomers coexist. The most relevant experimental information on anionic systems, up to size 40, comes from laser studies by Zhang et al [111]. These experiments clearly show that semiconductor clusters dissociate larger fragments with a preference for 6, 9 or 10 atoms. This is in sharp contrast to metal clusters that dissociate only monomers and dimers. Zhao and coworkers [112] studied the fragmentation behavior of the lowest-energy structures of Ge_2–Ge_{33} using all-electron DFT methods. They predict that the fragmentation products of Ge_6, Ge_7, and Ge_{10} clusters are abundant and appear frequently in fragmentation processes, which is in line with the experimental observations. The lowest-energy structures of germanium clusters (n = 11–33) are presented in Figure3 . It can be seen that the TTP motif is prevailing in almost all of these structures. For Ge_{17}–Ge_{26} they contain a Ge_6 link unit, except for Ge_{20}. All Ge_n clusters in the size range 27–29 contain a Ge_9 link unit, which acts as a linkage connecting to two small clusters. The lowest-energy structures of Ge_{19}-Ge_{29} are consistent with the calculated results of Yoo et al [79], though the latter discuss other competitive structures based on the Ge_9 link unit and octagonal subunits. The lowest-energy geometries of Ge_{30}-Ge_{33} keep a similar growth pattern with a Ge_9 linkage connecting with three small clusters including a Ge_4 cluster. The shape of the clusters is clearly prolate.

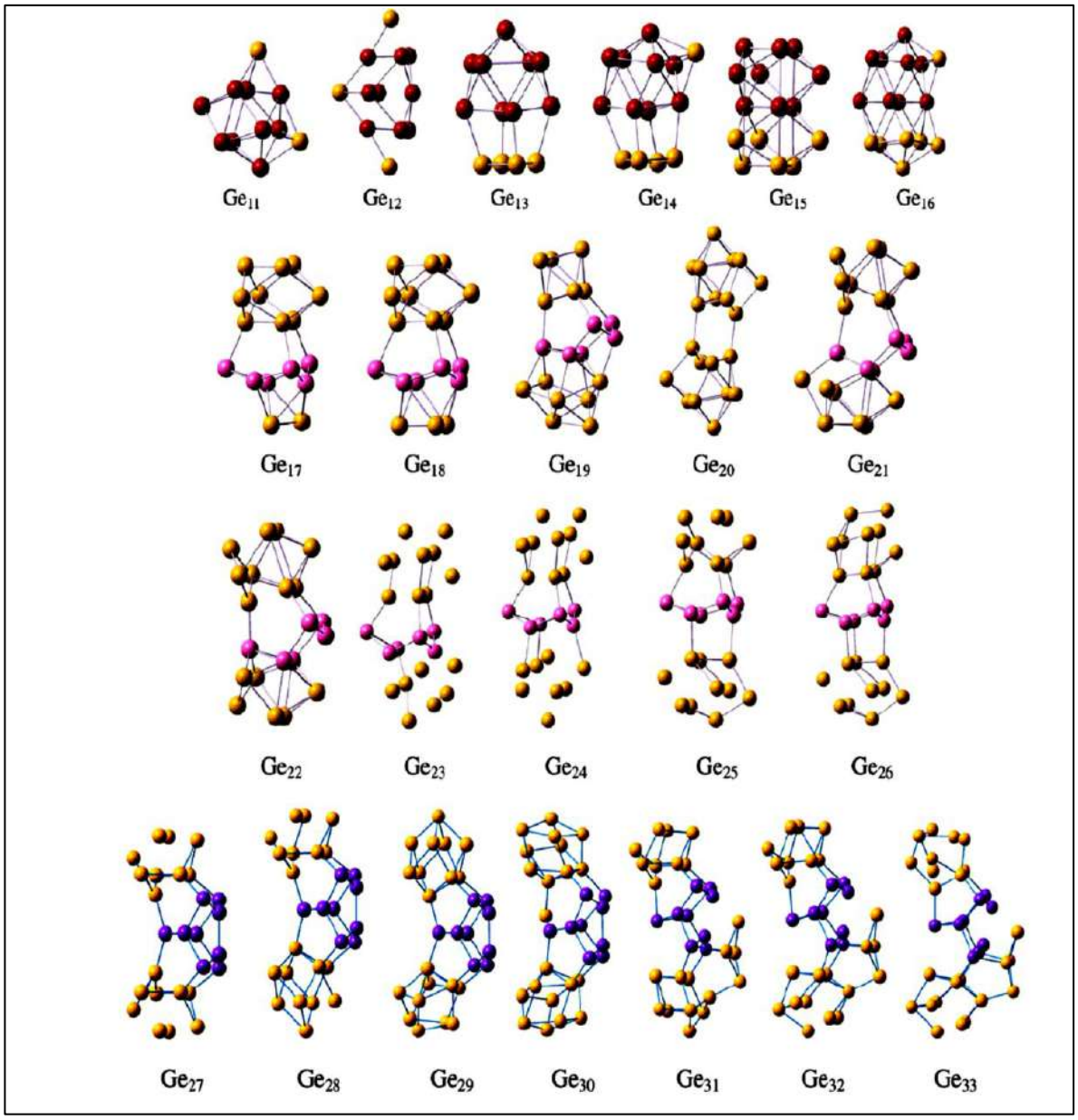

Figure.3 : Lowest-energy structures of germanium clusters (n = 11–33) **[112]**.

1.4.2. Doped germanium clusters

In recent years, there has been interest in doping germanium clusters with different materials in order to improve the electronic properties of germanium aggregates for possible applications. Zhao and Wang [113] studied geometries, stabilities and electronics properties of $FeGe_n$ (n = 9-16) clusters. They found that the encapsulation of one iron atom Fe in the pure Ge_n clusters contributes in strengthening the stabilities of the germanium framework and the HOMO-LUMO gaps of the $FeGe_n$ clusters which are usually smaller than those of the corresponding pure germanium clusters. In their study concerned with the properties of aluminum-doped small germanium clusters, Shi et al. [114] showed that the lowest energy structures of the $AlGe_n$ are similar to lowest energy structures of the pure corresponding germanium clusters. Li et al. [115] reported the effect of one atom of gold Au in anionic germanium clusters $AuGe_n^-$ (n = 1 – 13). They found that the clusters with n = 12 are the most stable ones compared to the other size. Electronic and magnetic properties of Mn, Co and Ni doped small germanium clusters have been investigated using spin polarized density functional theory by Kapila et al.[116]. They found that the Ni-doped Ge_n clusters are the more stable when compared to Co and Mn dope Ge_n clusters. Tang et al. [117] studied the structure and stability of the 3d transition metal endohedral $Ge_{12}M$ (M= Sc – Ni) clusters. They found that all $Ge_{12}M$ clusters have the doping energies (DEs) and the energies gap (Egs) comparable to the isolated compounds, which indicates their remarkably kinetic stability and the possibility for isolation. Mahtout et al. [23] calculated the electronic and magnetic properties of medium-sized $CrGe_n$ ($15 \leq n \leq 29$) clusters by using first principles DFT investigation. They showed that the structures of Ge_{n+1} and $CrGe_n$ become more compact and switch to near spherical structure with one or more core atoms and the clusters with size 17, 19, and 22 exhibit high stability. Katircioglu [118]reported that the C– C bonds are privileged over Ge–C bonds and Ge–Ge binding for different values of n and m in Ge_nC_{m-n} clusters.

The tunability of the GeSn band structure through Sn composition is an important advantage to implement optoelectronic devices operating in the Near Infra Red (NIR) and Mid Infra Red (MIR) wavelength ranges.

Recently, small $SnGe_n$ clusters have been studied in the range n < 5. Andzelm et al. [119] performed a DFT study on GeSn monomer, and they reported on the spectroscopic constants and electronic structure of the diatomic molecules GeSn in their low lying electronic states. They showed that the local spin density model potentials (LSD) used in their study form a

good description of chemical bonding and spectroscopic properties of molecules. Schmude and Gingenich [120] presented an experimental study on the small germanium-tin clusters and they find the atomization enthalpies of the GeSn, $GeSn_2$, Ge_2Sn, Ge_3Sn, Ge_4Sn molecules. A DFT investigation of Sn_mGe_n ($m + n \leq 5$) binary clusters has been performed by Samanta and Das [22]. They showed that the larger mixed tin and germanium clusters have higher binding energies and the larger HOMO–LUMO energy gaps, which implies their high stability. Han et al. [121] presented theoretical investigation of very small $SnGe_n$ (n=1 - 4) clusters. They calculated equilibrium geometry, enthalpy of reaction and natural population and they found that natural populations of these clusters indicate a charge transfer from Sn to Ge atoms.

1.4.3. Optical properties

The optical spectrum provides information on the electronic structure. In particular, the optical response of the clusters depends on their size and also on the cluster structure. This is an important feature, since the determination of the structure is, in general, a hard task, either for experimental techniques or for sophisticated total energy calculations and knowledge of the geometrical structure of a cluster is required as a basis for understanding many of its properties.

Experimentally, germanium nano-crystals of various large sizes were synthesized and their optical properties have been studied [122-124]. Ikezawa et. al. [122], they measured the optical absorption spectra of Germanium crystals in the far-infrared region at the temperatures of 2 ~ 292 K and they found the structures in the absorption spectra around 100 and 200 cm^{-1}. Also Heath et al.[123] synthesized three large Germanium quantum dots with the sizes over 200, 100, and 60 Å in their experimentally study. The extinction spectra of these Germanium quantum dots were measured with ultraviolet/visible and near infrared spectroscopy in the energy range of 0.6 ~ 5 eV. The highly crystalline germanium nanocrystals in the size range 2 ~ 10 nm were grown by Wilcoxon's group[124], and also they studied the optical absorption properties of Germanium nanocrystals with the diameters of 2.0 nm (about 150 Ge atoms) and 4.0 nm.

Theoretically, various models and methods have also been used to study the optical properties of Germanium nanocrystals [125-128]. Lorin X. et al [125] they reported first-principles calculations for diamond, Si, Ge, and GaAs that include the electron-hole interaction were used to calculate the frequency-dependent imaginary part of the dielectric

function. Independent-particle approximation and a pseudopotential-plane-wave method were used to calculate the nanoparticles up to 363 atoms [125]. Nesher et al. calculated the absorption spectra and optical gap of Germanium nanocrystals using time-dependent density functional theory within the adiabatic local density approximation. They predicted that the optical gaps of Germanium nanocrystals are smaller than that of Silicon for any size[128]. H.Ch. Weissker et al[127] calculated Spin-dependent excitation energies of Silicon and Germanium nanocrystals by means of a delta self-consistent field method considering the excitation of an electron-hole pair and including the electron-hole Coulomb interaction.

Absorption spectra of hydrogenated germanium nanocrystals over 800 atoms are calculated in real space using ab initio pseudopotentials constructed within the local density approximation by Dmitriy V.M et al[126]. A semi-empirical tight-binding approach were used to calculate the optical properties of Germanium nanoclusters with up to about 1000 atoms and the theoretical single-particle spectra showed that the bulk absorption peak is blue-shifted [129]. The experiment measured the absorption peak of the Germanium quantum dots with average radius from 12 to 60 Å showed a blue-shift of up to 0.1 eV and a strong reduction of their oscillator strengths due to the effect of quantum confinement[130]. J. Tauc [131] studied the infrared absorption bands in germanium amorphous, the analysis of their results has shown that the valence band wave functions are delocalized over distances of the order 10^2 A°.

The optical properties of Si-Ge semiconductor nano-onions[132] and different sized Silicon containing Germanium nanoclusters of spherical shape[133] were studied in detail. Hill et al. found that the band gaps of small Si-coated Ge Nano-onion with the diameter below about 30 Å are within the visible region of the spectrum[132]. The results of calculations of optical absorption spectra of silicon containing Germanium nanoclusters of spherical shape and different size are reported by V.N. Brudnyi et al[133], and they analyzed the optical transitions from the Germanium cluster levels to the silicon bulk energy band states. The optical absorption properties of Ge clusters and nanocrystalline with the sizes from ~ 2.5 to 15 Å have been studied at the B3LYP/6-31G level using time-dependent density functional theory by Wei Qin et all [67]. Hydrogen passivation and phosphorus doping on some selected Ge nanoparticles were also calculated. They found that with the increase of cluster size, the optical absorption spectra of change from many peaks to a continuous broad band and at the same time exhibit a systematic red shift. Doping phosphorus also causes the absorption spectra to shift

toward the lower energy region. The germanium clusters are found to have stronger absorption in the visible region in comparison with the crystalline ones, regardless phosphorus doping. V. N. Brudnyi et all [134] studied the electronic states and optical absorption spectra of germanium clusters in silicon matrix by the pseudo-potential method , it has been shown that the optical spectra are sensitive to the shape and size of the Germanium quantum dots.

Despite of these studies, many questions remain open. For example, what are the structural, electronic and the optical properties of germanium clusters when the size of the clusters changes from small to large? How about the effects on the structural, electronic and the optical properties when impurities are doped in germanium clusters? Further understanding of these questions would be very helpful to the relevant application of germanium clusters in advanced electronic and optical devices.

1.5. Motivation

In light of the previous studies, to the best of our knowledge, systematic and theoretical investigated on neutral and charged tin doped germanium $SnGe_n$ clusters with range of 5 to 17 atoms have been not reported so far. The main motivation behind the present work is to study the inclusion effect of one Sn on the electronic, magnetic and optical properties of different isomers of Ge_{n+1} clusters in the size range n=1-17 atoms and their evolution as a function of the size by using ab intio calculations. The properties and the associated adiabatic energies of charged tin doped germanium are also studied. Our investigation will provide noteworthy contribution for theoretical and experimental studies and also provide useful information for guiding the design of semiconductor nanostructure-based electronic and optoelectronic devices.

2. Theory and Computational methods

Introduction

In this chapter, we will outline the theoretical background for DFT and TDDFT and we will present and comment the computational methods and the computer programs implementation (numerical simulations) were we use to calculate ground state structures and their properties optic, electronic and energetic. The numerical simulations can be realized through several ab initio codes with pseudopotential approach electron like "SIESTA, PWSCF, VASP ..." or with all electron like "TBLMTO, WIEN2k, CRYSTAL, FPLO…", for what concern the total energy calculation part. In this work, the initial structures of the clusters used have been obtained by SIESTA ab initio DFT code. On the other side, the optical features of the optimized structures have been investigated by OCTOPUS TDDFT code.

2.1. Density functional theory

Before the calculation of electronic and optical properties using quantum mechanical methods can be performed, the ground state electronic structure must first be determined. In the following paragraphs, we will detail the calculation methods of ground state electronic structure.

2.1.1. The Schrodinger Equation

One of the principal aim of condensed matter physics is the theoretical study of the electronic properties of a system. To understand the behaviour of systems ranging from atoms and nanostructures to complex bulk systems, the resolution of the Schr¨odinger equation [135] has become the fundamental and the primary task of the many-body problem, the time-independent Schrödinger equation is given as

$$\hat{\mathrm{H}}\Psi(\mathrm{r}_1, \mathrm{r}_2, \dots, \mathrm{R}_1, \mathrm{R}_2, \dots) = E\Psi(\mathrm{r}_1, \mathrm{r}_2, \dots, \mathrm{R}_1, \mathrm{R}_2, \dots) \qquad 2.1$$

where $\Psi(\mathrm{r}_1, \mathrm{r}_2, \dots, \mathrm{R}_1, \mathrm{R}_2, \dots)$ is the all electron wave function, and $\hat{\mathrm{H}}$ represents the Hamiltonian of the interacting system, can be written as

$$\hat{H} = -\sum_i \frac{\hbar^2}{2m_e} \cdot \nabla_{r_i}^2 - \sum_i \frac{\hbar^2}{2M_i} \cdot \nabla_{R_i}^2 - \sum_{i,j} \frac{Z_i e^2}{4\pi\epsilon_0 |R_i - r_i|} + \sum_{i \neq j} \frac{e^2}{8\pi\epsilon_0 |r_i - r_j|} + \sum_{i \neq j} \frac{e^2 Z_i Z_j}{8\pi\epsilon_0 |R_i - R_j|} \quad 2.2$$

where m_e and M_i are the mass of the electron and nucleus, respectively. The first and the second term are represent the kinetic energy of the electrons and the nuclei, respectively. The remaining three terms are the potential energy from Coulomb interaction between electron and nucleus, electron and electron, and nucleus and nucleus, respectively[135]. To solve this equation exactly is impossible. Even solving this equation numerically is infeasible. In order to accurately calculate the electron wavefunctions and eigenvalues, a series of approximations must be made.

2.1.2. The Born-Oppenheimer (adiabatic) or approximation

The first approximation uses the large mass difference between the nuclei and the electrons, which causes almost immediate adaptation of the dynamics of electrons to the position of the nuclei. Therefore, the dynamics of the nuclei could be neglected, considering them as "frozen", which is the basis Born-Oppenheimer (BO) or adiabatic approximation[136]. The ion kinetic energy term in equation (3.1) becomes zero. The ion interaction term would also reduce to a constant expression, V_{ext}. This has significantly reduced the equation to a *ZN* body equation of the form:

$$H = -\sum_i \frac{\hbar^2}{2m_e} \cdot \nabla_{r_i}^2 + \sum_{i \neq j} \frac{e^2}{8\pi\epsilon_0 |r_i - r_j|} + V_{ext} = T + V + V_{ext} \quad 2.3$$

Although using this approximation, there's still another open question blinking on the paper: how to resolve the electron eigenvalues equation from the quantum theory point since it describe interactions between 10^{23} electrons per material and the index of the wavefunction runs over N-electrons?

2.1.3. The Hohenburg and Kohn Theorems

A further development towards finding a solvable set of equations came with the two theorems of Hohenburg and Kohn [137]in 1964 showed that indeed any property of an interacting system can be obtained from the ground state electron density, $n_0(r)$. This is the foundation of the DFT.

2.1.3.1. Theorem I

For any system of interacting particles in an external potential Vext(r), the potential Vext(r) is determined uniquely, up to a constant, by the ground state particle density, $n_0(r)$.

2.1.3.2. Corollary I

Considering that the Hamiltonian is fully determined from $n_0(r)$, except for a constant shift of the energy, it follows that the many body wavefunctions for all states (ground and excited) and the properties of the system are also completely determined.

2.1.3.3. Theorem II

A universal functional for the energy E[n] in terms of density n(r) can be defined for any external potential V_{ext}. For any particular V_{ext} , the ground state energy of the system is the global minimum of the energy functional, and the density n(r) which minimizes the functional is the exact ground state density $n_0(r)$[138].

An immediate consequence of this theorem is that if V_{ext} is known then this uniquely identifies an electron density. This can be used to calculate the other terms in the Hamiltonian, producing the full Hamiltonian. Therefore if the external potential, provided by the ions, is known then the full multi-electron wave function can be calculated.

Following the two theorems of Hohenberg and Kohn, the ground-state energy functional H[n] = E[n] is of the form

$$E(n) = \langle\psi|\hat{T} + \hat{V}|\psi\rangle + \langle\psi|\hat{V}_{ext}|\psi\rangle \qquad 2.4$$
$$= \quad F_{HK}(n) + \int n(r)V_{ext}(r)dr$$

where the functional $F_{HK}(n)$ incorporates the kinetic and the potential energy, coming from the all electron-electron interactions. Since this functional does not depend on the external potential, the kinetic and potential energies depend only on the density; hence the functional must be the same for any system. The $F_{HK}(n)$ function can be further split into

$$E(n) = T_S(n) + E_{int}(n) \qquad 2.5$$

where $T_S[n]$ is the kinetic energy, and $E_{int}[n]$ is the interaction energy [139], which is defined as

$$\boldsymbol{E_{int}(n)} = \frac{1}{2}\int \frac{n(r)n(\acute{r})}{|r-\acute{r}|}drd\acute{r} + \boldsymbol{E_{xc}(n)} \qquad 2.6$$

where the first term is the Hartree energy, and the second term is the exchange correlation energy, in which all the many particle interactions are gathered.

With these theories the ability to calculate the ground state electron density and many different properties of materials became possible. There still remained a few more theoretical developments before it became practical. This came in 1965 with the equations of Kohn and Sham.

2.1.4. The Kohn-Sham Equations

The essential change introduced in the Hohenberg and Kohn theory by the Kohn-Sham formalism[140] is the replacement of the many body equation with a single particle equation, while keeping constant the total number of interacting particles. According to the formalism, the total energy functional can be written as

$$\boldsymbol{E(n)} = \boldsymbol{T_S(n)} + \int \left[V_{ext}(r) + \frac{1}{2} V_H(r)\right] n(r)dr + \boldsymbol{E_{xc}(n)} \quad 2.7$$

$T_S[n]$ is the kinetic energy of the electrons, $E_{xc}[n]$ is the exchange-correlation functional, V_H is the Hartree potential, and V_{ext} is the external potential, defined

$$\boldsymbol{V_{ext}} = -\sum_{\boldsymbol{i}} \frac{\boldsymbol{Z_i}}{|\boldsymbol{R} - \boldsymbol{r}|} \quad 2.8$$

Minimizing the Eq. 2.7 with respect to the density yields a Schrodinger-like [138]

$$\boldsymbol{H_{eff}(r)}\psi_i(r) = \left[-\frac{1}{2}\nabla^2 + \boldsymbol{V_{eff}(r)}\right]\psi_i(r) = \varepsilon_i\psi_i(r) \quad 2.9$$

showing that the independent particles are moving in an effective potential, V_{eff} . In the V_{eff} the external potential, the Hartree potential and the exchange correlation potential are included. Using an initial guess of electron density to solve the KS equation, gives the KS wavefunctions, ψ_i, which are then used to calculate the electron density

$$n(r) = \sum_{i=1}^{N} |\psi_i(r)|^2 \quad 2.10$$

is later used to calculate new effective potential. This is repeated until self consistency[139] is achieved. From Eq. 2.9 the kinetic energy can be expressed by:

$$\boldsymbol{T_S(n)} = \sum_{i=1}^{N} \varepsilon_i - \int \boldsymbol{V_{eff}(r)} n(r)dr \quad 2.11$$

Ultimately, the total energy of the system is given by

$$\boldsymbol{E} = \sum_{i=1}^{N} \varepsilon_i - \frac{1}{2}\int \frac{n(r)n(\acute{r})}{|r-\acute{r}|} dr d\acute{r} - \int \boldsymbol{V_{xc}} n(r) dr + \boldsymbol{E_{xc}}(\boldsymbol{n}) \qquad 2.12$$

The most appealing property of this formalism is that the kinetic energy and the Hartree terms are explicitly separated and can be calculated accurately. Therefore, the limiting factor in providing accurate results is the exchange correlation term, the form of which, if it would be exactly known, would make this formalism an exact one. It is necessary, in fact, to find a good approximation for the exchange-correlation energy$\boldsymbol{E_{xc}}$. Once a good approximation for $\boldsymbol{E_{xc}}$ is obtained, the Kohn-Sham equations must be solved self-consistently [139]and then it is possible to obtain the ground state density of the interacting system and its total energy, as depicted in Figure4 .

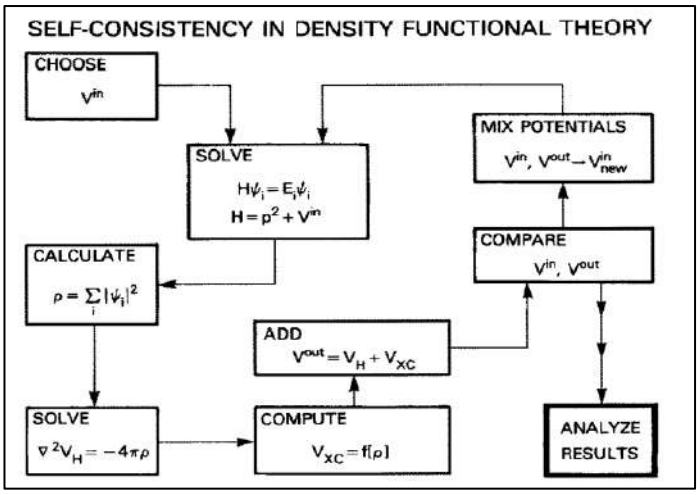

Figure.4 : Self-Consistency in Density Functional Theory [139]

2.1.5. Approximations to the exchange-correlation functional

In the following section an overview of the two most widely used approximations of the exchange-correlation functional is going to be presented.

2.1.5.1. LDA

The main difficulty in developing Kohn-Sham formalism is in the construction of exchange-correlation functional. The electron density is treated locally as a uniform electron gas, and the exchange-correlation energy is considered to be the same as the energy of the

uniform electron gas at any local point in space. In LDA[140] the exchange-correlation functional can be written as

$$E_{xc}^{LDA}(n) = \int \varepsilon_{xc}(n) n(r) dr \quad (2.13)$$

where ε_{xc} is the exchange-correlation energy per particle. The εxc can be further divided into exchange, ε_x, and correlation, ε_c, terms. The ε_x term can be explicitly evaluated from the Hartree-Fock method. On the other hand, the analytical form of the ε_c is not know. Thus numerical forms of εc are used, which have been obtained by fitting on accurate data from Quantum Monte Carlo calculations[141]. Despite the simplicity, LDA is one of the most widely used functionals in various studies.

2.1.5.2. GGA

In general, the electronic density of a system is not uniform and can even vary rapidly in space, for example, when switching from one electronic layer to another in an atom, or when we go from one atom to another in a molecule. In these cases the LDA approximation is not suitable. Therefore, the first improvement that can be made to the LDA method is expressing the exchange-correlation energy functional as a function of both the electron density and its gradient. This method is known as Generalised-Gradient approximation (GGA) [142, 143], in which the exchange-correlation functional is given by

$$E_{xc}^{GGA}(n) = \int \varepsilon_{xc}(n, |\nabla n|)(n) n(r) dr \quad (2.14)$$

where ε_{xc} can be expressed as the homogeneous ε_x enhanced by a factor F_{xc}. Then the exchange-correlation functional can be written as

$$E_{xc}^{GGA}(n) = \int \varepsilon_x^{LDA} F_{xc}(n, |\nabla n|)(n) n(r) dr \quad (2.15)$$

where F_{xc} is a functional of the electron density and its gradient. Compared to LDA, GGA gives often better results when calculating structural properties cohesive energies, phase transitions, and various other properties.

2.2. Pseudopotenials

The electronic ground state of any system can be described by the different methods which we presented in this chapter. But the problem is that calculations become more and more expensive as the number and size of atoms increases, because of the increase in the number of electrons. However, and in the most cases, the valence electrons are the only ones

to intervene in the interesting properties of the systems studied, for example in the establishment of chemical bonds. The core electrons are almost unaffected by environmental changes and remain unchanged from the situation in the isolated atom, it possible to group them with the nuclei, to constitute rigid ions: it is the approximation of the frozen cores[144]. Thus the number of electrons to be treated explicitly is much smaller than the real number of electrons and "big" systems become accessible to calculations. The interactions between valence electrons and ionic atomic cores are represented by pseudopotential. For Construction, a pseudo potential must be additive: it must be possible to obtain from calculations on the atom, and the total potential must be the sum of the pseudopotentials when several atoms are present. Also It must be transferable, i.e., the same atomic pseudo potential must be used in different chemical environments. The most pseudo potentials are built from calculations on the atom involving all electrons. Figure5 illustrates the schematic representation of the pseudo potential concept [145].

To explain the construction of a pseudo potential, firstly, consider exact core and valence states, $|\psi_c\rangle$ and $|\psi_v\rangle$, for which the Schrödinger equation can be expressed as

$$H|\psi_i\rangle = E_i|\psi_i\rangle \qquad 2.16$$

i stands for both core and valence states. The interest is to smoothen the valence states in the core region; thus, the core orthogonality wiggles can be subtracted from the valence states,

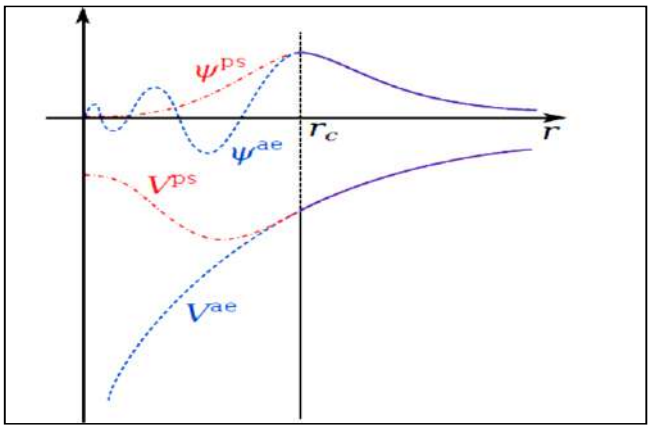

Figure.5 : The schematic representation of the pseudo potential concept**[145]**

leading to pseudostates, $|\phi_v\rangle$, written as

$$|\phi_v\rangle = |\psi_v\rangle + \sum_c |\psi_c\rangle \alpha_{cv} \quad 2.17$$

and

$$\alpha_{cv} = \langle \psi_c | \phi_v \rangle \quad 2.18$$

Inserting Eq. 2.17 into Eq. 2.16 we find that[146-148]

$$H|\phi_v\rangle = E_v|\psi_v\rangle + \sum_c E_c|\psi_c\rangle\alpha_{cv} \quad = E_v|\phi_v\rangle + \sum_c (E_c - E_v)|\psi_c\rangle\alpha_{cv} = E_v|\phi_v\rangle \quad 2.19$$

Hence,

$$\left[H + \sum_c (E_c - E_v)|\psi_c\rangle\langle\psi_c|\right]|\phi_v\rangle = E_v|\psi_v\rangle \quad 2.20$$

Through this the pseudo-Hamiltonian is written as follows

$$H^{\mathrm{ps}} = H + \sum_c (E_v - E_c)|\psi_c\rangle\langle\psi_c| \quad 2.21$$

And pseudopotential

$$V^{\mathrm{ps}} = V + \sum_c (E_v - E_c)|\psi_c\rangle\langle\psi_c| \quad 2.22$$

The first and the second terms in the pseudopotential are the true potential and the repulsive potential, respectively.

2.3. Basis sets

Let us have reminder in brief of the KS formalism before going into details regarding the basic concept of basis sets. In KS DFT, the electrons are moving under the effect of effective potential V_{eff}, thus the Kohn-Sham eigenvalue equation write as follows

$$H_{eff}(r)\psi_i(r) = \left[-\frac{\hbar^2}{2m_e}\nabla^2 + V_{eff}(r)\right]\psi_i(r) = \varepsilon_i\psi_i(r) \quad 2.23$$

From the Bloch theorem, and the periodicity of the effective potential V_{eff}, the single particle wavefunction can be written as

$$\psi_k(r) = e^{ik.r}u_k(r) \quad 2.24$$

To solve the the KS equation the single particle wavefunction can be expanded in a complete basis set of functions $\{\emptyset_i(r)\}$as follow

$$\psi_{nk}(r) = \sum_i c_{i,n}\emptyset_{i,k}(r) \quad 2.25$$

and the coefficients $c_{i,n}$ can be obtained by solving

$$\sum_j [\langle \emptyset_{i,k} | H | \emptyset_{j,k} \rangle - \varepsilon_{nk} \langle \emptyset_{i,k} | \emptyset_{j,k} \rangle] c_{j,nk} = 0 \qquad 2.26$$

The first term is the effective Hamiltonian and the second term is the overlap matrix element, and then can be obtained the eigenvalues by solving the secular equation

$$det[\langle \emptyset_{i,k} | H | \emptyset_{j,k} \rangle - \varepsilon_{nk} \langle \emptyset_{i,k} | \emptyset_{j,k} \rangle] = 0 \qquad 2.27$$

The basis sets can be formed in different ways depending on the studied systems and the required accuracy, and among the most widely used basis sets are linear muffin-tin orbitals (LMTO), linear combination of atomic orbitals (LCAO)[149], planes wave (PW), and linearised augmented plane waves (LAPW)

2.4. Success and limitations of the DFT

The numerous works carried out in recent years show that DFT calculations give good results for the fundamental states of very diverse systems (metallic, ionic, organometallic, transition metals, etc.) for many properties (molecular structures, vibration, ionization potentials ...). However, these methods still suffer from several defects. Thus, it would seem, until proven otherwise, that dispersion forces or van der Waals are not yet correctly treated in DFT except in the specially developed functional ones. Moreover, we do not always understand the good or bad results of the DFT on some systems. Moreover, there is no real criterion for choosing one functional over another. It is also difficult to find criteria to improve a given functional, which sometimes makes the use of the DFT difficult. A strong limitation is that excited states are not accessible in the formalism developed above. However, recent developments using a time-dependent formalism (TDDFT) as part of the linear response theory allow a description of the excited states.

2.5. Extending Density Functional Theory to Excited State Calculations

The ground-state formulation of DFT has allowed the calculation of many properties of materials. Some properties, however, depend not only on the ground state electron density, but also how that density responds to excitations (TDDFT)[150]. The first theorem of the Hohenburg and Kohn Theorems (DFT) only refers to the time-independent ground-state density of a system. A new theorem is therefore required, analogous in principle to the first Hohenburg and Kohn Theorem, but able to accommodate a time-dependent potential. This theorem was provided by the Runge-Gross Theorem in 1984[151], and is widely cited as the beginnings of modern TDDFT.

The Runge-Gross Theorem states that under certain conditions there is a one-to-one correspondence between the time-dependent external potential V_{ext}(r, t) and the time-dependent density n(r, t) of a system. This theorem means that, given the external potential of the system, the electron density can be calculated. The electron density can then be used to calculate the rest of the Hamiltonian, and the full many-body wavefunction can be derived.

The exchange-correlation potentials are a function of the full history of the density, and so are much more complex than in the ground-state case. Many approximations are made in order to make these calculations feasible, and there are several different approaches that fall under this heading.

The majority of methods adopted under TDDFT work within the time-propagation of the system. Under this method a perturbation of arbitrary time and spatial dependence may be considered. This method is usually referred to as an explicit propagation over time method. As shall be seen, there are a number of different approximations that must be made within this method, which further divide it. A short summary of this method and its approximations shall be given here, a more complete description of the explicit propagation method is given by Castro et. al[152].

2.5.1. Explicit Propogation Over Time

The essential aim of TDDFT theorem is to find the set of wavefunctions $\psi_n(t)$ that are solutions to the equation [153]

$$\boldsymbol{H_{KS}(t)|\psi_n(t)\rangle = i\frac{\partial}{\partial t}|\psi_n(t)\rangle} \qquad 2.28$$

At some time $\boldsymbol{t_0}$, assuming that the perturbation was switched, the set of wavefunctions up to this time it could be solved within standard DFT and there is a set of solutions to the system at time $\boldsymbol{t_0}$, $\boldsymbol{\psi_n(t_0)}$. The problem is then to find an expression for how the wavefunctions change from this initial solution. Now, the problem is reduced to finding a propagator $U(t, t_0)$ such that at any time $\boldsymbol{t > t_0}$ the solution is given by

$$|\psi_n(t)\rangle = U(t, t_0)|\psi_n(t_0)\rangle \qquad 2.29$$

Substituting this expression into equation (3.46) gives the equation

$$\boldsymbol{H_{KS}(t)}U(t, t_0)|\psi_n(t_0)\rangle = \boldsymbol{i\frac{\partial}{\partial t}}U(t, t_0)|\psi_n(t_0)\rangle \qquad 2.30$$

and

$$\boldsymbol{H_{KS}(t)}U(t,t_0) = \boldsymbol{i}\frac{\boldsymbol{\partial}}{\boldsymbol{\partial t}}U(t,t_0) \quad 2.31$$

After integral, can now be expanded out to form a Dyson series and introducting a time ordering operator[154]:

$$U(t,t_0) = 1 + \sum_{n=1}^{\infty}\frac{(-i)^n}{n!}\int_{t_0}^{t}dt_1\int_{t_0}^{t}dt_2 \ldots \int_{t_0}^{t}dt_n T[H_{KS}(t_1)\ldots H_{KS}(t_n)] \quad 2.32$$

Where T given by

$$T[A(x)B(y)] = \begin{cases} A(x)B(y) & if \;\; x_0 > y_0 \\ B(y)A(x) & if \;\; x_0 < y_0 \end{cases} \quad 2.33$$

x_0 and y_0 are the time coordinates of points x and y respectively. In equation (2.32), we can see that it is necessary to include the time-ordering operator to ensure that the correct order is maintained. Therefore, the propagator can be rewritten in terms of the time-ordered exponential

$$U(t,t_0) = Te^{-i\int_{t_0}^{t}d\tau H(\tau)} \quad 2.34$$

The expression above is too complex to compute directly, and so approximations must be made to find a calculable form of $U(t,t_0)$. The first commonly made approximation is that the Hamiltonian commutes with itself at different times. This allows the removal of the time-ordering operator T. In this case the integral over time can be removed and the familiar form for the time dependence remains[155],

$$U(t,t_0) = e^{-i(t-t_0)H} \quad 2.35$$

And

$$\psi_n(t) = e^{-iHt}\psi_n^0 \quad 2.36$$

where ψ_n^0 is the solution to the time-independent Kohn-Sham equation. Of course, this assumption is not relevant to TDDFT. Other approximations must therefore be made for the propagator.

For any three times t_1, t_2, t_3 the propagator can be rewritten as follow

$$U(t,t_0) = e^{-i(t-t_0)H} \quad 2.37$$

It is very important property of the time propagator, and one that allows simplification of the problem substantially. This property allows the problem to be broken into a series of time segments. The propagator can then be expressed by

$$U(t,t_0) = U(t_N,t_{\mathrm{N}-1})U(t_{N-1},t_{\mathrm{N}-2})\dots U(t_1,t_0) = \prod_{\mathrm{n}=0}^{\mathrm{N}-1} U(t_{n+1},t_{\mathrm{n}}) \qquad 2.38$$

For each time step to be a constant Δt, in which case the above expression can be further simplified to become

$$\prod_{\mathrm{n}=0}^{\mathrm{N}-1} U(t_n+\Delta t,t_{\mathrm{n}}) \qquad 2.39$$

And therefore, the wavefunctions which can now be written with the expression given in equation (2.34) to give [155]

$$|\psi_n(t+\Delta t)\rangle = Te^{-i\int_t^{t+\Delta t} d\tau H(\tau)}|\psi_n(t)\rangle \qquad 2.40$$

There are two levels of approximation remaining. Firstly, there needs to be an approximation of the integral of the Hamiltonian over the time step. Secondly the exponential of this integral must be calculated.

2.5.1.1. Methods for Approximating the Integral

The exponential midpoint rule is one of the simplest methods available and works by giving a first-order approximation to the integral term in equation 2.34. And the time propagator is given by [154]

$$U_{ST}(t+\Delta t,t) = e^{-\frac{i}{2}\Delta \mathrm{tT}}e^{-i\Delta \mathrm{tV}}e^{-\frac{i}{2}\Delta \mathrm{tT}} \qquad 2.41$$

where the potential operator V is defined by

$$V_{ext}(r,t+\Delta t/2) + \int \mathrm{dr}'\,\frac{\mathrm{n}(\mathrm{r}')}{|\mathrm{r}-\mathrm{r}'|} + V_{xc}[n](r,t) \qquad 2.42$$

where n is the electron density. The main advantage of this technique is it uses the fact that the kinetic energy operator is diagonal in Fourier space, and the potential operator is almost diagonal in real space, and separation of these operators makes calculating the exponential of the integral less computationally expensive.

The next question then is whether there is some other operator, say $\Omega(t+\Delta t,t)$ such that

$$U(t+\Delta t,t) = e^{\,\Omega(t+\Delta t,t)} \qquad 2.43$$

In 1954 W. Magnus developed such an expression for $\Omega(t+\Delta t,t)$ in the form of an infinite series of the form[156]

$$\Omega(t+\Delta t,t) = \sum_{\mathrm{n}=1}^{\infty} \Omega_{\mathrm{n}}(t+\Delta t,t) \qquad 2.44$$

Where

$$\Omega_{\mathrm{n}}(t+\Delta t,t)=\sum_{\mathrm{m}=0}^{\mathrm{n}-1}\frac{B_{\mathrm{m}}}{\mathrm{m}!}\int_{t}^{t+\Delta t}S_n^m(\tau)\,\mathrm{d}\tau \qquad 2.45$$

And B and S are expressed by

$$S_1^0(\tau)=-i\,H(\tau)$$

$$S_n^0(\tau)=0\ (k>1)$$

$$S_n^m(\tau)=\sum_{\mathrm{p}=1}^{\mathrm{n}-\mathrm{m}}\left[\Omega_{\mathrm{n}}(t+\Delta t,t),S_{n-p}^{m-1}(\tau)\right]\ (1\le m\le n-1)$$

Although the Magnus expansion method is the most sophisticated of the above techniques for approximating the integral, currently the Magnus expansion method was considered an "experimental" feature of Octopus [152, 157].

2.5.1.2. Methods for Approximating the Exponential

The Taylor expansion of an exponential is the most obvious method to find the exponential of the integral. That is

$$e^{\mathrm{A}}=\sum_{\mathrm{k}=0}^{\infty}\frac{1}{\mathrm{k}!}A^k \qquad 2.46$$

Therefore the N_{th} order approximation of the exponential of the operator is simply

$$e^{\mathrm{A}}\approx\sum_{\mathrm{k}=0}^{\mathrm{N}}\frac{1}{\mathrm{k}!}A^k \qquad 2.47$$

Where N can be any positive integer, and in practice $\mathrm{N}=4$ has is usually used, as it allows the use of larger time steps Δt whilst staying stable [152].

The Chebyshev expansion is another polynomial expansion of the exponential [158], it form a complete orthogonal basis set. The N_{th} order Chebyshev approximation of the exponential is defined as

$$e^{\mathrm{A}}\approx\sum_{\mathrm{k}=0}^{\mathrm{N}}\mathrm{c_k}\mathrm{T_k}(A) \qquad 2.48$$

where $\mathrm{T_k}$ is the Chebychev polynomial of order k.

The Chebychev expansion has the advantage over the Taylor expansion that it allows larger time steps Δt to be used, hence reducing the number of steps required for a full propagation, but it is less efficient than the Taylor expansion for small time steps.

The Lanczos method is a more sophisticated than those already mentioned. The Lanczos approximation of the exponential is defined as

$$e^{\mathrm{A}}v \approx \mathrm{V_k e^{Hk} e_1} \qquad 2.49$$

Where $\mathrm{e^{Hk}}$ can be calculated by any of the methods given by Moler and Loan [159]. The Lanczos method is capable of efficiently calculating the exponential up to quite large time steps Δt [157]. This makes it very useful for calculating systems over large time scales where very high-frequency data is not required.

2.5.2. Calculation of the Absorption Cross-Section

In order to calculate the optical absorption cross-section for a particle, a set of perturbed wavefunctions are defined in terms of the ground-state electron wavefunctions $\psi_n^0(r)$ by

$$\psi_n(r) = \mathrm{e^{i\kappa x_j}}\psi_n^0(r) \qquad 2.50$$

where κ is a small, positive, real constant and x_j is a unit vector in direction j. And then, these wavefunctions are used as a starting point and the system is propagated through time as it relaxes from the initial perturbation, giving the change to the ground-state density δρ(r, t). The change in the dipole moment in the direction i is given by

$$\delta\langle X_i\rangle(\omega) = \int \mathrm{d^3 r} x_i \delta\rho(r,\omega) \qquad 2.51$$

The polarisability element $\alpha_{ij}(\omega)$is defined in terms of the dipole moment in the direction i from a perturbation in the direction j, and can be calculated by[154]

$$\alpha_{ij}(\omega) = -\frac{\delta\langle(\omega)\rangle}{\lambda} \qquad 2.52$$

The absorption cross-section tensor for isolated particle is given by

$$\sigma(\omega) = \frac{4\pi\omega}{c}\Im m[\alpha(\omega)] \qquad 2.53$$

One of the strengths of the explicit time propagation method is the ability to deal with an arbitrary external potential. The linear response methods make the assumption of a sinusoidal perturbation. They also assume a small external perturbation and in practice also assume a perturbation without any spatial variation.

2.6. What TDDFT can do well

In the dynamics of the interacting system is qualitatively similar to the corresponding non-interacting system. The adiabatic approximation (LDA) for the exchange-correlation potential works well, and it is possible to use the same approximation in the time-dependent case that is

used to prepare the initial ground state of the system. In the case of linear-response calculations of the excitation spectrum of the system, the spectral features are dominated by single-particle excitation processes. In the case of the calculations of strongly excited systems under the influence of high intensity fields, the external field dominates over the electron-electron interactions, highly nonlinear multiphoton processes are prevalent (multiple ionization or high-harmonic generation) [152].

2.7. SIESTA our choice of DFT implementation

SIESTA [160, 161] "Spanish Initiative for Electronic simulations with Thousands of atoms" is a calculation method and computer code which solves problems related to ground state properties (Energy/volume curves, phase diagrams, phonons, molecular dynamic) at the level of density functional theory (DFT). Since its development, the computational power has risen substantially, allowing for calculations of various properties of small to considerably large systems, with > 1000 atoms. We used a version written in Fortran 90.

The system is reproduced identical to itself by periodicity. It suffices to define just one elementary cell, giving the angles and norms of the three vectors defining it, and then to give the positions of the atoms in this cell. When studying molecular systems such as clusters, they must be placed in cells large enough to avoid interactions between the system and its images of neighboring cells. These interactions must not exist because they are physically unfounded since the images are only there to reflect the artifice of the periodic boundary conditions.

The number of points k of the first Brillouin zone used for the self-consistent resolution of the Kohn-Sham equations can have a great influence on the result. In the case of molecular systems, the molecules or atoms of each cell are well separated and energy bands (i.e., molecular or atomic levels) are flat. It is enough then to take only one point k (in most cases one takes k = 0 which is called approximation of the point Γ). On the other hand, for a solid, it is necessary to take enough point k to represent well the structure of bands.

Structural relaxation is done by minimizing the total energy either with a static method, such as the conjugate gradient method [162] (in this method, it is a question of minimizing energy by moving in the configuration space , not according to the greatest slope, but in directions that accelerate convergence) or with dynamic method (Verlet, Nosé, simulated annealing, etc.). For that we fix the maximum tolerated force undergone by each atom. Constraints can also be imposed during the relaxation of the system by freezing, for example, the position of certain atoms.

In the following paragraphs, we will briefly discuss a concept of non-local pseudopotentials, basis sets based on atomic orbitals, and the basic method for calculating matrix elements and total energies implemented in SIESTA. For more details can be found in the Soler et al. review of the method [163].

2.7.1. Norm-conserving pseudopotentials

In computations solid-state, the first step in gaining efficiency in calculations is to generate a pseudo potential from a simple environment like spherical atom, termed "good" ab initio pseudopotential. The role of this pseudopotential is reproducing the logarithmic derivatives of the all electron wavefunction outside a given cutoff radius, rc. Hammann, Schlüter and Chiang, the first to propose pseudo potentials which satisfy all criteria [164], they were named norm-conserving pseudopotentials. From given all electron information, we can generating a screened pseudo potential,V^{sc}. However, this propos does not provide the form of the pseudo potential in the core region, for treat this problem we can use Troullier-Martins (TM) approach [165], one of the most widely used methods for determining the form of a pseudopotential in the core region. In the TM approach, the pseudo wavefunction is made to satisfy: (i) norm conservation of the charge density in the core region; (ii) continuity of the pseudo wavefunction and its logarithmic derivative and first energy derivative at rc; and (iii) smooth pseudopotential form, which comes from the zero curvature at the origin. The interaction between the atomic valence states in screened pseudopotential is different from valence states interactions in molecules or solids. Therefore, it is very useful to remove the screening to make the pseudopotential transferable to various environments; it is termed unscreened pseudopotential V^{usc}. The newly introduced pseudopotential has a spherically symmetric form which loads to possible to treat each angular momentum (l) separately, so l-dependent pseudopotential, V_l (r). It is possible to a made more efficient by introducing separable potentials that are non-local in the angles and radius which was proposed by Kleinman and Bylander (KB) [166].

2.7.2. LCAO basis set

The first introduced in quantum chemistry for describing molecular orbitals is the linear combination of atomic orbitals (LCAO) basis sets. They are essentially a superposition of atomic orbitals, given by

$$\emptyset_{nlm} = \sum_{i} \boldsymbol{C}_{i,nlm}\boldsymbol{\chi}_{i,nlm} \qquad 2.54$$

Where $\emptyset_{nlm}$is the basis orbital, $C_{i,nlm}$ are the AO coefficients and the summation is over the number of AO, $\chi_{i,nlm}$. Mostly used basis functions are the Slater Type Orbitals (STO) [167] and the Gaussian Type Orbitals (GTO) [168]. Both of these types of AO have the same form

$$\chi_{i,nlm}(r,\theta,\varphi) = R_{nl}(r)Y_{lm}(\theta,\varphi) \quad 2.55$$

The basis orbitals that are confined within a given cutoff radius are used in SIESTA for increase the efficiency. These basis orbitals have the following form

$$\emptyset_{i,nlm}(r) = R_{i,nl}(r_i)Y_{lm} \quad 2.56$$

where $r_i = r - \mathbf{R}_i$, and $R_{i,nl}$ is a numerical radial function. The index n indicates the number of orbitals which have different radial dependence, but the same angular dependence, referred to as multiple-ζ (zeta).

2.7.2.1. Single, multiple and polarized basis sets

The basis sets is a set functions that is used to represent the electronic wave function in the density functional theory. The basic description of a free atom can be obtained by considering only one basis function for each atomic orbital. This type of basis set is termed minimal basis set (use of minimum number of basis orbitals) also knows as single-zeta (single-ζ, SZ) basis set. The SZ basis set for hydrogen and helium is composed of just one s-function (1s) but ethers elements of periodic table, the different shells in the atoms from the same row, are considered together, e.g. 2sp (2s and 2p), 3sp,4sp,3 d shells, etc. In the case of lithium and beryllium, including only the s orbitals in the minimal basis set yields very poor results, thus p-functions are also added. The Double Zeta (DZ) basis set is two basis functions for every atomic orbital, the DZ basis set for hydrogen and helium has two s-functions (1s and 1s′), and for the second row elements has four s-functions (1s,1s′, 2s and 2s′) and two p-functions (2p and 2p′), six s-functions and four p-functions for third row elements. As in DZ, the core and valence orbitals in TZ (increasing the number of basis function by one will yield the Triple Zeta basis set) can be split, giving a triple split valence basis set. The basis sets next in size are Quadruple Zeta (QZ) and Quintuple Zeta (5Z). The LCAO basis sets can be improved by adding polarization functions, e.g. p-functions for hydrogen and helium, d-functions for the second row elements etc. In general, single or multiple polarization functions can be added to the multiple zeta basis sets, i.e. adding a single polarization function to a DZ basis set gives Double Zeta Polarized (DZP) basis set[169].

2.7.3. Matrix elements

For practical reasons the pseudopotential approximations and the LCAO basis set, which were discussed in the previous sections, were implemented in the SIESTA DFT method. Thus, the Hamiltonian can be written as

$$\boldsymbol{H} = \boldsymbol{T} + \sum_{\boldsymbol{i}} \boldsymbol{V_i^{na}}(\boldsymbol{r}) + \sum_{\boldsymbol{i}} \boldsymbol{V_i^{nl}} + \boldsymbol{\delta V_H}(\boldsymbol{r}) + \boldsymbol{V_{xc}}(\boldsymbol{r}) \qquad 2.57$$

where $\boldsymbol{i}$ is an atom index, $\boldsymbol{T}$ is the kinetic operator, $\boldsymbol{V_i^{nl}}$ I is the non-local $(\boldsymbol{nl})$ part of the KB pseudopotential, $\boldsymbol{V_i^{na}}$ is screened neutral-atom $(\boldsymbol{na})$ potential, $\boldsymbol{\delta V_H}(\boldsymbol{r})$ and $\boldsymbol{V_{xc}}(\boldsymbol{r})$ are the electrostatic and exchange-correlation potentials. The matrix elements of the $\boldsymbol{T}$ and $\boldsymbol{V_i^{nl}}$ are expressed as two-center integrals and calculated in reciprocal space then tabulated as functions of the relative position of the centers. The residual terms are calculated using real-space grid. The sum of neutral atom potentials are calculated and tabulated as a function of distance to atoms. The last two terms ($\boldsymbol{\delta V_H}(\boldsymbol{r})$, $\boldsymbol{V_{xc}}(\boldsymbol{r})$) depend on the self-consistent electron density, $\boldsymbol{\rho}(\boldsymbol{r})$, can be written as

$$\boldsymbol{\rho}(\boldsymbol{r}) = \sum_{\boldsymbol{\mu\nu}} \boldsymbol{\rho_{\mu\nu}} \emptyset_{\boldsymbol{\mu}}(\boldsymbol{r}) \emptyset_{\boldsymbol{\nu}}(\boldsymbol{r}) \qquad 2.58$$

where μ, νindicate the basis orbitals $\emptyset_{\boldsymbol{\mu/\nu}}$, and $\boldsymbol{\rho_{\mu\nu}}$ is the one-electron density matrix, defined as

$$\boldsymbol{\rho_{\mu\nu}} = \sum_{\boldsymbol{i}} \boldsymbol{c_{i\mu} n_i c_{i\nu}} \qquad 2.59$$

With

$$\boldsymbol{c_{i\mu}} = \langle \boldsymbol{\Psi_i} | \widetilde{\emptyset}_{\boldsymbol{\mu}} \rangle,$$

where $\boldsymbol{n_i}$ is the occupation of state of the Hamiltonian. To obtain the last two terms in Eq. 2.57, first the $\boldsymbol{\rho}(\boldsymbol{r})$ needs to be calculated at a given grid point, by calculating each of the atomic basis orbital at that point. The $\boldsymbol{\delta V_H}(\boldsymbol{r})$ can be obtained, by solving the Poisson's equation, and is added to the total grid potential, $\boldsymbol{H} = \boldsymbol{V^{na}}(\boldsymbol{r}) + \boldsymbol{\delta V_H}(\boldsymbol{r}) + \boldsymbol{V_{xc}}(\boldsymbol{r})$. Finally, the matrix elements of the total grid potential are calculated at every grid point, and added to the Hamiltonian matrix element [169].

2.7.4. Total energy

The Kohn-Sham total energy, based on the electron density obtained from Eq. 2.58, is constructed as follows

$$E_{tot} = \sum_{\mu\nu} \rho_{\mu\nu} H_{\mu\nu} - \frac{1}{2} \int dr V_H(r) \rho(r) \int dr \left(\varepsilon_{xc}(r) - V_{xc}(r)\right) \rho(r) + \frac{1}{2} \sum_{ij} \frac{e^2 Z_i Z_j}{|r_i - r_j|} \quad 2.60$$

where $\varepsilon_{xc}(r)\rho(r)$ is the exchange-correlation energy density and $Z_{i/j}$ are the valence pseudo-atom charges. The calculations can be further improved by avoiding the long-distance interactions of the last term. To do this, a diffuse ion charge ρ_i^{local} , having the same electrostatic potential as V_i^{local}, can be written as

$$\rho_i^{local}(r) = -\frac{1}{4\pi e} \nabla^2 V_i^{local}(r) \quad 2.61$$

The last term in Eq. 2.60 is constructed as follows

$$\frac{1}{2} \sum_{ij} \frac{e^2 Z_i Z_j}{|r_i - r_j|} = \frac{1}{2} \sum_{ij} \int dr V_i^{local}(r) \rho_j^{local}(r) - \sum_i U_i^{local}(r) \quad 2.62$$

Where

$$U_i^{local} = \int dr V_i^{local}(r) \rho_i^{local}(r)\, 4\pi r^2 \quad 2.63$$

Then, ρ^{na} can be defined as $\rho^{na} = \rho^{local} + \rho^{atom}$, and Eq.2.60 can be transformed into [169]

$$E_{tot} = \sum_{\mu\nu} \rho_{\mu\nu} \left(T_{\mu\nu} + V_{\mu\nu}^{nl}\right) + \frac{1}{2} \sum_{ij} dr V_i^{na}(r) \rho_j^{na}(r) \frac{1}{2} - \sum_i U_i^{local} + \int dr V^{na}(r)\, \delta\rho(r) + \frac{1}{2} \int dr \delta V_H(r) \delta\rho(r) + \int dr \varepsilon_{xc}(r)\, \rho(r) \quad 2.64$$

The first two terms are calculated by interpolation from initially calculated tables, as in the case of the matrix elements of the Hamiltonian. The third term is calculated from the Eq. 2.63, and the last three terms are calculated using a real space grid.

2.8. Octopus our choice of TDDFT implementation

Octopus is a scientific program aimed at the ab initio virtual experimentation on a hopefully ever-increasing range of system types. Electrons are described quantum-mechanically within density-functional theory (DFT), in its time-dependent form (TDDFT) when doing simulations in time. Nuclei are described classically as point particles. Electron-nucleus interaction is described within the pseudopotential approximation.

For optimal execution performance Octopus is parallelized using MPI and OpenMP and can scale to tens of thousands of processors. It also has support for graphical processing units (GPUs) through OpenCL and CUDA. Octopus is free software; it is coded in a combination of Fortan and C and has some scripts within it written in Perl. It also makes extensive use of libraries, requiring FFTW [170], LAPACK/BLAS [171, 172] and GSL [173] for compilation, so you are free to download it, use it and modify it.

In order to run Octopus, we need a few input files like the Cartesian coordinates of the atoms within the system (.xyz file), and the pseudopotentials for each of the species, although Octopus has default pseudopotentials it can use. The rest of the parameters are given in a single text file known as the inp file.

The program of octopus [154, 174] is based on TDDFT in the Kohn-Sham scheme and all calculations are expanded in a regular mesh in real space, so the simulations are performed in real time. The program has been successfully used to calculate linear and non-linear absorption spectra, harmonic spectra, laser induced fragmentation, etc. of a variety of systems. The main advantage of real space methods is the simplicity and intuitiveness of the whole procedure. First of all, quantities like the density or the wave-functions are very simple to visualize in real space. Furthermore, the method is fairly simple to implement numerically for 1-, 2-, or 3-dimensional systems, and for a variety of different boundary conditions. In real space methods the only convergence parameter is the grid-spacing, and decreasing the grid spacing always improves the result. Unfortunately, real-space methods suffer from a few drawbacks. For example, most of the real-space implementations are not variational, i.e., we may find a total energy lower than the true energy, and if we reduce the grid-spacing the energy can actually increase. Moreover, the grid breaks translational symmetry, and can also break other symmetries that the system may possess. This can lead to the artificial lifting of some degeneracies, to the appearance of spurious peaks in spectra. Another important parameter for OCTOPUS calculations is the radius parameter. Since OCTOPUS performs all

real space calculations using a sphere around each atom, it converge the density within each of these spheres. Also since we employ zero boundary conditions for clusters calculations, we do not need to specity a super-cell since this condition will take care of the non-periodic boundary conditions. Also this method of using spheres centered around each atom rather than a cell reduces the computational time drastically in real space calculations for clusters and molecules. A radius too large will not affect the calculations but a radius too small would make the wave function die out even before they reach adjacent atom. But all of the above problems can be minimized by correctly optimizing the radius and the spacing parameters as described in the sub-sections [154, 174].

2.8.1. Radius optimization

As mentioned earlier the radius parameter is a crucial parameter for OCTOPUS calculations. In order to get the correct value of the radius parameter, we minimize the energy by consecutively running OCTOPUS for a test system with a fixed value of spacing and vary over the radius parameter. We check for the total energy of the system and chose a radius parameter where the total energy is a minimum.

2.8.2. Grid Spacing

Methods of optimizing the grid spacing for a calculation are outlined within the Octopus tutorial [157]. Any real space grid must be sufficiently dense that the electron density is accurately represented, having a grid density that is too low results in the total energy dropping from the true value. Calculation times are directly proportional to number of grid points, and therefore scale with $1/x^3$, where x is the grid spacing. Similar to the case of radius optimization, even while optimizing spacing energy minimization is the only reliable criterion.

A similar set of tests were run on all the clusters under consideration and the value of radius and spacing obtained were the same proving the earlier point, that these parameters mainly depend on the pseudo-potentials under consideration. Once the spacing and radius parameters are fixed we calculate the photo-absorption spectra of the clusters using TDDFT method. Other variables like Convergence Criteria, Exchange-Correlation Potential, Extra States and Smearing were used in our calculation with default values.

2.8.3. Time Dependent run:

In our calculation, the photo-absorption spectrums were obtained by use TDDFT method [150, 175]. In this method, the basic variable is the one electron density $n(r,t)$,which is

obtained with the help of a fictitious system of non-interacting electrons, the Kohn-Sham system. The time-dependent Kohn Sham equations are [150, 175]

$$i\frac{\partial}{\partial t}\psi_i(r,t) = \left[\frac{-\nabla^2}{2} + v_{KS}(r,t)\right]\psi_i(r,t) \qquad 2.65$$

Where $\psi_i(r,t)$ are Kohn-Sham one electron orbitals. In terms these orbitals $n(r,t)$,can be written as

$$n(r,t) = \sum_{i}^{occ} |\psi_i(r,t)|^2 \qquad 2.66$$

The Kohn-Sham potential can be written as

$$v_{KS}(r,t) = v_{ext}(r,t) + v_{Hartree}(r,t) + v_{xc}(r,t) \qquad 2.67$$

where the first term is the external potential, the second Hartree potential and the last the exchange and correlation potential. For obtaining this potential we use adiabatic local density approximation (ALDA).

In order to calculate the absorption spectra by octopus cod we must choose between the three methods below: the Sternheimer response method, the Casida response method and the explicit propagation method. The aim of this work is to calculating the absorption cross-section spectra of pure and tin doped germanium clusters from 2 to 18 atoms which leads produced a lot of clusters, i.e. a lot of the calculations. The prime consideration for selecting the appropriate calculation method is the scaling of the calculation time it takes each method with system size and with number of the clusters to obtain. This excludes the Casida method as its calculation time scales proportionally to $N_R N^2_o N^2_u$ where N_o and N_u are the number of occupied and unoccupied states in the system, respectively, and N_R is the number of real-space points in the system. Calculations times for both the Sternheimer and explicit propagation methods are approximately directly proportionally to $N_R N_e$ and are therefore proportional to the number of atoms in the system squared [150], and in the other side, the Sternheimer method however also scales with the number of frequencies for which the absorption cross-section is required. This causes it is slow for the calculation of an entire cross-section spectrum, the explicit propagation method was therefore chosen for calculations. In this method the electrons are given some small momentum (K) to excite all the frequencies [176]. This is achieved by transforming the ground state wave function according to

$$\psi_i(r,\delta t) = e^{iKZ}\psi_i(r,0) \qquad 2.68$$

and then propagating these wave functions for some finite time. The spectrum is then obtained from dipole strength function S(ω) [176]

$$S(\omega) = \frac{2\omega}{\pi} Im\alpha(\omega) \quad 2.69$$

$$\alpha(\omega) = \frac{1}{K}\int dte^{i\omega t}[d(t) - d(0)] \quad 2.70$$

where the α (ω) is the dynamical polarizability and d(t) is dipole moment of the system. We can also define a quantity know as the oscillator strength to express the strength of the transition.

$$f_I(x) = \frac{2}{3}\omega_I \sum_{n\in x,y,z} |\langle\varphi_0|n|\varphi_I\rangle|^2 \quad 2.71$$

where φ 0 and φ I are the ground and excited state respectively. The oscillator strength is related to the dipole strength function defined earlier using the following relationship

$$S(\omega) = \sum_I f_I \times \delta(\omega - \omega_I) \quad 2.72$$

The sum over the oscillator strength gives the number off active electrons in the system,

$$\sum f_I = N \quad 2.73$$

where N is the number of active electrons in the system.

APPLICATIONS

3. The ground state structures of $SnGe_n^{(0,\pm1)}$ (n=1-17) clusters and their electronic properties

Introduction

The present chapter deals a theoretical study of structures of pure and tin doped germanium clusters, Ge_{n+1} and $SnGe_n$ (n=1-17), neutrals and cations in the framework of the DFT method. The aim is to find the ground state structures of these clusters and their electronic properties. The chapter is organized as follows: we describe the computational details in section 2, section 3 is devoted to discuss the obtained results and in section 4 we draw some conclusions.

3.1. Method

In this study, ab initio molecular orbital and density functional theory (DFT) calculations are performed by using the SIESTA software package [137, 140, 177] (the Spanich Initiative for Electronic Simulation with Thousand of Atoms). The density functional is treated by generalized gradient approximation (GGA) with exchange correlation potential developed by Perdew and Zanger[178] and Perdew, Burke and Ernserhof (PBE)[179]. Self-consistent field procedures are carried out with a convergence (SZ) basis set for Sn and Ge atoms. The ionic core criterion of 10^{-4} a.u. on the total energy and electron density. A big cubic supercell with dimension of 40 Å was used to create sufficient vacuum space to eliminate the image interactions. The k=0 (Γ) point approximation was used in Brillouin zone sampling. During simulation, volume of the system was kept constant and a single ζ potential were Bylander form[180]. The energy cut-off of150 Ry was use represented by norm-conserving Troullier-Martins[165] and non local pseudopotentiels factorized in the Kleinman- and PAO.EnergyShift is taken equal to 50 meV. To perform simulated annealing for pure germanium clusters, initial velocities were assigned to the system corresponding to 10 K. Random velocities, drawn from the Maxwell-Boltzmann distribution with the corresponding temperature, are assigned to atoms. The constraint of zero centre of mass velocity is imposed. The atoms were moved according to the velocity Verlet algorithm with a time step of 1 a.u.

Table1.: Average bond length a (Å), Binding energy Eb (eV), Adiabatic Electronic Affinity (AEA) (eV) and Adiabatic Ionisation Potential (AIP) (eV) for Ge_2 et Ge_3 clusters.

Cluster	Our Works				Theoretical values				Experimental values			
	a	E_b	AEA	AIP	*a*	E_b	AEA	AIP	*a*	E_b	AEA	AIP
Ge_2	2.625	1.28	2.060	7.753	2.548[d]	1.3[e]	2.10[i]	7.9[j]	/	1.32[g]	2.035[g]	7.58-7.76[j]
					2.54[b]	1.31[f]				1.41[m]	2.074[h]	
					2.413[c]	1.32[j]						
					2.41[a]	1.230[l]						
					2.61[k]	1.812[k]						
Ge_3	2.476	1.86	1.907	8.126	2.428[i]	1.92[e]	2.09[i]	7.92[j]	/	2.24[n]	2.23[g]	7.97-8.09[j]
					2.400[l]	1.98[d]				2.15[m]	2.23[h]	
					2.378[d]	2[a]						
					2.296[i]	2.04[c]						

[a] Ref.[181].
[b] Ref.[182].
[c] Ref.[114].
[d] Ref.[183].
[e] Ref.[184].
[f] Ref.[107].
[g] Ref.[49].
[h] Ref.[50].
[i] Ref.[56].
[j] Ref.[76].
[k] Ref.[23].
[l] Ref.[57].
[m] Ref.[88].
[n] Ref.[185]

The system of each cluster was taken at high temperature of 1000 K in 1000 steps. Then, they are equilibrated at this temperature in 1000 other steps. Finally, the system was slowly cooled to 0 K in 5000 steps. On the other hand, for tin doped germanium clusters, conjugate gradient method within Hellmann Feynman forces was used and all the forces are less than 10^{-2} eV/ Å. In order to find the global minimum structures of $SnGe_n$ clusters, at first we have optimized several isomers of pure germanium clusters with size of 2-18 atoms. Second, a great number of isomers for doped $SnGe_n$ were considered. We have initially relaxed different possible isomers of neutral $SnGe_n$ clusters. Then, the best obtained structures have been considered in their anionic and cationic configurations and relaxed. After conducting a simulation process, a comparative study between the properties of neutral and charged

clusters was performed. In the discussion, we consider only the lowest energy isomers determined in our optimizations. In order to test the method used in geometry optimization, with respect to the exchange-correlation functional to the size and to the cutoff radii of basis sets, we performed calculations on Ge_2 and Ge_3 clusters. Our results shown in Table1 are in good agreement with theoretical and experimental results of the literature.

3.2. Results and discussions

3.2.1. Structural properties

In cluster physics, one of the most important things in studying the properties of clusters is to determine their ground states geometries. The most obtained stable structure and their corresponding isomers for pure and tin doped germanium clusters are shown in Figure.6 and Figure7, respectively. In these Figures, (a) isomer is the most stable structure. The energetic ordering of isomers for Ge_{n+1} and $SnGe_n$ (n=1-17) clusters are given in Table2 and Table 3 , respectively. In these tables, the parameters of the most stable structures for each size are reported in bold character. In Table.4, we give the average Ge-Ge and Sn-Ge bond lengths of the lowest energy structures of $SnGe_n^{(0,\pm1)}$ clusters. Figure.8 presents the most stable structures of anionic and cationic $SnGe_n^{(\pm1)}$ clusters and their parameters are described in Table.5.

In the case of clusters with two atoms, we obtained a SnGe monomer with bond length of 2.805 Å, which is in good agreement with the theoretical value [165] of 2.753Å. The binding energy equals 1.19eV/atom which is smaller than that of Ge_2 monomer (1.28eV/atom). For charged monomer, the bond length is 2.910 Å and 2.495 Å for $SnGe^+$ and $SnGe^-$, respectively, while the binding energy is 1.285 and 1.819 eV/atom, respectively. The cationic monomer is more stable than the neutral and anionic monomers.

The triangular structure is the lowest energy structure for Ge_3 with symmetry C_{2v} and average bond length of Ge-Ge of 2.476 Å. For $SnGe_2$ cluster, which has a triangular structure, with C_s symmetry, the average bond lengths Ge-Ge and Sn-Ge are 2.472 Å and 2.658 Å, respectively. The geometric structure of the anion cluster of $SnGe_2$ is also triangular, whereas its cation cluster is angular with C_s symmetry.

For Ge_4, the most stable structure is the rhombus (D_{2h}) with the bond length of 2.714 Å and the binding energy E_b=2.25eV/atom. The same structure is obtained by Wang et al[57] in their theoretical study and Li et al[76] in their experimental study on the Ge_n systems. In the

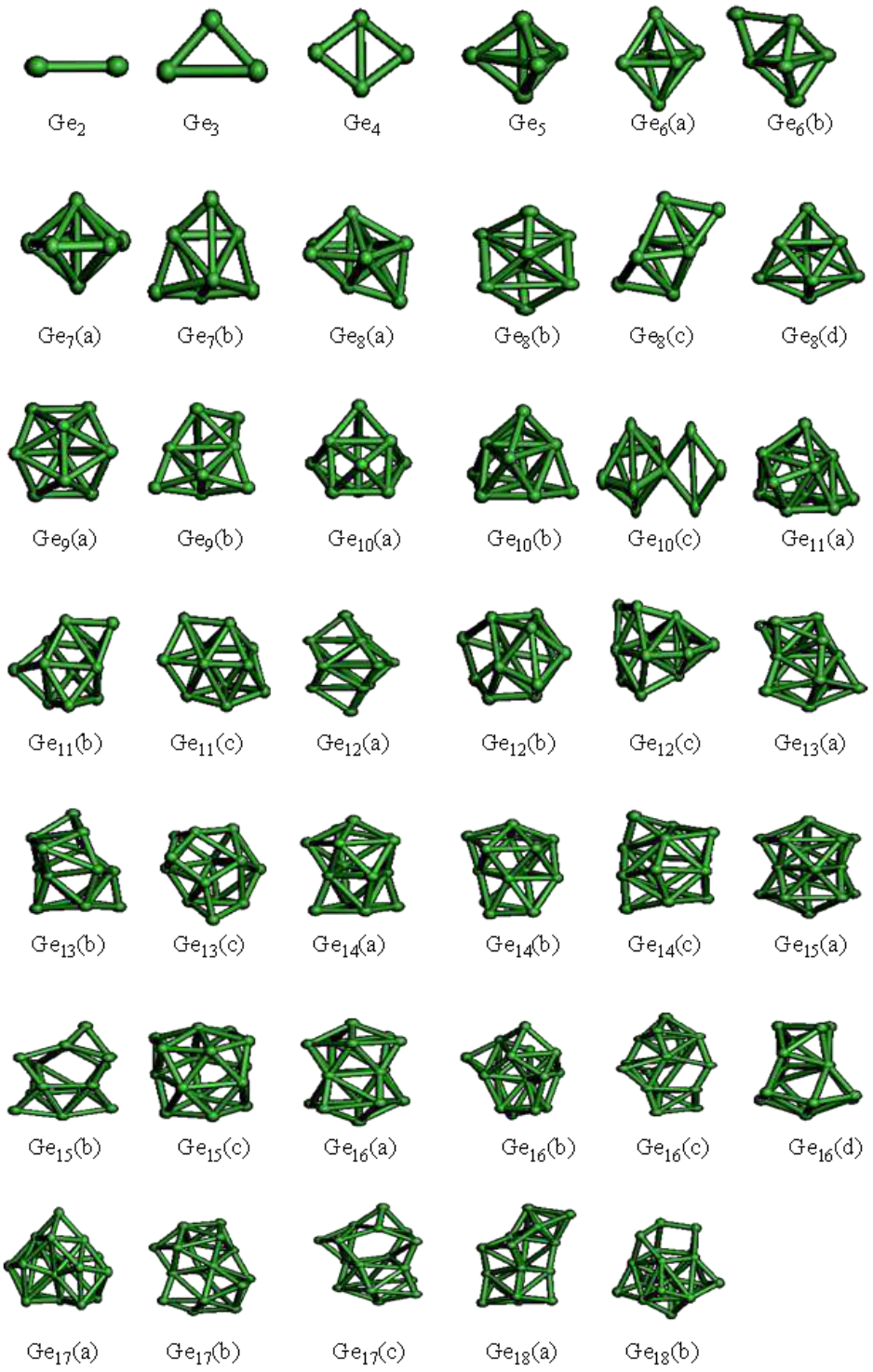

Figure.6 : Ground state structures and their isomers for Ge_{n+1} (n = 1-17) clusters

Table2.: Symmetry group, binding energy per atom E_b (eV/atom), HOMO-LUMO gap ΔE(eV) and average bond length for pure Ge_{n+1} (n=1-17) clusters, the bold character is the parameter of the most stable structure.

Size (n+1)	Symmetry group	E_b (eV/atm)	ΔE (eV)	*a* (Å)
1	**(a) $D_{\infty h}$**	**1.28**	**0.367**	**2.625**
2	**(a) C_{2v}**	**1.86**	**1.368**	**2.476**
3	**(a) D_{2h}**	**2.25**	**1.152**	**2.714**
4	**(a) D_{3h}**	**2.44**	**1.815**	**2.668**
5	**(a) C_{2v}**	**2.55**	**1.650**	**2.823**
	(b) C_s	2.49	1.321	2.811
6	**(a) D_{5h}**	**2.66**	**1.557**	**2.900**
	(b) C_{2v}	2.59	2.111	2.722
7	**(a) C_s**	**2.64**	**1.179**	**2.796**
	(b) C_2	2.61	1.143	2.837
	(c) C_{2h}	2.61	1.153	2.836
8	**(a) C_{2v}**	**2.70**	**1.588**	**3.000**
	(b) C_1	2.64	1.306	2.854
9	**(a) C_{3v}**	**2.80**	**1.609**	**2.857**
	(b) C_s	2.73	1.415	2.854
	(c) C_{2v}	2.60	0.817	2.849
10	**(a) C_s**	**2.76**	**1.148**	**2.857**
	(b) C_1	2.76	1.140	2.857
	(c) C_2	2.73	1.143	2.944
11	**(a) C_{2v}**	**2.76**	**1.536**	**2.884**
	(b) C_1	2.75	1.113	2.940
	(c) C_s	2.71	1.299	2.855
12	**(a) C_1**	**2.77**	**0.982**	**2.943**
	(b) C_2	2.75	1.235	2.836
	(c) C_s	2.75	1.096	2.788
13	**(a) C_s**	**2.83**	**1.372**	**2.867**
	(b) C_1	2.80	1.335	2.888
	(c) C_2	2.76	1.014	2.871
14	**(a) C_{2v}**	**2.82**	**0.864**	**2.925**
	(b) C_1	2.78	1.116	2.768
	(c) C_s	2.77	1.163	2.862
15	**(a) C_{2h}**	**2.83**	**1.164**	**2.893**
	(b) C_1	2.78	0.978	2.852
	(c) C_1	2.77	1.172	2.825
	(d) C_1	2.77	1.138	2.875
16	**(a) C_s**	**2.82**	**0.884**	**2.893**
	(b) C_1	2.82	0.908	2.861
	(c) C_1	2.82	1.116	2.836
17	**(a) C_1**	**2.81**	**1.322**	**2.822**
	(b) C_1	2.79	0.626	2.845

case of $SnGe_3$ cluster, the ground state structure showed a C_{2v} symmetry with Sn–Ge and Ge–Ge bond distance of 2.857 Å and 2.741 Å, respectively. Rhombus structure is also found to be the most stable structure for charged $SnGe_3$ cluster.

The ground state of Ge_5 cluster is a trigonal bipyramid with D_{3h} symmetry and average bond length of 2.668 Å. Our calculations indicate that the $SnGe_4$ cluster has also trigonal bipyramid with C_{2v} structure. Their Ge-Ge bond length increases to 2.665 Å and Sn-Ge bond length is found to be 2.852 Å. This structure is in agreement with Samanta et al[22] results. For the charged cluster, the capped tetrahedron structure is the most stable structure with C_{2v} symmetry. The energy binding of $SnGe_4^+$ is 2.316eV/atom which is smaller than that of $SnGe_4^-$ (2.833eV/atom).

The capped trigonal bipyramid with (C_{2v}) symmetry is obtained for Ge_6 cluster, in agreement with the result of Li et al[76]. For n=5, $SnGe_5$ (a) is the most stable isomer with C_s symmetry. Their corresponding Ge-Ge and Sn-Ge bonds length are 2.850Å and 2.911Å, respectively. The same form is obtained by Wang and Han[186]. The capped trigonal bipyramid configuration with C_{2v} is also stable for $SnGe_5^+$. However, the anion $SnGe_5^-$ is a distorted octahedron with (C_{2v}) symmetry.

For Ge_7, the pentagonal bipyramid with D_{5h} symmetry and the lowest binding energy of 2.66 eV/atom is suggested. Our results are in good agreement with previous theoretical studies [57, 76, 187]. Three different isomers are found for $SnGe_6$. The most stable one is $SnGe_6$ (a) with C_s symmetry, bond lengths Ge-Ge and Sn-Ge of 2.714Å and 2.927Å, respectively. The pentagonal bipyramid is the most stable structure for $SnGe_6^-$ and $SnGe_6^+$.

For n = 8, the face capped pentagonal bipyramid is obtained for pure Ge_8 cluster with C_s symmetry, binding energy of 2.64 eV/atom and average bond length of 2.796 Å. The same structure is reported by Wang et al [57]. A similar structure as Ge_8 is obtained in the case of $SnGe_7$ and $SnGe_7^{\pm}$ with C_1 symmetry. The Ge-Ge bond length is much larger in the case of $SnGe_7^+$ and $SnGe_7^-$ (2.892 Å and 2.862 Å) clusters compared to the corresponding neutral $SnGe_7$ cluster (2.581 Å).

For Ge_9, the bicapped pentagonal bipyramid Ge_9 (a) with C2v symmetry is the most stable structure with binding energy of 2.70 eV/atom and average bond length Ge-Ge of 3Å. In the corresponding doped cluster, the most stable structure is $SnGe_8$ (a) with Cs symmetry. Its Ge-Ge and Sn-Ge average distances are 2.939 Å and 3.062 Å, respectively. The same structure

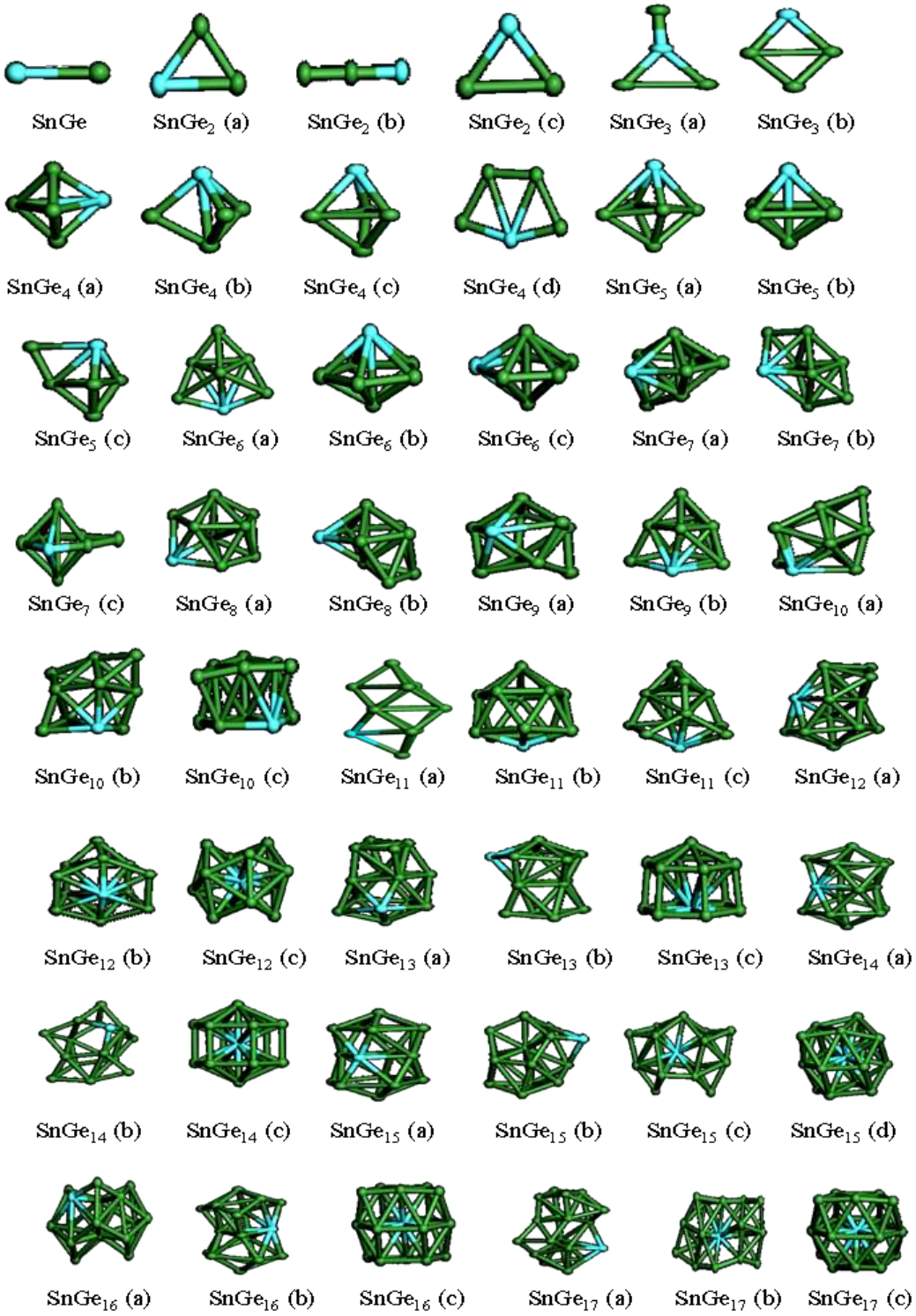

Figure.7 :Ground state structures and their corresponding isomers for $SnGe_n$ (n = 1-17) clusters.

and symmetry is found for cationic $SnGe_8^+$. However, the anionic $SnGe_8^-$ cluster presents a different structure with C_1 symmetry.

The lowest energy structure, among the three best structures observed in the case of Ge_{10} cluster, is Ge_{10} (a) with C_{3v} symmetry, which is in good agreement with Wang et al [57] results. In the doped clusters case, the ground state structure is $SnGe_9$ (a) with C_s symmetry. The Sn atom occupies a peripheral position. The averages Ge-Ge and Sn-Ge distances are 2.851 Å and 3.059 Å, respectively. The results indicate that the $SnGe_9^+$ and $SnGe_9^-$ structure are completely different to the neutral $SnGe_9$ structure. The average Ge-Ge distance of cationic cluster 0.353 Å is smaller than that in the neutral $SnGe_9$.

For Ge_{11}, the most stable structure is Ge_{11} (a) with C_s symmetry. Substituting Ge by Sn leads to a somewhat similar structure. The ground state structure of $SnGe_{10}$ (a) is given in Figure7 with C_s symmetry. Its calculated binding energy is 2.73 eV/atom, while the bond lengths Ge-Ge and Sn-Ge are 2.846 Å and 3.088 Å, respectively.

We observe that the obtained results suggest that the majority lowest energies clusters of germanium pure are layered structure beginning n = 12. In Figure.6 , we show that the ground state structure of Ge_{12} has stacked structure with C_{2v} symmetry. Substituting Ge by Sn doesn't perturb significantly the structure because the structure of $SnGe_{11}$ is very similar to that of Ge_{12}. The binding energy of $SnGe_{11}$ is only 0.02eV/atom, which is less than that of Ge_{12}. The stacked structure is also stable for $SnGe_{11}^+$ specie with C_1 symmetry. The layered structure has found also for Ge_{13}. It consists in a triangle Ge_3 and bicapped square antiprism Ge_{10}, in 1-5-4-3 layers. Similar layered structure Ge_{14} (a) is obtained for Ge_{14} with 1-5-4-4 layered. In this case, the Ge_3 unit of the best isomer Ge_{13} is replaced by a rhombus Ge_4.

The lowest energy structures of Ge_{15}, Ge_{16}, and Ge_{17} are stacked structures with 1-5-3-5-1, 1-5-4-5-1 and 1-5-5-5-1 layers, respectively. These layered structures have also been found by Wang et al[57]. Two isomers with spherical configuration and one Ge core atom are found for Ge_{16} and Ge_{18}, as shown in Figure.6 . The most stable structure Ge_{18} (a) of Ge_{18} consists in three connected pentagonal parties Ge_7, dimer Ge_2 and capped tetragonal prism Ge_9 but this isomer is not a layered structure.

In all the $SnGe_n$ isomers clusters, with $n < 12$ size, the Sn atom occupies a peripheral position. In $n > 12$ case, the Sn atom can occupy a core position. For example in $SnGe_{12}$, Sn occupies a peripheral position in $SnGe_{12}$ (a) structure and occupies a core position in $SnGe_{12}$ (b) and $SnGe_{12}$ (c) structures. Compared to other isomers, $SnGe_{12}$ (a) structure has the highest

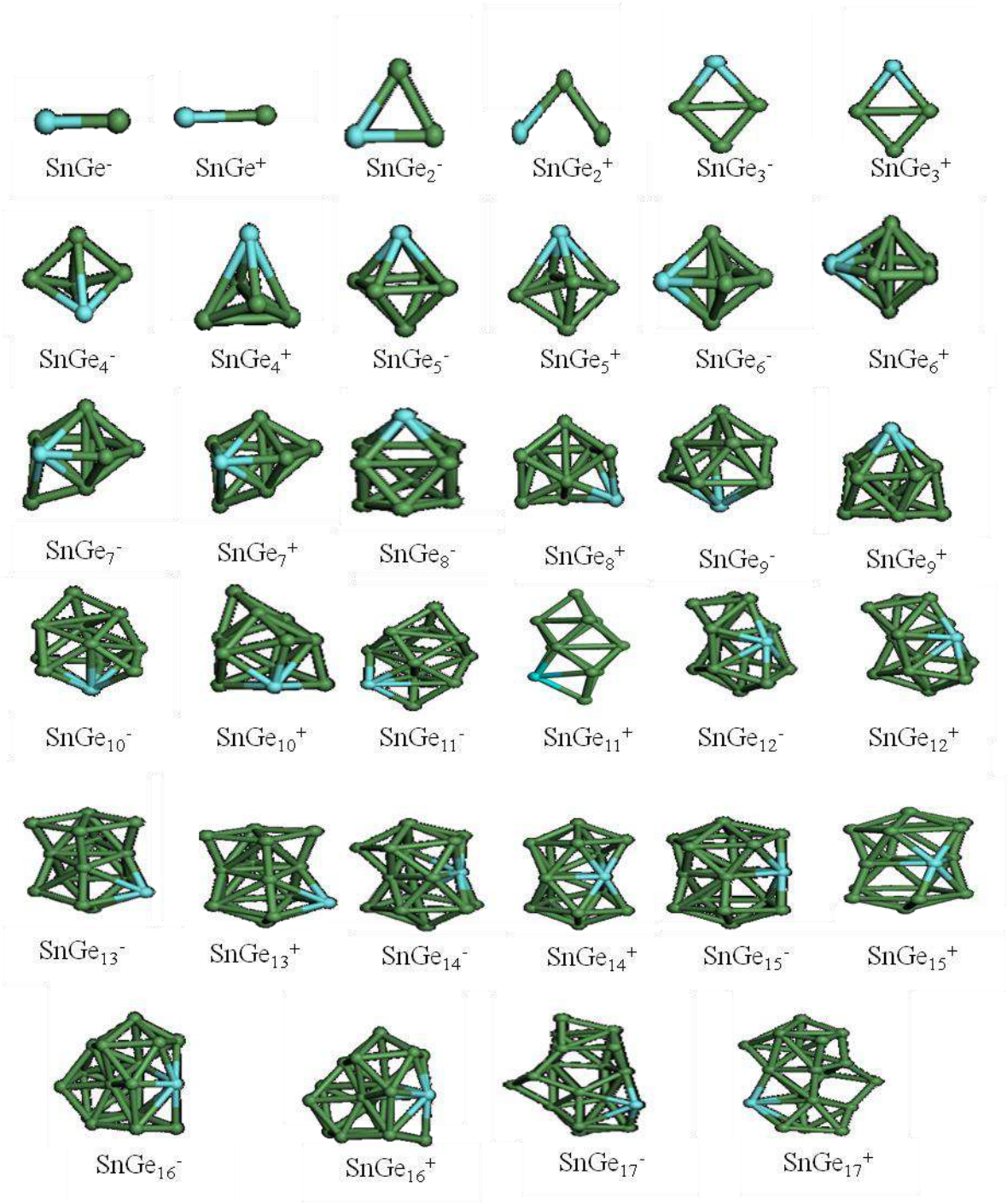

Figure.8:. Ground state structures of cationic and anionic $SnGe_n^{(\pm1)}$ (n = 1-17) clusters

stability. For charged $SnGe_{12}^{\pm}$, we obtained the same structures with the same symmetry C_1 and Sn-Ge bond length for cation and anion clusters of 3.078 Å and 3.029 Å, respectively. Two stacked structures (a) and (b) and hexagonal prism (c) are optimized for $SnGe_{13}$. The calculated results show that the $SnGe_{13}$ (a) isomer is the most stable geometry and have the same form with pure germanium Ge_{14}. The stacked structure is also stable for $SnGe_{13}^{\pm}$. $SnGe_{14}$ (a) structure, where the Sn atom is located at the surface, is similar to Ge_{15} structure. Two other isomers (b) and (c), with Sn atom at the center of thestructure, are also found for $SnGe_{14}$. The same structure with C_s symmetry, have been obtained for $SnGe_{14}^{+}$ and $SnGe_{14}^{-}$. $SnGe_{15}$ cluster have four stable structures.

The most stable one is the $SnGe_{15}$ (a) with C_s symmetry, which is obtained by substitution of Ge atom by Sn atom in the Ge_{16} cluster. The other isomers $SnGe_{15}$ (b, c, d) have spherical structures with Sn atom in surface for (b) and in a core position for (c, d). The $SnGe_{15}$ (a) structure is conserved for the cationic $SnGe_{15}^{+}$ cluster.

$SnGe_{16}$ and $SnGe_{16}^{\pm}$ have the same stable structure Ge_{17} (a) with C_1 symmetry, $SnGe_{16}$ has two other isomers. Three $SnGe_{17}$ isomers are shown in Figure7. The $SnGe_{17}$ (a) isomer has the same form of Ge_{18} and it is the most stable structure. The $SnGe_{17}$ (b) cluster is similar spherical structure and $SnGe_{17}$ (c) cluster is spherical structure, Sn atom is located in the centre position in both structures. The same structure as $SnGe_{17}$ (a) is found for cationic $SnGe_{17}^{+}$ with C_1 symmetry. Different forms of anionic $SnGe_{17}^{-}$ cluster are obtained.

3.2.2. Electronic properties

3.2.2.1. Binding energy

In order to explore the relative stability of different species, we calculate the binding energy per atom for the Ge_{n+1} and $SnGe_n^{(0\pm1)}$ (n = 1-17) clusters. The binding energy per atom ($E_{b/atom}$) is considered, in cluster science, as a sensitive quantity that reflects the relative stability. The different values of $E_{b/atom}$ for the lowest energy structures are calculated as:

$$E_b(Ge_{n+1}) = ((n+1)E(Ge)-E(Ge_{n+1}))/(n+1) \quad 3.1$$

$$E_b(SnGe_n) = (nE(Ge) + E(Sn) - E(SnGe_n))/(n+1) \quad 3.2$$

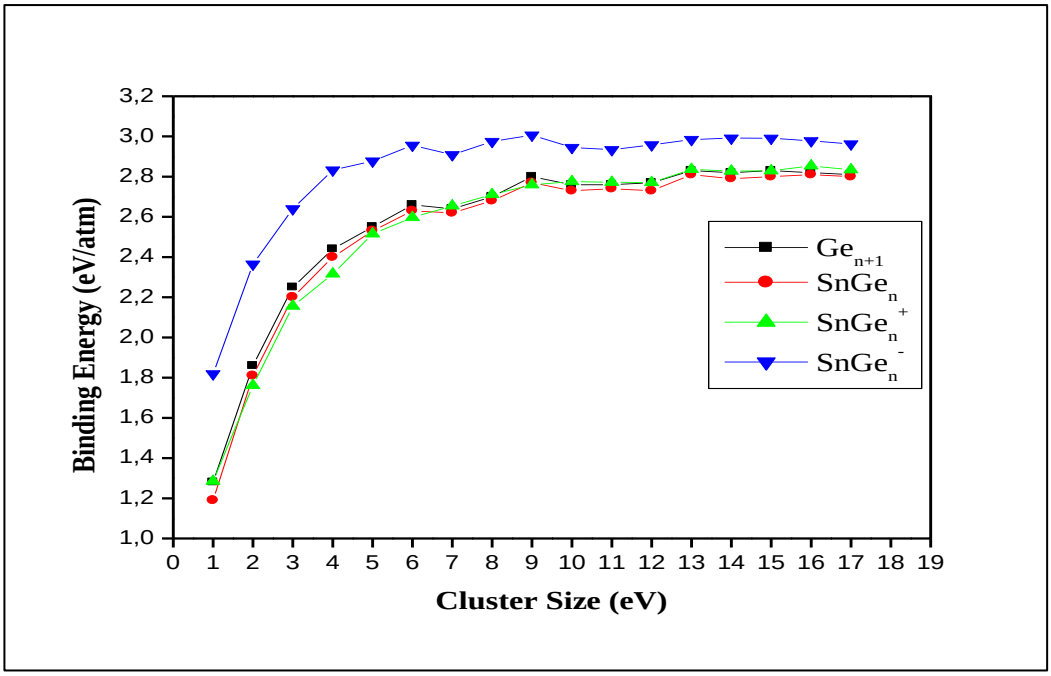

Figure.9: Size dependence of the binding energies of Ge_{n+1} and $SnGe_n^{(0,\pm1)}$ (n=1-17) clusters.

$$E_b(SnGe_n^{-1}) = ((n-1)E(Ge) + E(Sn) + E(Ge^{-1}) - E(SnGe_n^{-1}))/(n+1) \quad 3.3$$

$$E_b(SnGe_n^{+1}) = (nE(Ge) + E(Sn^{+1}) - E(SnGe_n^{+1}))/(n+1) \quad 3.4$$

where E(Ge)$E(Ge)$, E(Sn), E(Ge^{-1})$E(Ge)$ and E(Sn^{+1}) are the total energy of free Ge, Sn, Ge^- and Sn^+ atoms, respectively. E(Ge_{n+1})$E(Ge_{n+1})$ is the total energy of Ge_{n+1}, E($SnGe_n$)$E(SnGe_n)$ is the total energy of $SnGe_n$ and E($SnGe_n^{\pm}$)$E(SnGe_n^{\pm})$ is the total energy cationic and anionic $SnGe_n^{\pm}$ clusters. The obtained results of binding energies per atom for pure Ge and neutral and charged tin doped germanium clusters are given in Table2, Table 3 and Table.5, respectively and their variations versus the cluster size are plotted in Figure9. For all species, the binding energy per atom increases with the cluster size. This behavior implies that the cluster stability is enhanced whenever the cluster size increased. The graphs show a thermodynamic instability of smaller clusters. In the case of $SnGe_n$ clusters, the binding energy per atom increases significant increasing in the average binding energies of the clusters of small size rang (n < 9), which is due to the rapidly from 1.19eV/atom in SnGe cluster to 2.77eV/atom in $SnGe_9$. For clusters of size n > 9, we can see a slow increasing in E_b to reach the saturation plateau at 2.8eV/atom. From Figure9, we also observe that there is a

high competition in the evolution of the binding energies between $SnGe_n$ and its corresponding Ge_{n+1} cluster. This means that the Sn atoms haven't an immediate and direct effect on the relative stability of pure germanium clusters. The anionic clusters exhibit a high stabilities compared to the others cationic and neutral ones. Local peaks are observed in the curve of binding energies of Ge_{n+1} and $SnGe_n$ for n=6, n=9 and n=13. This means that the corresponding clusters are more stable than their neighbors.

3.2.2.2. Fragmentation energy

In the other hand, we calculated the fragmentation energy which is considered as a good criterion for predicting the relative stability of the clusters for spontaneous fragmentation. In this works, the size dependence of the fragmentation energies (E_f) for Ge_{n+1} and $SnGe_n^{(0,\pm1)}$ clusters are studied. The fragmentation energy values for different clusters can be calculated by using the following formulas:

$$E_f(Ge_{n+1}) = E(Ge_n) + E(Ge) - E(Ge_{n+1}) \quad (3.5)$$

$$E_f(SnGe_n^{(0\pm1)}) = E(SnGe_{n-1}^{(0\pm1)}) + E(Ge) - E(SnGe_n^{(0\pm1)}) \quad (3.6)$$

Where E(Ge)$E(Ge)$, $E(Ge_{n+1})$ $E(Ge_{n+1})$ and $E(SnGe_n^{(0\pm1)})$ $E\left(SnGe_n^{(0\pm1)}\right)$ are the total energy of free Ge atom, Ge_{n+1} cluster and $SnGe_n^{(0\pm1)}$ cluster respectively.

Based on the above formulas, the calculated fragmentation energy values and their evolution with the cluster size are shown in Figure10. We observe that there are oscillating behaviors with an odd-even decreasing tendency in the evolution of fragmentation energy for all the species. Two parts can be distinguished for Ge_{n+1} and $SnGe_n$ clusters. For n<9, the clusters with n even values are more stable than n odd values. However, for n>9, the clusters with n odd values are more stable than n even values. This confirms that the size n=9 is the stability transition size of these two species.

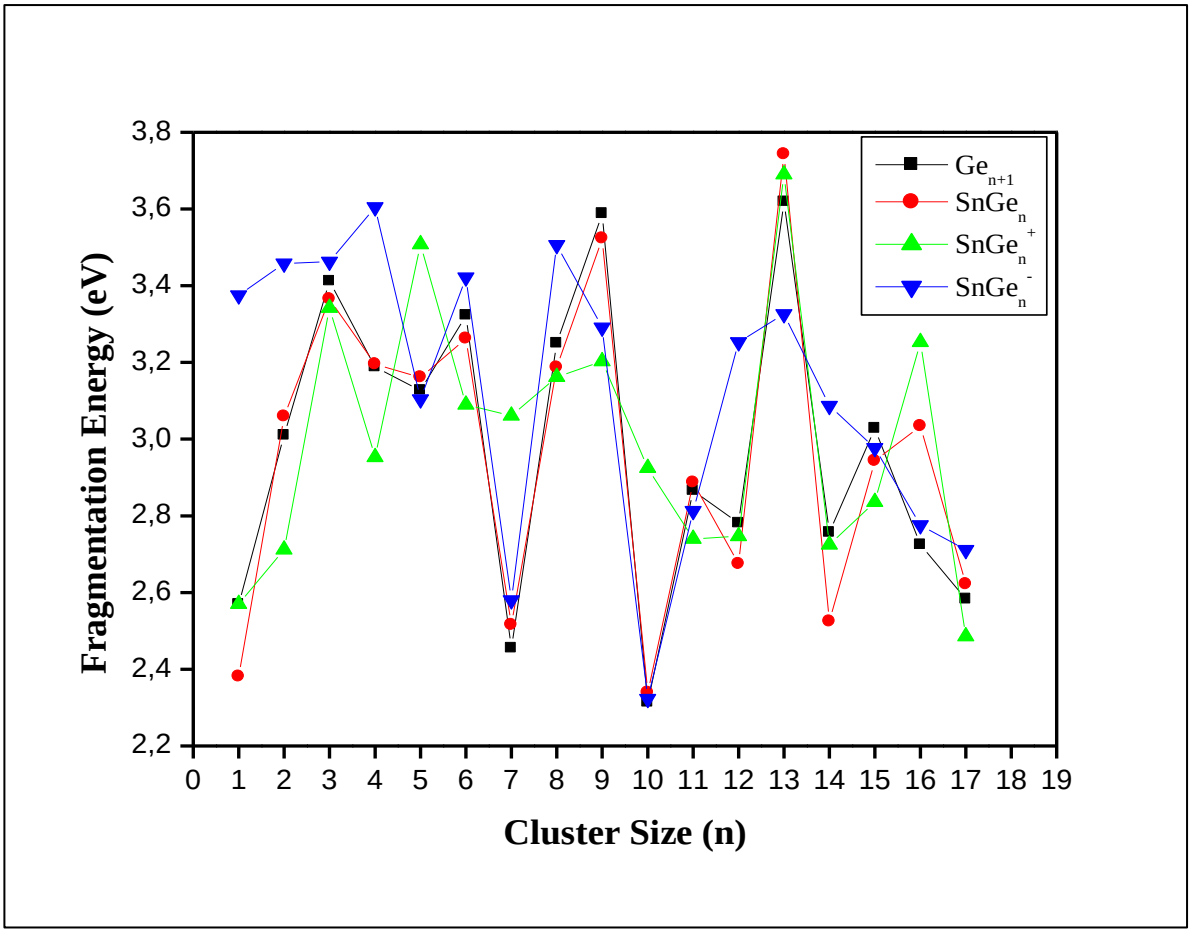

Figure.10: Size dependence of the fragmentation energy of Ge_{n+1} and $SnGe_n^{(0,\pm1)}$ (n=1-17) clusters.

Local maxima of the fragmentation energy of Ge_{n+1}, $SnGe_n$, $SnGe_n^+$ and $SnGe_n^-$ clusters appear at $Ge_{4,10,14}$, $SnGe_{3,9,13,16}$, $SnGe^+_{3,5,13,16}$ and $SnGe^-_{4,6,8,13}$, respectively, which indicates that these clusters are more stable than their neighbors.

3.2.2.3. Second difference energy

In order to analyze the relative stability of Ge_{n+1} and $SnGe_n^{(0\pm1)}$ clusters, we calculate second order difference of total energy (Δ_2E). For the ground state structures the second difference energies for all species are defined by:

$$\Delta_2E(Ge_{n+1}) = E(Ge_{n+2}) + E(Ge_n) - 2E(Ge_{n+1}) \quad (3.1)$$

$$\Delta_2E(Ge_{n+1}) = E(SnGe_{n+1}^{(0\pm1)}) + E(SnGe_{n-1}^{(0\pm1)}) - 2E(SnGe_n^{(0\pm1)}) \quad (3.2)$$

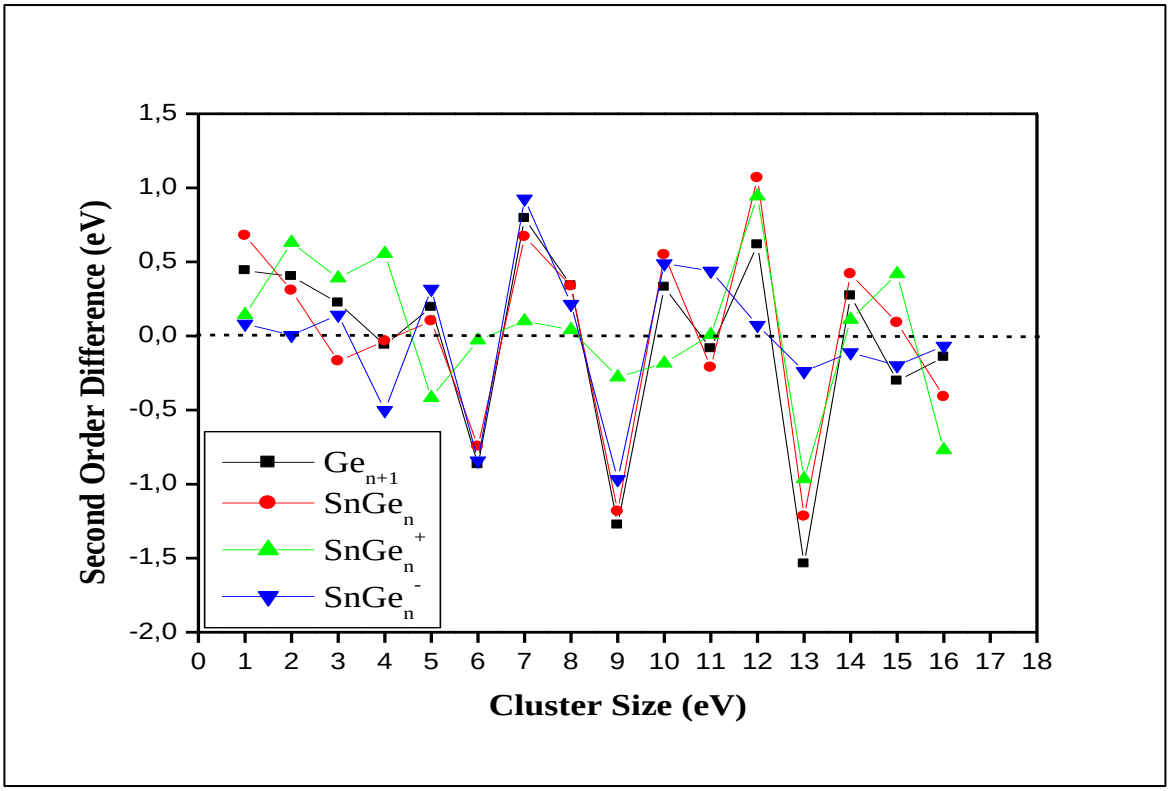

Figure.11: Second energy differences for Ge_{n+1} and $SnGe_n^{(0,\pm1)}$ (n=1-17) clusters.

where E is the total energy of corresponding cluster. It is very known in cluster physics that the small systems with positive value of Δ_2E are more stable than the systems with negative value of Δ_2E. The calculated values of Δ_2E and their evolution as function of the n size for Ge_{n+1} and $SnGe_n^{(0\pm1)}$ are shown in Figure11. From the Figure11, the very pronounced peaks are observed at the sizes n = 1,5,7,10,12,14 for pure Ge_{n+1} and $SnGe_n$ clusters, which demonstrate that the clusters corresponding for these sizes are more stable compared to their neighbors for both species. The explanation of this behavior can be given with a direct relationship between the stability of Sn doped germanium and their corresponding pure Ge_{n+1} with the same size. Except for the two size n = 7 and n=10, we observe that the structure $SnGe_n$ clusters kept unchanged after the encapsulation of Sn atom in pure germanium cage. We also observe that the local peaks at sizes n=2,4, 12 and n=7, 10, 11 for $SnGe_n^+$ and $SnGe_n^-$ clusters, respectively indicating that the corresponding clusters have a higher relative stability compared to neighboring clusters.

3.2.2.4. HOMO-LUMO gap

In order to understand the chemical reactivity and kinetic stability of the clusters, we calculate the energy differences between the highest occupied and lowest unoccupied molecular orbital (HOMO-LUMO) of the Ge_{n+1} and $SnGe_n^{(0,\pm1)}$ clusters. In Figure12, we show the evolution of the HOMO-LUMO gaps as a function of the size for the ground states of different species studied in this thesis. We observe a high oscillation of HOMO-LUMO gaps values for the very small size clusters (n<4). From n = 4 this behavior decreases when the size increases. Many local maxima are observed at n = 2, 4, 8, 9, 11, 13, 15, 17 for both pure and doped germanium clusters, which indicates that these clusters are less reactive than their neighbors and have high chemical stability. The HOMO-LUMO gap of $SnGe_3$ is lower than that of Ge4, which indicates that the doping Sn atom enhance the chemical activity of the cluster. We note that the cluster of tin doped germanium at n = 6 have a large value of HOMO-LUMO gap, which indicates that SnGe6 is the most chemically stable structure and can be used as the building blocks in many new nanomaterials with specific properties. The ionization of $SnGe_n$ leads to a considerable reduction of the HOMO-LUMO gaps compared to the case of neutral clusters.

This indicates that the chemical activity of charged $SnGe_n^{\pm}$ clusters is higher than that of neutral $SnGe_n$ clusters. Moreover, the clusters of Ge_2, $SnGe_{1,3}$ and $SnGe^{-}_{12,13,16,17}$ have small values of HOMO-LUMO gaps, which indicates that they have partially metallic character.

3.2.2.5. Ionization potential and electron affinity

In cluster physics, the ionization potential and electron affinity are considered as suitable parameters to determine the stability of clusters and reflecting the variation of the electronic structure with the size. In order to determine the required energies to add or remove an electron from the lowest energy structures of neutral $SnGe_n$ clusters, we have calculated the adiabatic electron affinity (AEA) and adiabatic ionization potential (AIP),taking in the account the structural relaxation. The vertical ionization potential (VIP) and vertical electron affinity (VEA) are respectively the energy required to remove or add an electron on the neutral clusters without structural relaxation.

The ionization potential (IP) is an important character in understanding electronic properties of clusters and giving more information about clusters metallic character. From Figure13 (a), we can see that VIP and AIP values decrease as the cluster size the increase. It is well known that when the IP is small, the cluster will be more close to a metallic character.

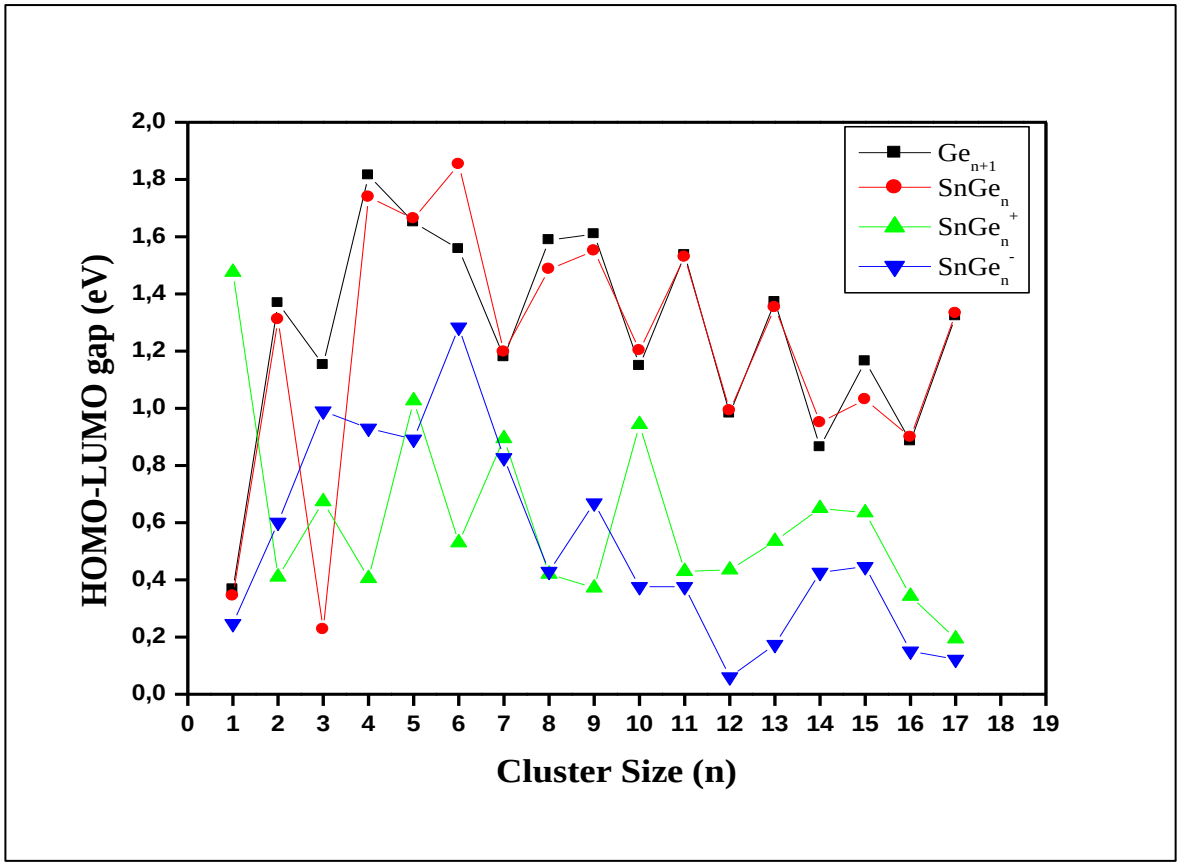

Figure.12: Size dependence of the HOMO-LUMO gaps of Ge_{n+1} and $SnGe_n^{(0,\pm1)}$ (n=1-17) clusters.

This means that the clusters of $SnGe_n$ with size more than 9 atoms exhibit a high metallic character. The smallest VIP and AIP values are observed in $SnGe_{14,16}$ clusters, indicating that these clusters are more readily ionized than the others. The highest value of $SnGe_4$ VIP can be explained by its related symmetry.

The calculated AEA and VEA of $SnGe_n$ clusters are presented in Figure13 (b). We can see that the electron affinity increases whenever the cluster size increases. Consequently, the $SnGe_n$ clusters with large sizes will liberate more energy when they capture one electron. We also observe some maximal local peaks in this graph at n = 8, 12, 14 for AEA and n = 7, 9, 15 for VEA, which means that these clusters are energetically less stable than their neighbors.

3.2.2.6. Chemical hardness

On the other hand, the chemical hardness (η) of cluster can be examined in order to understand its chemical stability. A large values of η indicates that corresponding clusters are

less reactive [188, 189]. For the ground state structures, the chemical hardness is evaluated by using the following formula:

$$\eta = VIP - VEA \qquad 3.3$$

The obtained results for the most stable structures of $SnGe_n$ clusters are listed in Table 3 and plotted in the Figure13 (c) as a function of the size n. We observe that the chemical hardness of $SnGe_n$ clusters decreases when the size increases. This means that clusters with small size are less reactive and more stable than clusters with large size. We can also see from graph that the $SnGe_4$ cluster has the highest chemical hardness value, which indicates that this cluster is more stable than its neighbors. In addition, other local peaks at n = 2, 6 and 8 for $SnGe_n$ are less reactive than the other clusters.

3.2.3. Magnetic properties

One of the most important properties which make a special characteristic of these small clusters is their magnetic behavior. Indeed, we can observe very small clusters with very specific magnetic response which can have many important applications in nanotechnologies. In our case, the magnetic properties are evaluated by the assessment of the total spin magnetic moment for each cluster size. It is defined as the difference between the total Mullikan charge populations for electrons with spin up and electrons with spin down. The calculated total spin magnetic moment values of $SnGe_n$ clusters are reported in Table 3 . We observe that all the ground states of $SnGe_n$ clusters are generally nonmagnetic structures, except the case of $SnGe_1$ which have a total spin magnetic moment of 2 μ_b. In order to explore this specific case we plot the total and the partial densities of states for $SnGe_1$ cluster (DOS and PDOS) (Figure 14). We observe, from the figure, that the total spin magnetic moment in SnGe monomer is mainly due to the 4p and 5p orbital of Ge and Sn atoms, respectively. In the case of the anionic and cationic $SnGe_n$ clusters, the obtained total spin magnetic moments have been reported in Table.5. We observe that their total spin magnetic moments of ionized structures are different compared to those obtained in neutral structures and they are generally equal to 1 μ_b. This means that the charge of the systems can affect the magnetic response of the tin doped germanium clusters.

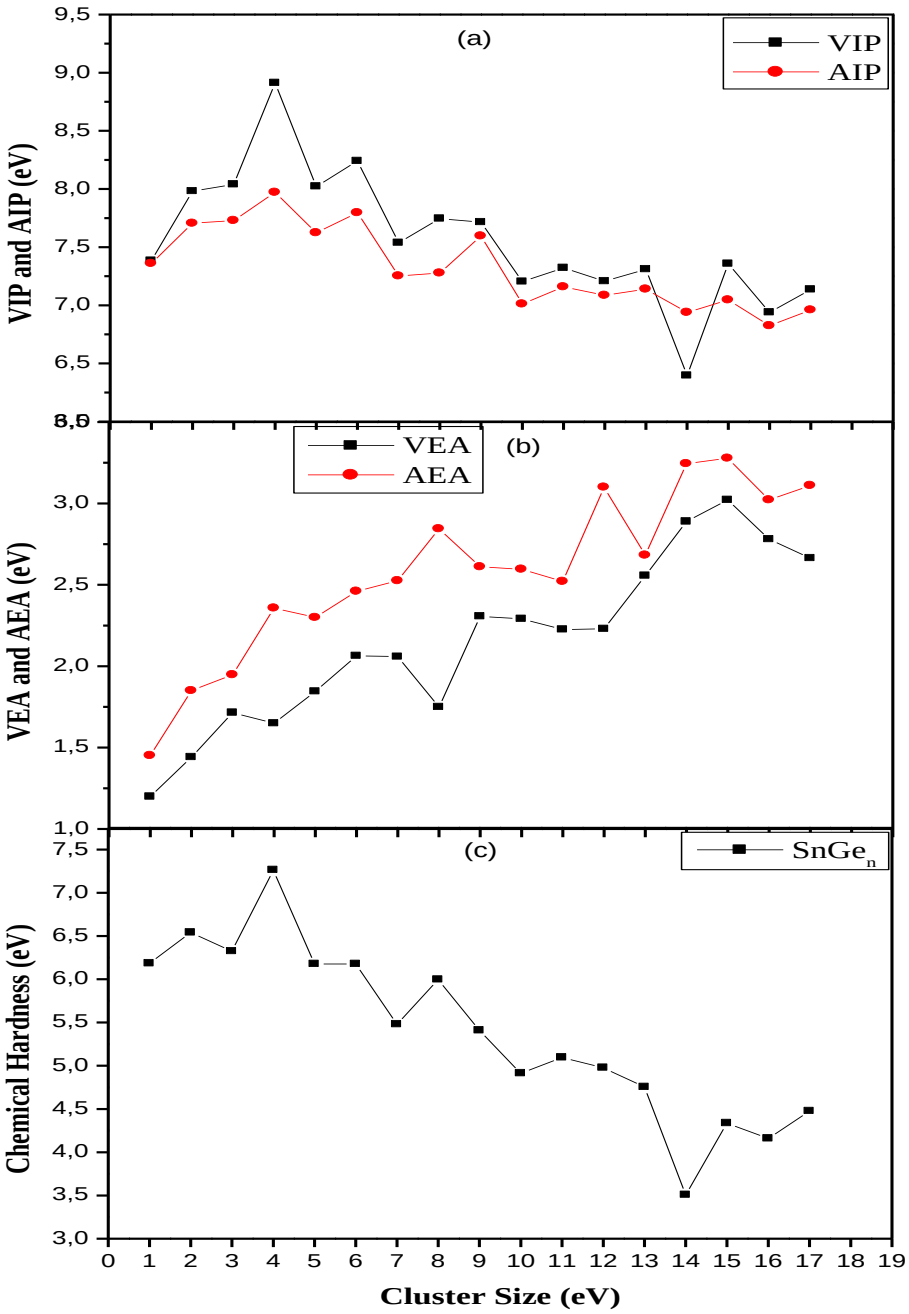

Figure.13: (a) Vartical (VIP) and adiabatic (AIP) ionization potential; (b) Vartical (VEA) and adiabatic (AEA) electron affinity, (c) chemical hardness for $SnGe_n$ (n=1-17) clusters.

Table .3 : Symmetry group, binding energy per atom E_b (eV/atom), HOMO-LUMO gap ΔE(eV), Vertical Electronic Affinity (VEA) (eV), Vertical Ionisation Potential (VIP) (eV), Chemical Hardness η (eV) and total spin magnetic moments μ (μ_B) for $SnGe_n$ (n=1-17) clusters.

Size (n)	Symmetry group	E_b(eV/atom)	ΔE(eV)	VEA(eV)	VIP(eV)	η (eV)	μ (μ_b)
1	**(a) $C_{\infty v}$**	**1.19**	**0.344**	**1.199**	**7.383**	**6.184**	**2.000**
2	**(a) C_s**	**1.81**	**1.311**	**1.441**	**7.982**	**6.541**	**0.000**
	(b) $C_{\infty v}$	1.71	1.643	1.264	8.719	7.455	0.000
	(c) C_{2v}	1.80	0.984	1.702	7.936	6.234	0.000
3	**(a) C_{2v}**	**2.20**	**0.227**	**1.715**	**8.039**	**6.324**	**0.000**
	(b) C_{2v}	1.79	1.132	2.386	7.072	4.686	0.000
4	**(a) C_{2v}**	**2.40**	**1.739**	**1.649**	**8.912**	**7.263**	**0.000**
	(b) C_{3v}	2.35	1.556	1.255	8.447	7.192	0.000
	(c) C_s	2.19	0.499	2.687	7.367	4.680	2.000
	(d) C_{2v}	2.14	0.889	2.959	6.840	3.881	2.000
5	**(a) C_s**	**2.53**	**1.663**	**1.845**	**8.022**	**6.177**	**0.000**
	(b) C_s	2.48	1.450	2.056	7.798	8.742	0.000
	(c) C_s	2.44	1.228	1.873	7.786	5.913	0.000
6	**(a) C_1**	**2.63**	**1.853**	**2.064**	**8.241**	**6.177**	**0.000**
	(b) C_1	2.61	1.512	2.357	8.153	5.796	0.000
	(c) C_{2v}	2.53	1.451	1.590	7.856	6.266	0.000
7	**(a) C_1**	**2.62**	**1.197**	**2.059**	**7.538**	**5.479**	**0.000**
	(b) C_1	2.59	1.149	2.076	7.416	5.340	0.000
	(c) C_s	2.58	0.947	2.047	7.179	5.132	0.000
8	**(a) C_1**	**2.68**	**1.486**	**1.749**	**7.745**	**5.996**	**0.000**
	(b) C_1	2.68	1.515	1.978	7.425	5.447	0.000
9	**(a) C_s**	**2.77**	**1.551**	**2.306**	**7.714**	**5.408**	**0.000**
	(b) C_1	2.69	1.434	2.197	7.497	5.300	0.000
10	**(a) C_s**	**2.73**	**1.202**	**2.291**	**7.204**	**4.913**	**0.000**
	(b) C_1	2.72	1.031	2.378	7.133	4.755	0.000
	(c) C_1	2.71	1.121	2.511	7.324	4.813	0.000
11	**(a) C_1**	**2.74**	**1.529**	**2.225**	**7.321**	**5.096**	**0.000**
	(b) C_{5v}	2.70	1.155	2.583	7.388	4.805	0.000
	(c) C_s	2.67	1.104	2.667	7.359	4.692	0.000
	(d) C_1	2.64	1.027	3.628	6.242	2.614	0.000
12	**(a) C_1**	**2.73**	**0.992**	**2.230**	**7.207**	**4.977**	**0.000**
	(b) C_{2v}	2.70	1.014	2.822	7.421	4.599	0.000
	(c) D_{3d}	2.62	1.046	2.754	6.804	4.050	0.000
13	**(a) C_1**	**2.81**	**1.353**	**2.556**	**7.310**	**4.754**	**0.000**
	(b) C_1	2.78	1.310	2.585	7.329	4.744	0.000
	(c) C_1	2.60	0.554	2.913	6.951	4.038	0.000
	(d) C_{6v}	2.72	0.517	3.115	7.122	4.007	0.000
14	**(a) C_s**	**2.79**	**0.950**	**2.889**	**6.396**	**3.507**	**0.000**
	(b) C_1	2.75	1.078	2.721	7.125	4.404	0.000
	(c) D_{6h}	2.58	0.010	2.916	6.358	3.442	0.002
	(d) C_1	2.73	1.097	2.690	7.070	4.380	0.000
15	**(a) C_2**	**2.80**	**1.031**	**3.022**	**7.357**	**4.335**	**0.000**
	(b) C_1	2.77	0.997	2.758	7.026	4.268	0.000
	(c) C_s	2.69	0.591	2.975	6.816	3.841	0.000
	(d) C_{2v}	2.64	0.520	2.758	6.424	3.666	0.000
16	**(a) C_1**	**2.81**	**0.899**	**2.780**	**6.939**	**4.159**	**0.000**
	(b) C_1	2.80	0.994	2.953	7.069	4.116	0.000
	(c) C_{2h}	2.74	0.537	2.571	6.348	3.777	0.000
17	**(a) C_1**	**2.80**	**1.332**	**2.664**	**7.136**	**4.472**	**0.000**
	(b) C_s	2.71	1.018	2.747	6.863	4.116	0.000
	(c) C_{2v}	2.69	1.015	2.219	6.826	4.607	0.000

Table.4: **Average bond length a_{Ge-Ge} and a_{Sn-Ge} for neutral, cationic and anionic $SnGe_n^{(0\pm1)}$ (n = 1-17) clusters.**

Cluster size (n)	$SnGe_n$		$SnGe_n^+$		$SnGe_n^-$	
	a_{Ge-Ge} (Å)	a_{Sn-Ge} (Å)	a_{Ge-Ge} (Å)	a_{Sn-Ge} (Å)	a_{Ge-Ge} (Å)	a_{Sn-Ge} (Å)
1	/	2.805	/	2.910	/	2.495
2	2.472	2.658	2.626	2.833	2.551	2.900
3	2.741	2.857	2.656	2.884	2.689	2.844
4	2.665	2.852	2.691	3.026	2.683	2.861
5	2.850	2.911	2.867	2.974	2.856	3.034
6	2.714	2.927	2.912	3.010	2.452	3.047
7	2.581	3.130	2.892	3.154	2.862	3.042
8	2.939	3.062	2.978	3.107	2.908	2.999
9	2.851	3.059	2.498	3.008	3.022	2.976
10	2.846	3.088	3.033	3.071	2.848	3.002
11	2.866	3.052	2.873	3.086	2.641	2.996
12	2.904	3.059	2.931	3.078	2.901	3.029
13	2.860	3.083	2.787	3.049	2.850	3.057
14	2.980	3.038	2.855	3.054	2.917	2.969
15	2.906	2.907	2.925	2.929	2.882	2.931
16	2.895	3.037	3.081	3.029	2.897	3.021
17	2.865	2.996	2.837	2.986	2.854	3.002

Table.5 : (A) Symmetry group, binding energy per atom E_b (eV/atom), HOMO-LUMO gap ΔE(eV), total spin magnetic moments μ (μ_B), adiabatic Ionisation Potential (AIP) (eV) for cationic $SnGe_n^+$ (n=1-17) clusters.(B) Symmetry group, binding energy per atom E_b (eV/atom), HOMO-LUMO gap ΔE(eV), total spin magnetic moments μ (μ_B), adiabatic electron affinity (AEA) (eV) for anionic $SnGe_n^-$

	(A) $SnGe_n^+$					(B) $SnGe_n^-$				
Cluster size (n)	Symmetry group	E_b (eV/atm)	ΔE (eV)	μ (μ_b)	AIP (eV)	Symmetry group	E_b (eV/atm)	ΔE (eV)	μ (μ_b)	AEA (eV)
1	$C_{\infty v}$	1.285	1.476	3.000	7.360	$C_{\infty v}$	1.819	0.247	1.000	1.451
2	C_s	1.761	0.410	1.000	7.706	C_s	2.365	0.601	1.000	1.850
3	C_{2v}	2.156	0.674	1.000	7.729	C_{2v}	2.640	0.990	1.000	1.948
4	C_{2v}	2.316	0.405	1.000	7.971	C_{2v}	2.833	0.930	1.000	2.357
5	C_{2v}	2.515	1.027	1.000	7.624	C_{2v}	2.878	0.892	1.000	2.300
6	C_{2v}	2.597	0.530	1.000	7.796	C_{2v}	2.956	1.284	0.996	2.460
7	C_1	2.655	0.894	0.999	7.252	C_1	2.909	0.827	1.000	2.525
8	C_1	2.711	0.420	0.998	7.277	C_1	2.975	0.430	0.998	2.844
9	C_s	2.760	0.372	0.997	7.597	C_s	3.007	0.669	0.999	2.611
10	C_1	2.775	0.944	0.997	7.012	C_s	2.945	0.376	0.999	2.596
11	C_1	2.772	0.430	0.992	7.158	C_1	2.934	0.376	0.994	2.521
12	C_1	2.771	0.435	0.995	7.086	C_1	2.958	0.061	0.997	3.100
13	C_1	2.836	0.535	0.992	7.139	C_1	2.985	0.174	0.976	2.682
14	C_s	2.828	0.650	0.999	6.939	C_s	2.992	0.426	0.985	3.244
15	C_2	2.829	0.635	0.994	7.046	C_2	2.991	0.446	0.945	3.278
16	C_1	2.854	0.343	0.991	6.824	C_1	2.978	0.151	0.966	3.022
17	C_1	2.834	0.194	0.969	6.960	C_1	2.963	0.122	0.976	3.110

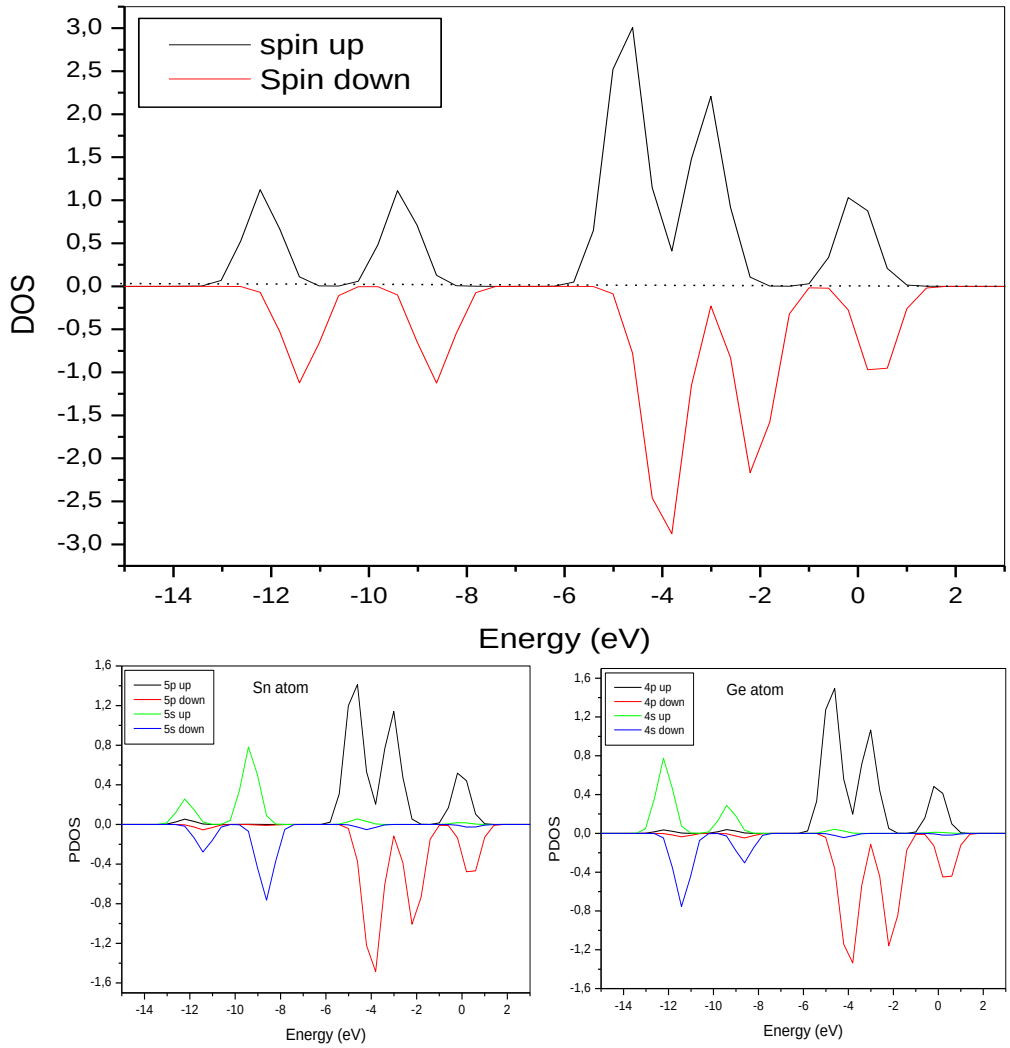

Figure.14 : The total density of states (DOS) for SnGe monomer and the projected density of states (PDOS) for Sn and Ge atoms in SnGe.

4. The Photo-Absorption spectra of $SnGe_n$ (n=1-17) clusters and their optical properties

Introduction

In this chapter we present the calculated optical absorption features of the pure germanium and tin doped germanium clusters. The aim is to understand the roles played by the size of the cluster and the presence of the impurity, Tin atom, on the electronic structure of the germanium clusters and to investigate how these features can be manipulated and engineered by simply handling with the size of the system and with dopo within the system. We employ Time Dependent Density Functional Theory within Local Density Approximation using OCTOPUS package to calculate the absorption spectra for those clusters.

4.1. Method

The initial structures of the clusters used for our calculations have been obtained by SIESTA package (see chapter 3). In this work, the local density approximation was employed to keep consistency with the geometry optimization process. OCTOPUS uses a uniform grid in real space, which is located inside the sum of n spheres, one around each atom of the n-atom cluster. A minimization of energy with respect to the radius and the grid spacing was carried out for all clusters. For optimal energy minimization, we used the radius of each sphere to be 6-8 Å and the grid spacing 0.16-0.18 Å.

We used a real-time TDDFT approach, based on the explicit propagation of the time-dependent Kohn–Sham equations. In this approach, one first excites the system from its ground state by applying a delta electric field. The Kohn–Sham equations are then propagated forward in real time[152], and the time-dependent density n(r,t) readily computed. From this quantity one can then obtain the absorption cross-section as explained in refs. [174], and [190]. In our work, the total propagation time was chosen to be 15 $\hbar$/eV, and the time step 0.001 $\hbar$/eV. This approach has already been used for cluster and molecular systems: metal and semiconducting clusters [191-194], aromatic hydrocarbons [190, 195, 196].

Throughout the calculations the ions were kept static. The approximated enforced time reversal symmetry (aetrs) method was employed in order to approximate the evolution

operator. Numerically the exponential of the Hamiltonian, which is used to approximate the evolution operator, was evaluated using a simple Taylor expansion of the exponential. In order to verify our calculation with experimental data, we chose to compare the absorption spectra of the most stable cluster of GeH_4 with available experimental data as our benchmark.

4.1.1. Benchmark

Before getting the absorption spectra of GeH_4 cluster, we need to calculate the ground state of this cluster and optimized him. For this cluster, we use the bond length 1.5 from ref. [197]. Figure15 shows the structure of GeH_4, the green sphere is the germanium atoms and the weight spheres are Hydrogen atoms. A typical graph of radius optimization is shown in Figure16. The figure corresponds to GeH_4 system and at a value of 3.5 Å the energy reaches a minimum. Once the energy reaches a minimum we can chose any value of the radius parameter. But at the same time it is important to note that choosing a larger radius would considerably increase the computational time. Figure17 shows the value of total energy plotted as a function of the spacing parameter for GeH_4 system with a range on the x axis is 0.10 to 0.22 Å. The spacing parameter of 0.20 Å would be the ideal spacing since the energy change only 0.01 eV.

The study of optical properties depends on transition from the occupied levels to the unoccupied levels. The structures in the photo-absorption spectra are specified by these transitions. Thus, we are interested in calculating these differences in energy and compare them with the energy differences deduced from the experimental spectra, Table6 shows this comparison. We have also included the TDDFT results of G. Nesher et al[128] along with the transitions identification. The uppermost occupied states result from a hybridisation of the germanium and hydrogen states while the lowest unoccupied states are primarily germanium states. Thus the energy gap is dependent on the bonding and anti-bonding germanium states. The transitions between these states have been identified as 5s, 5p, 5d states (these refer to the angular momentum character of the final states). In the absence of experimental data for the Ge clusters sizes studied here, our only point of experimental reference is the optical measurement of Itoh et al[198] for GeH_4. Here, our TDLDA-calculated optical gap value is 8.75 eV, which compares very well to the experimental value of 8.32 eV.

Figure18 shows the photo-absorption spectra obtained for GeH_4 using TDDFT. Here we plot the spectrum for the range from 0 eV to 12 eV, the entire spectrum gives us a better understanding of the optical properties. It can be quite clearly seen from the spectrum that

Time Dependent run give quite accurate answers if the parameters are chosen correctly. The calculated photo-absorption cross-section (using TDDFT) seems to be in good agreement with the TDLDA results of G. Nesher[128].

A similar set of tests were run on all the clusters under consideration and the value of radius and spacing obtained were the same proving the earlier point, that these parameters mainly depend on the pseudo-potentials under consideration. Once the spacing and radius parameters are fixed we calculate the photo-absorption spectra of the clusters using TDDFT metho

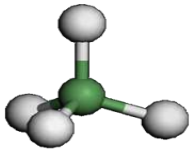

Figure.15 : Ground state structure of GeH_4 cluster.

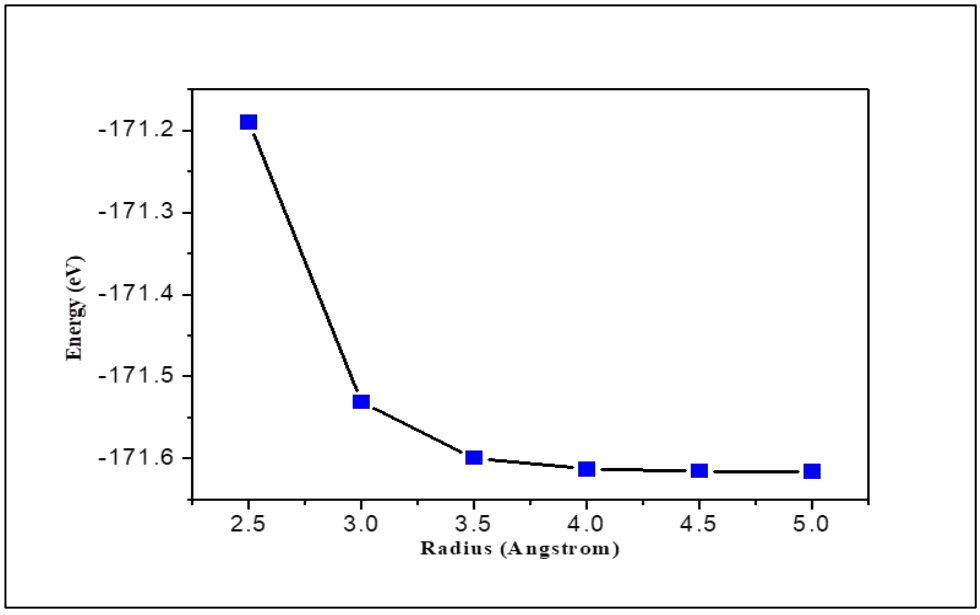

Figure.16: Energy as a function of radius parameter for GeH_4.

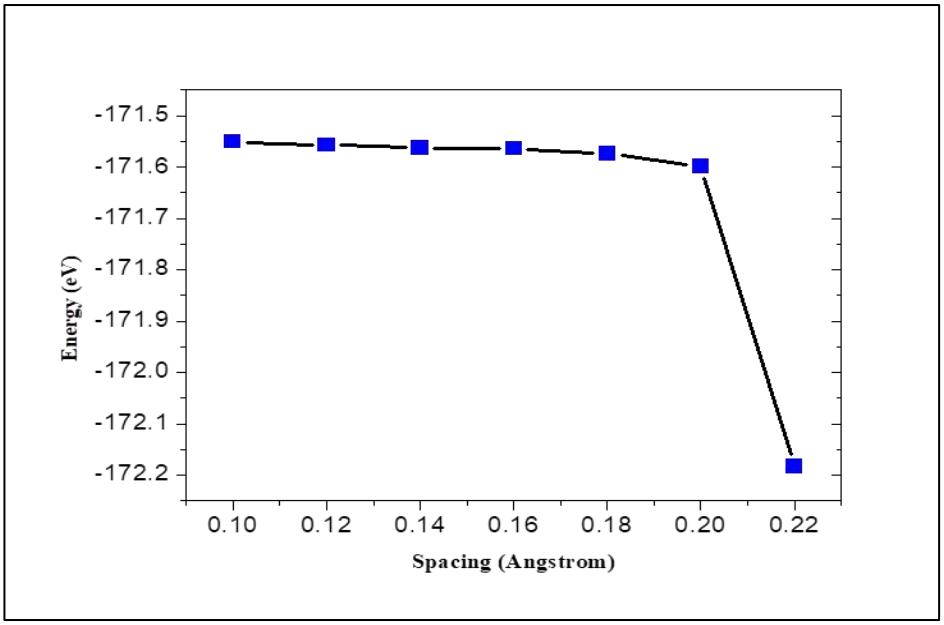

Figure.17: Energy as a function of spacing parameter for GeH_4.

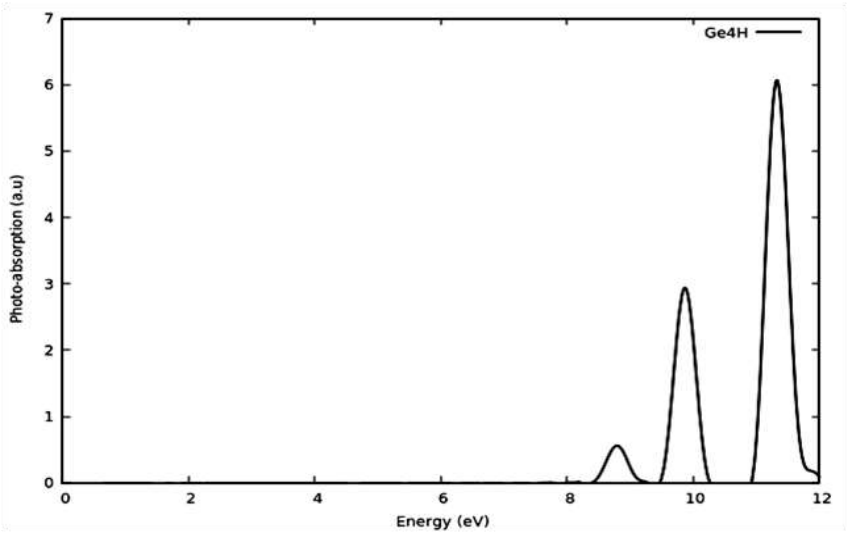

Figure.18: Photo-Absorption spectrum as a function of Energy for GeH_4.

Table6.: Excitation energies in eV for GeH_4 cluster.

Cluster	Transition	Present work	Theory			Experiment[c]
			TDLDA[a]	QMC[b]		
				VMC+CPP	DMC+CPP	
GeH_4	5s	8.75	8.15	10.27	9.48	8.32
	5p	9.83	9.06	10.58	10.11	9.36
	5d	11.31	9.50	/	/	10.39

a [128]

b [199]

c [198, 200, 201]

4.2. Results and Discussion

4.2.1. Optical absorption spectra of Pure germanium clusters

For Ge_n (n=2-18) clusters, the optical absorption spectra essentially depend on the two properties: the size of the clusters and their electronic structure, the calculated optical absorption spectra of Ge_n (n=2-18) clusters in the high energy and infrared-visible light region are plotted in Figure19 and Figure20. From Figures, we can see that the main absorption intensity of Ge_2-Ge_{18} clusters is concentrated in the ultraviolet region, especially in the far ultraviolet region (about 6 ~ 10 eV, i.e. 120 ~ 200 nm).

A general trend for the optical absorption spectra can be found in Figs :(1) An empty gap area exists at the lowest energies, and some minor peaks appear about 1.5-4 eV. (2) Several main peaks appear in the interesting near ultraviolet region of about 5-10 eV. (3) Above near ultraviolet region, high-energy region is of little interest because the TDDFT method is insufficient to describe behavior of the electrons in this region which is dominated by ionization processes[190]. (4) The increase of the numbers of atoms, the sizes of these Germanium clusters grow, and their absorption spectra converted gradually from many peaks to broad absorption bands. It can be also observed that in the low energy region the absorption

spectra of small clusters present much larger oscillator strengths than that of larger clusters. As germanium clusters size continues to increase, their structure motifs are sphere-like or prolate structures (see the chapter 3) and the number of optical absorption peaks decrease. Compared with the small clusters, the absorption peaks are not so sharp. Each peak is extended to both sides, forming an absorption band consisted of multiple peaks. The positions of absorption are also shifted toward the lower energy region. In general, increasing the number of atoms can enhance the absorption intensity because there will be more electronic states available for optical transition. Our results are agreement with Ref [67].

4.2.2. Effect of single Sn atom in pure germanium clusters

To see the effect of adding a single Sn atom to Ge_n clusters, we have also calculated the photo-absorption spectra of $SnGe_n$ clusters which are also shown in Figure21 and Figure22 compared with the germanium clusters results. Each figure shows the calculated photo-absorption cross-section of germanium and Sn doped germanium clusters. A compared with pure germanium, The absorption spectra after Sn doping are characterized by the emergence of a dominant and relatively broad peak between 6 and 10 eV, accompanied by broad absorption peaks also at the same region but smaller intensities . This common feature is coupled to a blue shift of the main peak with increasing cluster size.

For small clusters (up to n=7) we find that the photo-absorption spectra is a combination of many peaks and looks like that of isolated atoms. For example, in the case of clusters with two atoms, we obtained a SnGe monomer with the binding energy equals 1.19eV/atom which is smaller than that of Ge_2 monomer. The spectrum of the SnGe cluster shows marked differences from pure Ge_2. In general, we notice that the absorption of SnGe is concentrated more in blue shift region and his peaks are broader compared to the Ge_2 cluster. We can see also that the number of peaks in the Sn doped Ge cluster is less than pure Ge2 cluster. Let us now focus on the positions of the main peaks. From spectra, the main adsorption peak of Sn-doped Ge cluster is 7.9 eV where is located in high energies region compared to the Ge_2 cluster, and non absorption in spectrum of Ge2 cluster at this energy.

For SnGe2 cluster, the triangular structure is the lowest energy structure Like Ge_3. After an overview of the two spectra of these clusters we can observe that there are clear differences between the two spectra in positions and the oscillator strengths of the peaks. For example at the energy 5.2 eV the absorption spectrum of the SnGe2 cluster has the highest peak while no absorption in this region is shown for the absorption spectrum of a pure germanium cluster.

We can also observe that the addition of the tin in this case resulted in a decrease in both of the values of oscillator strengths and in the number of absorption peaks, this addition also led to the widening of the absorption peaks.

After compared the two photo-absorption spectra of $SnGe_3$ and Ge_4, in general, we notice that the absorption of both two clusters is concentrated in blue shift region and a similarity between the two spectra in the infrared-visible and near the ultraviolet regions (around 6 eV). The addition of one atom of the tin in this case made some peaks appear and others disappear. For example, at energy 6.5 and 9.2 the absorption is almost non-existent for Ge_4 cluster while at the same energy the absorption equal 3.8 and 4.3 a.u. for $SnGe_3$ cluster, respectively. The addition of the tin to the pure germanium clusters not only changed the positions of the peaks, but also reduced the intensity of oscillator strength.

In the case of a cluster of five atoms, the trigonal bipyramid structure is ground state for each two Ge_5 and $SnGe_4$ clusters with differences symmetries D_{3h} and C_{2v} respectively. The photo-absorption spectra of each cluster were presented in fig. Broadly, we can observe similarity between two spectra in all energy regions and that is due to the same structure, only some of the differences we will touch it now. The first difference that we can note him is the energy displacement towards the infrared energy region after adding the tin. We can note also increase in the intensity of oscillator strength, these differences can be explained by different symmetry of two structures. Like pure Ge_5 cluster the shape of the spectrum of $SnGe_4$ cluster changes compared to the other clusters from many peaks to broad absorption bands, this band started from 6 eV to 10 eV. The calculated positions of the absorption peaks for $SnGe_4$ show two intense transitions at 6.50 and 9.50 eV and smaller ones at 3.50, 4.2, 5.5, 7.2, 7.8 and 8.40 eV.

The ground state structure of $SnGe_5$ cluster is more stable compared to pure Ge_6 cluster. We produced the absorption spectrum for the minimum energy structure of $SnGe_5$ obtained in these calculations was presented in fig. Through the figure we can observe that both spectra have the same shape in the infrared and visible regions. From 5.2 eV the shape of the spectra changes this is due to the effect of adding tin to pure germanium. From figure, we can see that some peaks appear and others disappear for example at energy 6.5 eV the absorption is almost non-existent for Ge_6 cluster while at the same energy the absorption equal 3 a.u. for $SnGe_3$ cluster. We can also see a significant increase in the intensity of oscillator strength exactly at 9.8 eV. In contrast, the opposite occurs in other energies for example at 9 eV.

From the optical spectra cross-section of $SnGe_6$ and Ge_7 clusters, in general, we can observe similarity between two spectra along the axis of energy, only some of the differences in positions and the oscillator strengths of the some peaks. Also we can observe and clearly that the absorption of the two spectra are concentrated in blue shift energy. The absorption band of the $SnGe_6$ cluster is broader than in the case of Ge_7 cluster. The calculated positions of the absorption peaks for $SnGe_6$ show three intense transitions at 5.50, 6.28 and 9 eV and smaller ones at 5, 4.2, 7.5, 8.2 and 9.7 eV. From spectra, we can see that some peaks appear and others disappear for example at energy 5.5 eV the absorption is almost non-existent for Ge_7 cluster while at the same energy the absorption equal 8 a.u. for $SnGe_3$ cluster this also happened in 6.28 and 7.5 eV. We can also see a reduction in the intensity of oscillator strength exactly at 7 and 10 eV.

In the case of $SnGe_7$, in general, adding tin to the pure germanium cluster in this case did not make much difference only some of the differences in positions and the oscillator strengths of the some peaks. The absorption in both spectra is characterized by broad absorption range carries intense peaks started from 5 eV to 10 eV. Through spectra, we can observe a significant absorption in the visible region of Ge_8 cluster compared to $SnGe_7$ cluster. So we say that add the tin to the pure cluster has made the absorption drift towards the ultraviolet region and also changed the positions of some peaks such as in energy 6 eV the absorption of Ge_8 cluster equal 2 a.u against equal 6 a.u for $SnGe_7$ cluster.

The photo-absorption spectra of Ge_9 and $SnGe_8$ clusters, In this case, are very similar, so this great similarity leads us to say that the addition of tin has not changed the optical properties of the Ge_9 cluster except in some positions we observe a slight decrease or a slight increase in intensity of the oscillator strength exactly between 6.5-9.5 eV Apparently, and compatible to the case of Ge_{10}, the calculated spectrum of $SnGe_9$ does not show any transition between 0 and 3 eV. Generality the $SnGe_9$ spectrum has a similar overall shape as the Ge_{10} spectrum, and, in particular, three peaks are present in the Ge_{10} spectrum at the same positions.

Note that there is a slight difference between the two spectra and the appearance of two peaks at the energies 6 and 9 eV after the encapsulation of Sn atom in pure germanium cage.

In the case of $SnGe_{10}$, there is a remarkable similitude between Ge_{11} and $SnGe_{10}$ spectra that are mainly formed of four broad structures between 5 and 10 eV that are energetically almost equidistant and increasing in intensity. From the Figure22, the very pronounced peaks are observed at the energies 3.8, 5, 6.5, 7.7, 8.6 eV for pure Ge_{11} and $SnGe_{10}$ clusters. After

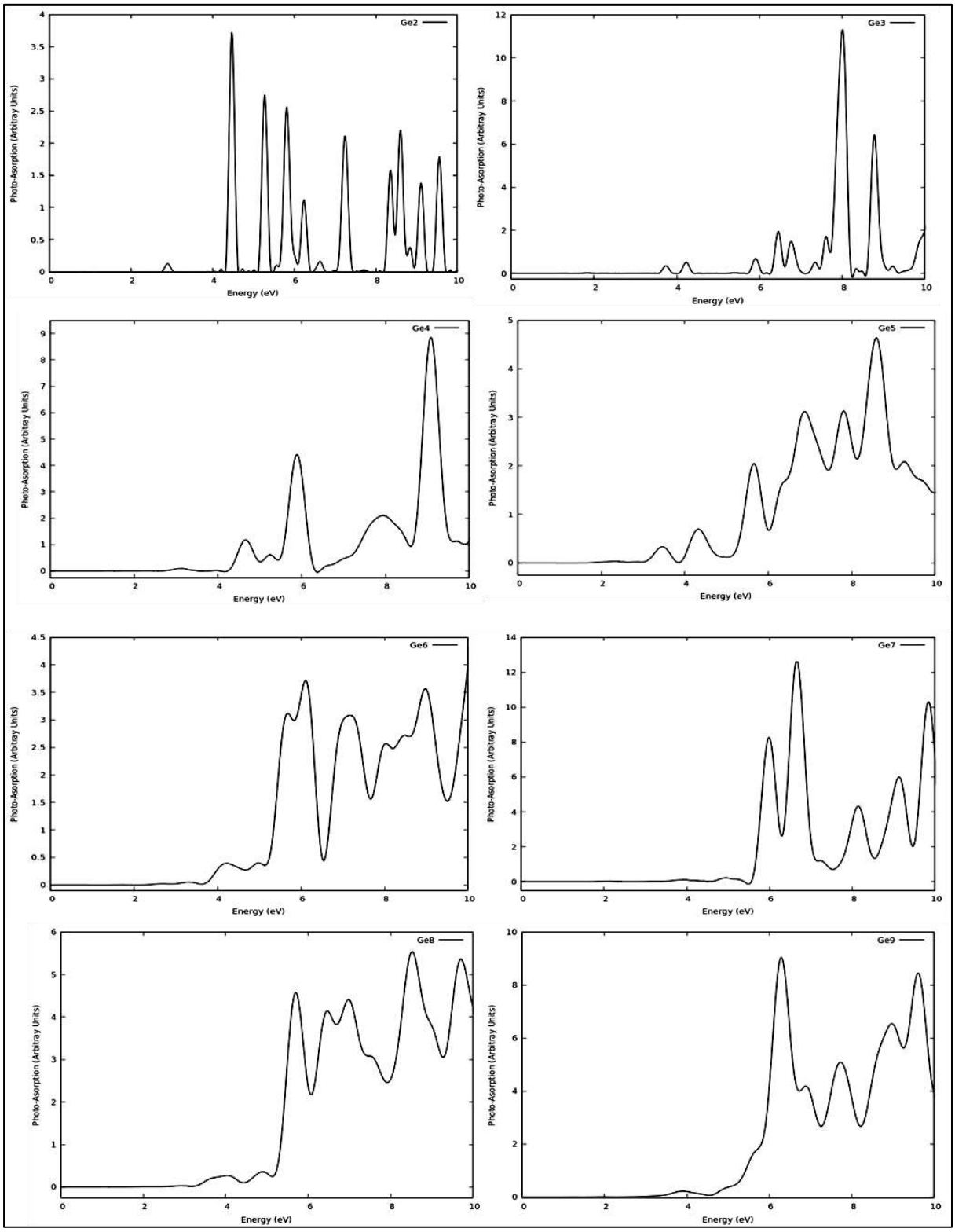

Figure.19: The Photoabsorption spectrum of Ge_n (n= 2,9) clusters.

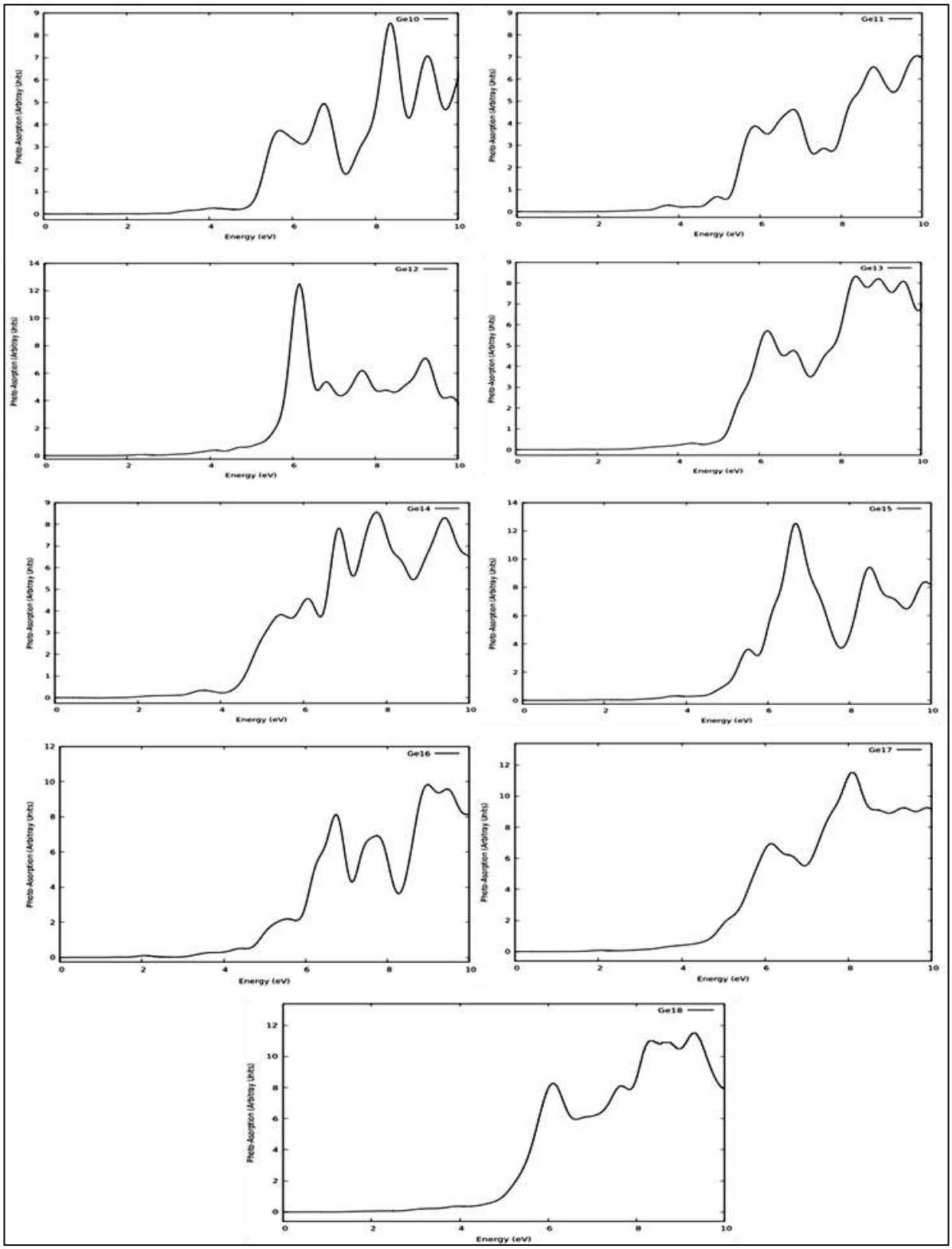

Figure.20: The Photo-absorption spectra of Ge_n (n= 10,18) clusters.

Table7 : Optical gap energies in eV, HOMO-LUMO energies in eV, Exciton binding energies in eV of Ge_n and $SnGe_{n-1}$ clusters .

Clusters	Optical gap (eV)	HOMO-LUMO gap (eV)	Exciton binding energy (eV)
Ge_2	2.89	0.344	-2.546
SnGe	2.61	0.344	-2.276
Ge_3	1.75	1.311	-0.439
$Sn Ge_2$	1.95	1.311	-0.639
Ge_4	2.36	1.643	-0.717
$Sn Ge_3$	2.24	0.227	-2.013
Ge_5	2.42	0.984	-1.436
$Sn Ge_4$	2.23	1.739	-0.491
Ge_6	2.65	0.227	-2.423
$Sn Ge_5$	2.55	1.663	-0.887
Ge_7	2.25	1.557	-0.693
$Sn Ge_6$	1.96	1.853	-0.107
Ge_8	2.20	1.179	-1.021
$Sn Ge_7$	1.30	1.197	-0.103
Ge_9	2.00	1.588	-0.412
$Sn Ge_8$	1.72	1.486	-0.234
Ge_{10}	2.11	1.609	-0.501
$Sn Ge_9$	1.88	1.551	-0.329
Ge_{11}	2.00	1.148	-0.852
$Sn Ge_{10}$	1.81	1.202	-0.608
Ge_{12}	2.40	1.536	-0.864
$Sn Ge_{11}$	2.31	1.529	-0.781
Ge_{13}	1.63	0.982	-0.648
$Sn Ge_{12}$	1.51	0.992	-0.518
Ge_{14}	2.30	1.372	-0.928
$Sn Ge_{13}$	2.50	1.353	-1.147
Ge_{15}	1.97	0.864	-1.106
$Sn Ge_{14}$	2.03	0.950	-1.080
Ge_{16}	2.06	1.164	-0.896
$Sn Ge_{15}$	1.97	1.031	-0.939
Ge_{17}	2.09	0.884	-1.206
$Sn Ge_{16}$	2.00	0.899	-1.101
Ge_{18}	2.29	1.322	-0.968
$Sn Ge_{17}$	1.97	1.332	-0.638

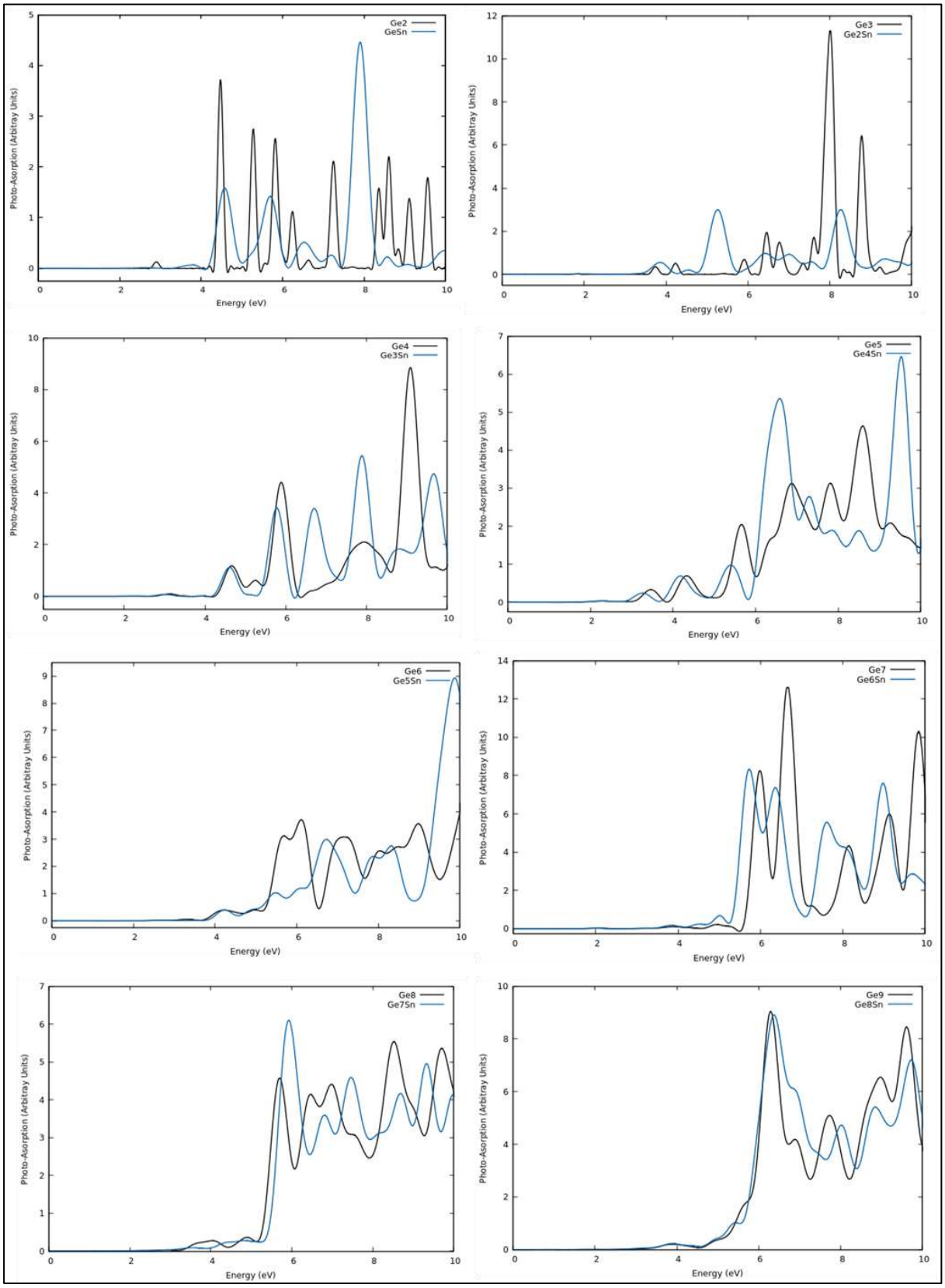

Figure.21: The Photoabsorption spectrum of $SnGe_n$ (n=1,8) clusters.

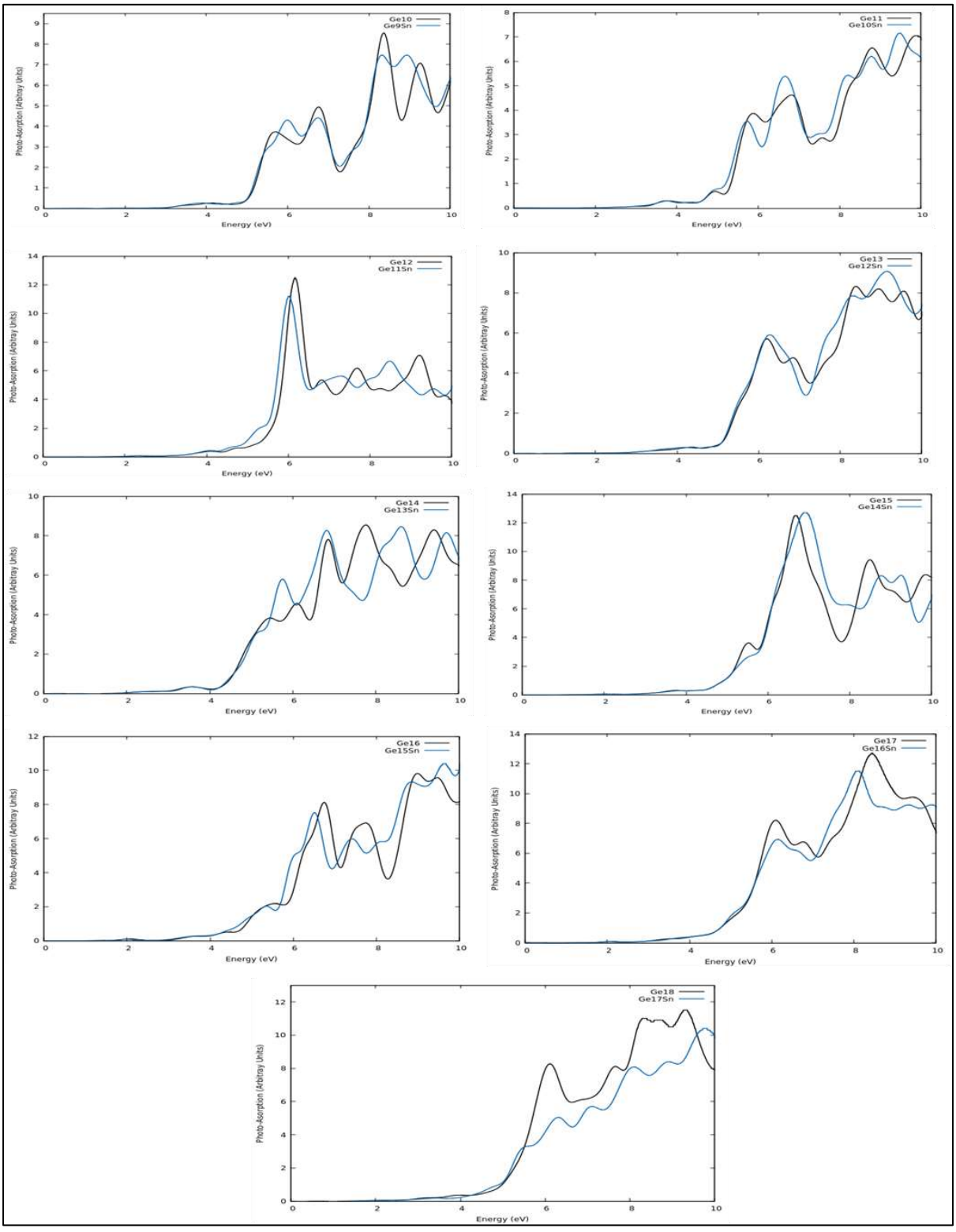

Figure.22: The Photo-absorption spectrum of $SnGe_n$ (n=9,17) clusters.

adding tin to the pure germanium cluster, new peaks are observed at the energies 8, 9.4 eV for pure Ge_{11} and $SnGe_{10}$ clusters. The photo-absorption spectrum of $SnGe_{11}$ represented in Figure22 shows three main peaks at 3.42 and 3.91 eV and two a less intense at 4.38 eV. Both spectra obtained for the lowest-energy structures of pure and doped germanium cluster have very similar shapes with broad absorption band started from 5.5 eV to 10 eV. We can note some differences like the emergence of new peaks at 7 and 8.5 eV and the disappearance of peaks like 7.7 and 9.8 eV. Through the spectra of $SnGe_{12}$ and Ge_{13} clusters, in general, we can observe that the absorption of the two spectra is concentrated in blue shift energy. We can note similarity between two spectra along the axis of energy, only some of the differences in positions and the oscillator strengths of the some peaks. From spectra, we can see that some peaks appear and others disappear for example at energy 6.8 eV the peak disappear for $SnGe_{12}$ and 8.5 eV. We can see also that the transitions for $SnGe_{12}$ are broader than in Ge_{13}.

In the case of clusters composed 14 atoms, the photo-absorption of pure and tin doped germanium clusters were studied. The photo-absorption spectra of each cluster were presented in fig. from figure, substituting Ge by Sn leads to a somewhat similar spectrum. In the region of 2 to 5 we note that there has been no change in the form of absorption spectrum. The absorption in both spectra is characterized by broad absorption band carries intense peaks started from 4 eV to 10 eV. Clearly the difference between two spectrums show in positions of those intense peaks, Let's take examples, The emergence of new peaks at energies 5.7 eV, 8.6 eV, 9.8 eV and other disappearance at energies 5.5 eV, 6.2 eV, 7.8 eV, 9.5 eV.

In Figure22 is shown the comparison between the photo-absorption spectra of Ge_{15} and $SnGe_{14}$ clusters. It can be seen that the impurity state, due to tin atom, have a slight influence of the optical spectrum that shows peaks in the optical region at 6.9, 8.5 and 9.4 eV and no more the intense peaks at 6.7, 8.3 and 9.8 eV in the tin doped germanium cluster; moreover the absorption spectrum of the doped cluster, in the optical region below 5 eV, remains similar to the corresponding spectrum of the undoped cluster.

From the spectra of Ge_{16} and $SnGe_{15}$ clusters, like previous clusters, It can be seen also in this case that the tin atom have a slight influence of the optical spectrum that shows broad peaks in the optical region at 6, 6.4, 7.4 and 8.8 eV and no more the intense peaks at 6.7 and 7.7 eV in the tin doped germanium cluster; moreover the absorption spectrum of the doped cluster, in the optical region below 5 eV, remains similar to the corresponding spectrum of the undoped cluster.

The calculated optical absorption spectrum of $SnGe_{17}$ cluster has been compared in Figure22 with the corresponding spectra of the Ge_{18} cluster. Once again substituting Ge by Sn leads to a somewhat similar spectrum of corresponding one. In the region of 2 to 5.6 we note that there has been no change in the form of absorption spectrum. The absorption in both spectra is characterized by broad absorption band started from 5 eV to 10 eV. On the contrary, in the region of 5.6 to 10 we note change in the positions of peaks and decrease in intensities of oscillator strength. We note also the peaks has became more broader than from before.

4.2.3. Optical gap energy

In Table7 we present the optical absorption gaps of the various clusters. The optical gap of a cluster defined by a neutral excitation is the energy difference between the lowest dipole-allowed excited state and the ground state. In our work the optical gap energy, E_{opt}, which is defined as the energy of first well defined peak in the absorption spectrum [202], provides another measure of the excitation energy obtained through TD-DFT calculations. As shown in Figure23, these are well-defined transitions even though the optical absorption strength is so weak that it is not even visible on the scale of Figures (20-23). Thus the present definition represented the lowest calculated gap. The HOMO-LUMO gap and the optical gap are known to differ because of the attractive interaction between the electron and the electron-hole formed during electron excitation. Our results shown in Table7 are in good agreement with theoretical results of the literature[67].

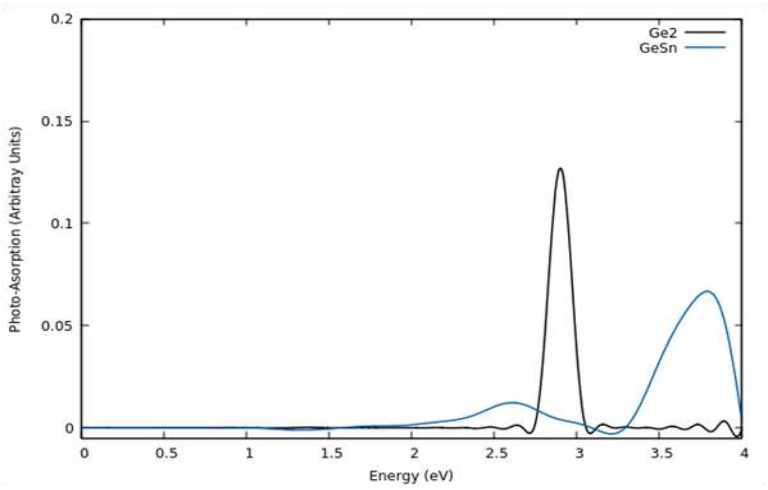

Figure.23: Detail of the low-energy absorption spectrum of Ge_2 and SnGe clusters.

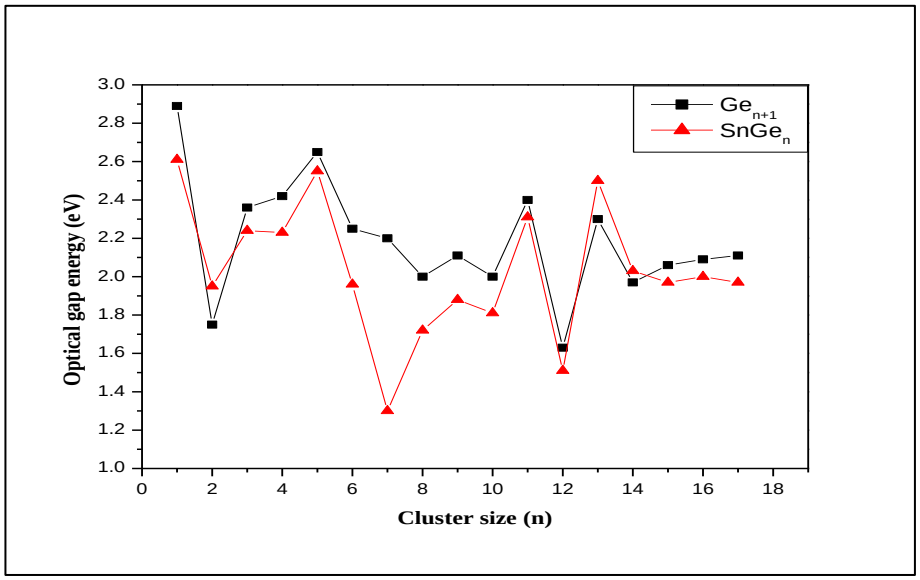

Figure.24: Optical gap energies of various Ge_{n+1} (black line) and $SnGe_n$ (red line) clusters as a function of the number of germanium atoms (n).

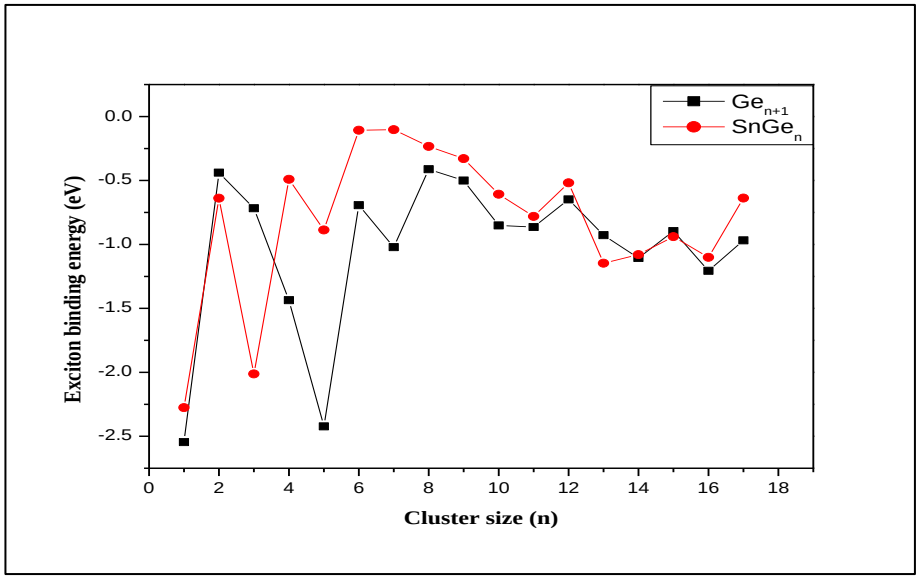

Figure.25: Exciton binding energies of various Ge_n (black line) and $SnGe_{n-1}$ (red line) clusters as a function of the number of germanium atoms (n).

In Figure24 we plot the optical gap as a function of the cluster size (n) for various Ge_{n+1} (black Line) and $SnGe_n$ (red Line) clusters (n=1-17). With the increase of cluster size, the optical gap exhibits a oscillating downward trend; and the local minimum values of the optical gap are found at n = 2, 8, 10, 12 and 14 for Ge_n and at n =2, 7, 10 and 12 for $SnGe_{n-1}$ as marked in Figure24. These results indicate that the electrons in the clusters of these sizes are easier to be excited than their neighboring clusters. It also shows a general trend that the addition of a single Sn atom reduces the optical gap as compared to the germanium clusters. As the number of germanium atoms in the cluster increase we find that the effect of a single Sn atom decreases. The dependence of the optical gap on the size of the clusters can be explained with the help of the quantum confinement model. According to this model, the observed photoluminescence comes from the recombination of electron-hole pairs confined in the clusters [203, 204].

4.2.4. The exciton binding energy

The exciton binding energy (E_x) of a cluster is defined as the difference between the HOMO-LUMO gap (E_g) and optical gap (E_{opt}),

$$E_x = E_g - E_{opt} \qquad 4.1$$

The exciton binding energy gives the energy required to separate an electron-hole pair, which should be taken into account when designing solar cells and optoelectronic devices [205]. Estimates of the exciton binding energies for each cluster are also displayed alongside the optical gaps in Table7 .

Figure25 shows the exciton binding energies versus sizes of the clusters (n) for pur and doped germanium clusters; we can see that the variations of the exciton binding energy with size and structure of clusters are large. Figure25 also displays the opposite trend of increasing exciton binding energy as cluster size increases. Interestingly, those calculations predict an optical gap that is higher than the HOMO- LUMO gap, which results in negative exciton binding energies. This is a trend that is well known in TDLDA calculations [206], and can likely be attributed to underestimation of the single particle transition energies. The Figure25 shows also the effect of add one tin atom on the exciton binding energies of germanium clusters, we can see clear increases of the exciton binding energies values.

For germanium clusters, the exciton binding energy ranges from 0.412 eV to 2.546 eV. These energies are much greater than the energies associated with bulk diamond structure of

germanium semiconductors, which are on the order of 4.7 meV[207]. This major increase of the Coulomb interaction part of the exciton binding energy is caused by the increased overlap of the electron and hole wave-functions.

The local maximum values of the exciton binding energies are found at n = 2, 6, 8, 12, 15 and 17 for Ge_n and at n =2, 4, 6, 12 and 15 for $SnGe_{n-1}$ as marked in Figure25. These results indicate that those clusters with larger exciton binding energy are less reactive chemical so chemical stability higher than their neighboring clusters, which are often desirable for light emitting devices. Whereas the opposite, the local minimum values of the exciton binding energy at n = 1, 5, 7, 11, 14 and 16 for Ge_n and at n = 1, 3, 5, 11, 13 and 16 for $SnGe_{n-1}$, may be favorable for photovoltaic applications.

Conclusions and future works

In this thesis, we applied ab initio computation techniques to study the structural, electronic and optical properties of germanium clusters and the study of structural, electronic, magnetic and optical properties of germanium clusters doped with tin atoms. We were able to familiarize ourselves with the basics of ab initio calculus, DFT, TDDFT and pseudopotentials. This gave us the opportunity to fully understand the SIESTA and Octopus packages to find the ground state structures of the germanium clusters and their the photo-absorption spectra.

In the case of pure germanium clusters, the lower energy structures of clusters with size n (n = 2-18) are obtained by DFT-GGA calculations with a molecular dynamics method, ie simulated annealing, application in the SIESTA code.

The lower energy structures obtained for the clusters are completely different and in no case constitute a fragment of the solid crystal. All the Ge_{n+1} and $SnGe_n^{(0,\pm1)}$ clusters adopt planar structures for very small size and near spherical and spherical compact structures as the size increase. In $SnGe_n^{(0,\pm1)}$ clusters, the Sn atom prefers the peripheral position when n<12 and occupies a core position for n>12. The structure $SnGe_n$ clusters kept unchanged after the encapsulation of Sn atom in pure germanium cage. For $\mathbf{Ge_{n+1}}$ and $SnGe_n^{(0,\pm1)}$ clusters, the binding energy per atom increases with the increasing of the size. The strong increasing in stability of the small clusters is related to the thermodynamic instability of smaller systems. The fragmentation energy calculations indicates that the clusters $Ge_{4,10,14}$ and $SnGe_{3,9,13,16}$ and $SnGe^{+}_{3,5,13,16}$ are more stable than their neighbors. The second energy difference analysis show that the clusters of Ge_{n+1} and $SnGe_n$ clusters at n = 1, 5, 7, 10, 12, 14 are more stables. The HOMO-LUMO gaps of all systems showed a decreasing behavior with the increasing of the size from n=4 and the charged clusters showed a considerable reduction of the HOMO-LUMO gaps compared to the case of neutral ones. The ionization potentials and electron affinity calculations showed that the clusters of $SnGe_n$ with a size more than 9 atoms exhibit high metallic character and will liberate more energy when they capture one electron. However, the chemical hardness of $SnGe_n$ showed that the clusters with large size are less reactive and more stable. All of the ground states of $SnGe_n$ clusters are nonmagnetic structures, except the case of $SnGe_1$. Their total spin magnetic moment is mainly due to the 4p and 5p orbital of Ge and Sn atoms, respectively.

The optical response of germanium clusters with numbers of atoms between 2 and 18 atoms was studied using TDDFT. As results using different calculation methods have been shown to be quite dependent on the calculation approach, trends in the optical absorption spectra should not be identified by bringing together sets of calculations from different sources. Rather, the complete range should be coverd in a continuous fashion, using a single meth, as has been done here. The trends idenified were:

The absorption spectra of clusters are dominated by a series of distinct peaks. The position of these peaks changes rapidly by the addition of only a few atoms, or alterations of the atomic structure.

The absorption spectra become smoother as the cluster size increases. Compared with the small clusters, the absorption peaks are not so sharp. Each peak is extended to both sides, forming an absorption band consisted of multiple peaks.

The main absorption peaks of these clusters are in the ultraviolet region, especially in the far ultraviolet region. With the increase of cluster size, their absorption spectra converted gradually from many peaks to broad absorption bands, and extend gradually toward the lower energy region and their optical gap becomes smaller and smaller.

A compared with pure germanium, The absorption spectra after Sn doping are characterized by the emergence of a dominant and relatively broad peak between 6 and 10 eV, accompanied by broad absorption peaks also at the same region but smaller intensities . This common feature is coupled to a blue shift of the main peak with increasing cluster size.

With the increase of cluster size, the optical gap exhibits a oscillating downward trend; and the local minimum values of the optical gap are found at n = 2, 8, 10, 12 and 14 for Ge_n and at n =2, 7, 10 and 12 for $SnGe_{n-1}$. These results indicate that the electrons in the clusters of these sizes are easier to be excited than their neighboring clusters. It also shows a general trend that the addition of a single Sn atom reduces the optical gap as compared to the germanium clusters.

All these specific properties make the $SnGe_n$ clusters good potentials candidates for many eventual applications in nanotechnologies. We had to mention that it is very interesting for the future to calculate the frequencies of vibration in order to obtain the best and more stable isomers, and to calculate emission spectra of these clusters.

References

[1] D. A. Miller, Optical interconnects to electronic chips, Applied optics, 49 (2010) F59-F70.
[2] M. Moskovits, Chemical Physics of Atomic and Molecular Clusters ed G Soles, in, Amsterdam: North-Holland) p, 1990.
[3] M. A. Duncan *Advances in Metal and Semiconductor Clusters: Cluster Materials*; Elsevier, 1998.
[4] W. A. De Heer, The physics of simple metal clusters: experimental aspects and simple models, Reviews of Modern Physics, 65 (1993) 611.
[5] R. Berry and J. Jellinek, Theory of Atomic and Molecular Clusters, in, J. Jellinek (Ed.), 1999.
[6] R. L. Johnston *Atomic and molecular clusters*; CRC Press, 2002.
[7] Y. Kawazoe, T. Kondow and K. Ohno In *Clusters and Nanomaterials*; Springer, 2002.
[8] J. A. Alonso, Structure and properties of atomic nanoclusters, in, Imperial College Press, London, 2005.
[9] P. Jena and A. W. Castleman Jr *Nanoclusters: a bridge across disciplines*; Elsevier, 2010.
[10] Y. Wang, X. Li, F. Wang, B. Xu, J. Zhang, Q. Sun and Y. Jia, Li2O clusters for high-capacity hydrogen storage: A first principles study, Chemical Physics, 415 (2013) 26-30.
[11] P. Jena and A. Castleman, Clusters: A bridge across the disciplines of physics and chemistry, Proceedings of the National Academy of Sciences, 103 (2006) 10560-10569.
[12] M. Loos, Chapter 1-nanoscience and nanotechnology, Carbon Nanotube Reinforced Composites: CNR Polymer Science and Technology, (2015) 1-36.
[13] R. Saini, S. Saini and S. Sharma, Nanotechnology: the future medicine, Journal of cutaneous and aesthetic surgery, 3 (2010) 32.
[14] C. N. R. Rao, A. Müller and A. K. Cheetham *The chemistry of nanomaterials: synthesis, properties and applications*; John Wiley & Sons, 2006.
[15] A. K. Bandyopadhyay *Nano materials*; New Age International, 2008.
[16] R. J. Narayan, P. N. Kumta, C. Sfeir, D.-H. Lee, D. Choi and D. Olton, Nanostructured ceramics in medical devices: applications and prospects, Jom, 56 (2004) 38.
[17] C. Darnault, K. Rockne, A. Stevens, G. A. Mansoori and N. Sturchio, Fate of environmental pollutants, in, JSTOR, 2005.
[18] R. Sivaraj, H. A. Salam, P. Rajiv and V. Rajendran In *Environmental Sustainability*; Springer, 2015.
[19] C. Kittel and P. McEuen *Introduction to solid state physics*; Wiley New York, 1996.
[20] P. Harrison and A. Valavanis *Quantum wells, wires and dots: theoretical and computational physics of semiconductor nanostructures*; John Wiley & Sons, 2016.
[21] J. Jeevanandam, A. Barhoum, Y. S. Chan, A. Dufresne and M. K. Danquah, Review on nanoparticles and nanostructured materials: history, sources, toxicity and regulations, Beilstein journal of nanotechnology, 9 (2018) 1050-1074.

[22] P. N. Samanta and K. K. Das, Electronic structure, bonding, and properties of SnmGen (m+n⩽ 5) clusters: A DFT study, Computational and Theoretical Chemistry, 980 (2012) 123-132.
[23] S. Mahtout and Y. Tariket, Electronic and magnetic properties of CrGen (15⩽n⩽29) clusters: A DFT study, Chemical Physics, 472 (2016) 270-277.
[24] A. L. Efros and M. Rosen, The electronic structure of semiconductor nanocrystals, Annual Review of Materials Science, 30 (2000) 475-521.
[25] P. Harrison, Quantum Wells, Quantum Wires, and Quantum Dots, in, New York: Wiley, 2000.
[26] P. O. Anikeeva, J. E. Halpert, M. G. Bawendi and V. Bulovic, Quantum dot light-emitting devices with electroluminescence tunable over the entire visible spectrum, Nano letters, 9 (2009) 2532-2536.
[27] T. J. Bukowski and J. H. Simmons, Quantum Dot Research: Current State and Future Prospects, Critical Reviews in Solid State and Materials Sciences, 27 (2002) 119-142.
[28] A. J. Nozik, Quantum dot solar cells, Physica E: Low-dimensional Systems and Nanostructures, 14 (2002) 115-120.
[29] E.-C. Cho, S. Park, X. Hao, D. Song, G. Conibeer, S.-C. Park and M. A. Green, Silicon quantum dot/crystalline silicon solar cells, Nanotechnology, 19 (2008) 245201.
[30] A. J. Nozik, Nanoscience and nanostructures for photovoltaics and solar fuels, Nano letters, 10 (2010) 2735-2741.
[31] C. Murray, D. J. Norris and M. G. Bawendi, Synthesis and characterization of nearly monodisperse CdE (E= sulfur, selenium, tellurium) semiconductor nanocrystallites, Journal of the American Chemical Society, 115 (1993) 8706-8715.
[32] A. P. Alivisatos, Semiconductor clusters, nanocrystals, and quantum dots, Science, 271 (1996) 933-937.
[33] Y. Ding, S. Zhou, F. B. Juangsa, M. Sugaya, Y. Asano, X. Zhang, Y. Zhao and T. Nozaki, Optical, electrical, and photovoltaic properties of silicon nanoparticles with different crystallinities, Applied Physics Letters, 107 (2015) 233108.
[34] M. G. Mavros, D. A. Micha and D. S. Kilin, Optical properties of doped silicon quantum dots with crystalline and amorphous structures, The Journal of Physical Chemistry C, 115 (2011) 19529-19537.
[35] H. Freitag, M. Mavros and D. Micha, Optical absorbance of doped Si quantum dots calculated by time-dependent density functional theory with partial electronic self-interaction corrections, The Journal of Chemical Physics, 137 (2012) 144301.
[36] X. Pi and C. Delerue, Tight-binding calculations of the optical response of optimally P-doped Si nanocrystals: a model for localized surface plasmon resonance, Physical Review Letters, 111 (2013) 177402.
[37] I. Vasiliev and R. Martin, Optical properties of hydrogenated silicon clusters with reconstructed surfaces, physica status solidi (b), 233 (2002) 5-9.
[38] A. Puzder, A. Williamson, J. C. Grossman and G. Galli, Surface control of optical properties in silicon nanoclusters, The Journal of Chemical Physics, 117 (2002) 6721-6729.
[39] L. Ramos, J. Furthmüller and F. Bechstedt, Influence of oxygen on optical properties of Si nanocrystallites, Applied Physics Letters, 87 (2005) 143113.

[40] W. Qin, W.-C. Lu, L.-H. Xia, L.-Z. Zhao, Q.-J. Zang, C. Wang and K. Ho, Theoretical study on the structures and optical absorption of Si 172 nanoclusters, Nanoscale, 7 (2015) 14444-14451.
[41] L.-Z. Zhao, W.-C. Lu, W.-S. Su, W. Qin, C. Wang and K. Ho, Si 78 double cage structure and special optical properties, Physical Chemistry Chemical Physics, 17 (2015) 27734-27741.
[42] W.-H. Yang, W.-C. Lu, C. Wang and K. Ho, How Big Does a Si Nanocluster Favor Bulk Bonding Geometry?, The Journal of Physical Chemistry C, 120 (2016) 1966-1970.
[43] W. Shockley, The theory of p-n junctions in semiconductors and p-n junction transistors, Bell System Technical Journal, 28 (1949) 435-489.
[44] A. Satta, A. R. Peaker, A. Theuwis, A. N. Larsen, B. Depuydt, B. De Jaeger, C. Quaeyhaegens, C. O. Chui, C. Deguet, C. Claeys, D. Esseni, E. Simoen, E. Sangiorgi, E. Kasper, F. Letertre, I. Romandic, J. Vanhellemont, J. Coutinho, K. C. Saraswat, M. De Jonghe, M. Heyns, M. Meuris, M. Caymax, M. Houssa, P. Clauws, P. Palestri, R. Jones, T. Akatsu, V. Markevich and W. De Baets In *Germanium-Based Technologies*; C. Claeys and E. Simoen, Eds.; Elsevier: Oxford, 2007.
[45] L. Tang, S. E. Kocabas, S. Latif, A. K. Okyay, D.-S. Ly-Gagnon, K. C. Saraswat and D. A. Miller, Nanometre-scale germanium photodetector enhanced by a near-infrared dipole antenna, Nature Photonics, 2 (2008) 226-229.
[46] M. Oehme, J. Werner, M. Kaschel, O. Kirfel and E. Kasper, Germanium waveguide photodetectors integrated on silicon with MBE, Thin Solid Films, 517 (2008) 137-139.
[47] S. Saito, A. Z. Al-Attili, K. Oda and Y. Ishikawa, Towards monolithic integration of germanium light sources on silicon chips, Semiconductor Science and Technology, 31 (2016) 043002.
[48] L. S. Keith, O. M. Faroon, N. Maples-Reynolds and B. A. Fowler In *Handbook on the Toxicology of Metals*; Elsevier, 2015.
[49] G. R. Burton, C. Xu, C. C. Arnold and D. M. Neumark, Photoelectron spectroscopy and zero electron kinetic energy spectroscopy of germanium cluster anions, The Journal of Chemical Physics, 104 (1996) 2757-2764.
[50] G. R. BURTON, C. XU and D. M. NEUMARK, STUDY OF SMALL SEMICONDUCTOR CLUSTERS USING ANION PHOTOELECTRON SPECTROSCOPY: GERMANIUM CLUSTERS (Gen, n=2−15), Surface Review and Letters, 03 (1996) 383-388.
[51] Y. Negishi, H. Kawamata, F. Hayakawa, A. Nakajima and K. Kaya, The infrared HOMO–LUMO gap of germanium clusters, Chemical Physics Letters, 294 (1998) 370-376.
[52] K. A. Gingerich, R. Schmude Jr, M. Sai Baba and G. Meloni, Atomization enthalpies and enthalpies of formation of the germanium clusters, Ge 5, Ge 6, Ge 7, and Ge 8 by Knudsen effusion mass spectrometry, The Journal of Chemical Physics, 112 (2000) 7443-7448.
[53] D. A. Hostutler, H. Li, D. J. Clouthier and G. Wannous, Exploring the Bermuda triangle of homonuclear diatomic spectroscopy: the electronic spectrum and structure of Ge 2, The Journal of Chemical Physics, 116 (2002) 4135-4141.
[54] S. Bals, S. Van Aert, C. Romero, K. Lauwaet, M. J. Van Bael, B. Schoeters, B. Partoens, E. Yücelen, P. Lievens and G. Van Tendeloo, Atomic scale dynamics of ultrasmall germanium clusters, Nature communications, 3 (2012) 897.

[55] J. De Haeck, T. B. Tai, S. Bhattacharyya, H. T. Le, E. Janssens, M. T. Nguyen and P. Lievens, Structures and ionization energies of small lithium doped germanium clusters, Physical Chemistry Chemical Physics, 15 (2013) 5151-5162.
[56] P. Deutsch, L. Curtiss and J.-P. Blaudeau, Electron affinities of germanium anion clusters, Ge n−(n= 2–5), Chemical physics letters, 344 (2001) 101-106.
[57] J. Wang, G. Wang and J. Zhao, Structure and electronic properties of Ge n (n= 2–2 5) clusters from density-functional theory, Physical Review B, 64 (2001) 205411.
[58] J. Wang, M. Yang, G. Wang and J. Zhao, Dipole polarizabilities of germanium clusters, Chemical physics letters, 367 (2003) 448-454.
[59] H. Kikuchi, M. Takahashi and Y. Kawazoe, Special Issue on Advances in Computational Materials Science and Engineering IV-Theoretical Investigation of Stable Structures of Ge6 Clusters with Various Negative Charges, Materials Transactions-JIM, 47 (2006) 2624-2628.
[60] S. Ma and G. Wang, Structures of medium size germanium clusters, Journal of Molecular Structure: THEOCHEM, 767 (2006) 75-79.
[61] W.-J. Zhao and Y.-X. Wang, Geometries, stabilities, and magnetic properties of MnGe n (n= 2–16) clusters: Density-functional theory investigations, Journal of Molecular Structure: THEOCHEM, 901 (2009) 18-23.
[62] X.-J. Li, H.-J. Ren and L.-M. Yang, An investigation of electronic structure and aromaticity in medium-sized nanoclusters of gold-doped germanium, J. Nanomaterials, 2012 (2012) 3-3.
[63] R. Trivedi, K. Dhaka and D. Bandyopadhyay, Study of electronic properties, stabilities and magnetic quenching of molybdenum-doped germanium clusters: a density functional investigation, RSC advances, 4 (2014) 64825-64834.
[64] A. Soltani and M. B. Javan, Carbon monoxide interactions with pure and doped B 11 XN 12 (X= Mg, Ge, Ga) nano-clusters: a theoretical study, RSC advances, 5 (2015) 90621-90631.
[65] Y. Jin, Y. Tian, X. Kuang, C. Lu, J. L. Cabellos, S. Mondal and G. Merino, Structural and electronic properties of ruthenium-doped germanium clusters, The Journal of Physical Chemistry C, 120 (2016) 8399-8404.
[66] X.-Q. Liang, X.-J. Deng, S.-J. Lu, X.-M. Huang, J.-J. Zhao, H.-G. Xu, W.-J. Zheng and X. C. Zeng, Probing Structural, Electronic, and Magnetic Properties of Iron-Doped Semiconductor Clusters Fe2Ge n–/0 (n= 3–12) via Joint Photoelectron Spectroscopy and Density Functional Study, The Journal of Physical Chemistry C, 121 (2017) 7037-7046.
[67] W. Qin, W.-C. Lu, L.-Z. Zhao, K. M. Ho and C. Z. Wang, Optical absorption properties of Ge2–44 and P-doped Ge nanoparticles, Computational Materials Science, 140 (2017) 148-158.
[68] M. Salazar-Villanueva, A. Cruz-López, A. Zaldívar-Cadena, A. Tovar-Corona, M. Guevara-Romero and O. Vazquez-Cuchillo, Effect of the electronic state of Ti on M-doped TiO2 nanoparticles (M= Zn, Ga or Ge) with high photocatalytic activities: A experimental and DFT molecular study, Materials Science in Semiconductor Processing, 58 (2017) 8-14.
[69] S. Mahtout, C. Siouani and F. Rabilloud, Growth behavior and electronic structure of noble metal-doped germanium clusters, The Journal of Physical Chemistry A, 122 (2018) 662-677.

[70] E. Tazikeh-Lemeski, A. Soltani, M. T. Baei, M. B. Javan and S. M. Rad, Theoretical study on pure and doped B 12 N 12 fullerenes as thiophene sensor, Adsorption, 24 (2018) 585-593.
[71] D. Bandyopadhyay, Electronic structure and stability of anionic AuGe n (n= 1–20) clusters and assemblies: a density functional modeling, Structural Chemistry, 30 (2019) 955-963.
[72] S. Zhou, X. Yang, Y. Shen, R. B. King and J. Zhao, Dual transition metal doped germanium clusters for catalysis of CO oxidation, Journal of Alloys and Compounds, 806 (2019) 698-704.
[73] M. Lasmi, S. Mahtout and F. Rabilloud, The effect of palladium and platinum doping on the structure, stability and optical properties of germanium clusters: DFT study of PdGen and PtGen (n= 1–20) clusters, Computational and Theoretical Chemistry, 1181 (2020) 112830.
[74] S. Ŏgüt and J. R. Chelikowsky, Structural changes induced upon charging Ge clusters, Physical Review B, 55 (1997) R4914.
[75] A. A. Shvartsburg, B. Liu, Z.-Y. Lu, C.-Z. Wang, M. F. Jarrold and K.-M. Ho, Structures of germanium clusters: where the growth patterns of silicon and germanium clusters diverge, Physical Review Letters, 83 (1999) 2167.
[76] S.-D. Li, Z.-G. Zhao, H.-S. Wu and Z.-H. Jin, Ionization potentials, electron affinities, and vibrational frequencies of Ge n (n= 5–10) neutrals and charged ions from density functional theory, The Journal of Chemical Physics, 115 (2001) 9255-9259.
[77] B.-X. Li, P.-L. Cao, B. Song and Z.-Z. Ye, Electronic and geometric structures of Gen− and Gen+ (n= 5–10) clusters in comparison with corresponding Sin ions, Physics Letters A, 307 (2003) 318-325.
[78] S. Bulusu, S. Yoo and X. C. Zeng, Search for global minimum geometries for medium sized germanium clusters: Ge 12–Ge 20, The Journal of Chemical Physics, 122 (2005) 164305.
[79] S. Yoo and X. C. Zeng, Search for global-minimum geometries of medium-sized germanium clusters. II. Motif-based low-lying clusters Ge 21–Ge 29, The Journal of Chemical Physics, 124 (2006) 184309.
[80] D. Feldmann, R. Rackwitz, E. Heinicke and H. J. Kaiser, Photoablösung von Elektronen der Ionen B-, Ga-, In-, Tl-, Ge-, Sn- und Pb- / Photodetachment of Electrons of the Ions B-, Ga-, In-, Tl-, Ge-, Sn- and Pb, in: Zeitschrift für Naturforschung A, 1977, pp. 302.
[81] S. Li, R. J. V. Zee and W. W. Jr., Magneto-infrared spectra of the Si2, Ge2, and Sn2 molecules in rare-gas matrices, The Journal of Chemical Physics, 100 (1994) 7079-7086.
[82] J. Thøgersen, L. D. Steele, M. Scheer, C. A. Brodie and H. K. Haugen, Electron affinities of Si, Ge, Sn and Pt by tunable laser photodetachment studies, Journal of Physics B: Atomic, Molecular and Optical Physics, 29 (1996) 1323.
[83] M. Scheer, R. C. Bilodeau, C. A. Brodie and H. K. Haugen, Systematic study of the stable states of ${\mathrm{C}}^{\mathrm{\ensuremath{-}}},$ ${\mathrm{Si}}^{\mathrm{\ensuremath{-}}},$ ${\mathrm{Ge}}^{\mathrm{\ensuremath{-}}},$ and ${\mathrm{Sn}}^{\mathrm{\ensuremath{-}}}$ via infrared laser spectroscopy, Physical Review A, 58 (1998) 2844-2856.

[84] L. Wang and J. Zhao, Competition between supercluster and stuffed cage structures in medium-sized Ge n (n= 30–39) clusters, The Journal of Chemical Physics, 128 (2008) 024302.
[85] W. Qin, W.-C. Lu, L.-Z. Zhao, Q.-J. Zang, G.-J. Chen, C. Wang and K. Ho, Platelike structures of semiconductor clusters Ge n (n= 40–44), The Journal of Chemical Physics, 131 (2009) 124507.
[86] W. Qin, W.-C. Lu, Q.-J. Zang, L.-Z. Zhao, G.-J. Chen, C. Wang and K. Ho, Geometric structures of Ge n (n= 34–39) clusters, The Journal of Chemical Physics, 132 (2010) 214509.
[87] G. Köhl, Massenspektrometrische Untersuchungen an Germanium, in: Zeitschrift für Naturforschung A, 1954, pp. 913.
[88] A. Kant and B. H. Strauss, Atomization Energies of the Polymers of Germanium, Ge2 to Ge7, The Journal of Chemical Physics, 45 (1966) 822-826.
[89] T. P. Martin and H. Schaber, Mass spectra of Si, Ge, and Sn clusters, The Journal of Chemical Physics, 83 (1985) 855-858.
[90] J. E. Kingcade, H. M. Nagarathna-Naik, I. Shim and K. A. Gingerich, Electronic structure and bonding of the dimeric germanium molecule from all-electron ab initio calculations and equilibrium measurements, The Journal of Physical Chemistry, 90 (1986) 2830-2834.
[91] F. W. Froben and W. Schulze, Matrix-isolation spectroscopy of germanium molecules, Surface Science, 156 (1985) 765-769.
[92] T. M. Miller, A. E. S. Miller and W. C. Lineberger, Electron affinities of Ge and Sn, Physical Review A, 33 (1986) 3558-3559.
[93] C. C. Arnold, C. Xu, G. R. Burton and D. M. Neumark, Study of the low-lying states of Ge2 and Ge−2 using negative ion zero electron kinetic energy spectroscopy, The Journal of Chemical Physics, 102 (1995) 6982-6989.
[94] K. Kaya, H. Kawamata, Y. Negishi, T. Hayase, R. Kishi and A. Nakajima, Photoelectron spectroscopy of silicon and germanium-fluorine binary cluster anions (SinF m − , GenF m −), Zeitschrift für Physik D Atoms,Molecules and Clusters, 40 (1997) 5-9.
[95] Y. Negishi, H. Kawamata, T. Hayase, M. Gomei, R. Kishi, F. Hayakawa, A. Nakajima and K. Kaya, Photoelectron spectroscopy of germanium-fluorine binary cluster anions: the HOMO-LUMO gap estimation of Gen clusters, Chemical Physics Letters, 269 (1997) 199-207.
[96] J. Harris and R. O. Jones, Multiplet structure and charge distributions in silicon and germanium dimers, Physical Review A, 18 (1978) 2159-2166.
[97] W. Xu, Y. Zhao, Q. Li, Y. Xie and H. F. Schaefer Iii, The germanium clusters Ge n (n= 1–6) and their anions: structures, thermochemistry and electron affinities, Molecular Physics, 102 (2004) 579-598.
[98] R. King, I. Silaghi-Dumitrescu and A. Kun, A density functional theory study of five-, six-and seven-atom germanium clusters: distortions from ideal bipyramidal deltahedra in hypoelectronic structures, Journal of the Chemical Society, Dalton Transactions, (2002) 3999-4004.

[99] R. King and I. Silaghi-Dumitrescu, Density functional theory study of nine-atom germanium clusters: effect of electron count on cluster geometry, Inorganic chemistry, 42 (2003) 6701-6708.
[100] R. King, I. Silaghi-Dumitrescu and A. Lupan, Density functional theory study of 11-atom germanium clusters: effect of electron count on cluster geometry, Inorganic chemistry, 44 (2005) 3579-3588.
[101] R. King, I. Silaghi-Dumitrescu and A. Lupan, Density functional theory study of eight-atom germanium clusters: effect of electron count on cluster geometry, Dalton Transactions, (2005) 1858-1864.
[102] R. King, I. Silaghi-Dumitrescu and A. Lupan, New low symmetry low energy structures of 11-atom bare germanium clusters: A density functional theory study, Chemical Physics, 327 (2006) 344-350.
[103] R. King, I. Silaghi-Dumitrescu and M. Uţa, Density functional theory study of 10-atom germanium clusters: effect of electron count on cluster geometry, Inorganic chemistry, 45 (2006) 4974-4981.
[104] R. B. King, I. Silaghi-Dumitrescu and M. M. Uţă, Density functional theory study of twelve-atom germanium clusters: conflict between the Wade–Mingos rules and optimum vertex degrees, Dalton Transactions, (2007) 364-372.
[105] R. King and I. Silaghi-Dumitrescu, The role of "external" lone pairs in the chemical bonding of bare post-transition element clusters: the Wade–Mingos rules versus the jellium model, Dalton Transactions, (2008) 6083-6088.
[106] R. King, I. Silaghi-Dumitrescu and M. Uţă, Beyond the Wade− Mingos Rules in Bare 10-and 12-Vertex Germanium Clusters: Transition States for Symmetry Breaking Processes, Journal of chemical theory and computation, 4 (2008) 209-215.
[107] M. Menon, A transferable nonorthogonal tight-binding scheme for germanium, Journal of Physics: Condensed Matter, 10 (1998) 10991.
[108] Z.-Y. Lu, C.-Z. Wang and K.-M. Ho, Structures and dynamical properties of C n, Si n, Ge n, and Sn n clusters with n up to 13, Physical Review B, 61 (2000) 2329.
[109] F.-S. Liang and B.-X. Li, Stable structures of Gen (n= 21–25) clusters, Physics Letters A, 328 (2004) 407-413.
[110] J. Hunter, J. Fye, M. Jarrold and J. Bower, Structural transitions in size-selected germanium cluster ions, Physical Review Letters, 73 (1994) 2063.
[111] Q. L. Zhang, Y. Liu, R. Curl, F. Tittel and R. Smalley, Photodissociation of semiconductor positive cluster ions, The Journal of Chemical Physics, 88 (1988) 1670-1677.
[112] L.-Z. Zhao, W.-C. Lu, W. Qin, Q.-J. Zang, C. Wang and K. Ho, Fragmentation behavior of Gen clusters (2⩽ n⩽ 33), Chemical Physics Letters, 455 (2008) 225-231.
[113] W.-J. Zhao and Y.-X. Wang, Geometries, stabilities, and electronic properties of FeGen (n= 9–16) clusters: Density-functional theory investigations, Chemical Physics, 352 (2008) 291-296.
[114] S. Shi, Y. Liu, C. Zhang, B. Deng and G. Jiang, A computational investigation of aluminum-doped germanium clusters by density functional theory study, Computational and Theoretical Chemistry, 1054 (2015) 8-15.

[115] X. Li, K. Su, X. Yang, L. Song and L. Yang, Size-selective effects in the geometry and electronic property of bimetallic Au–Ge nanoclusters, Computational and Theoretical Chemistry, 1010 (2013) 32-37.
[116] N. Kapila, V. Jindal and H. Sharma, Structural, electronic and magnetic properties of Mn, Co, Ni in Ge n for (n= 1–13), Physica B: Condensed Matter, 406 (2011) 4612-4619.
[117] C. Tang, M. Liu, W. Zhu and K. Deng, Probing the geometric, optical, and magnetic properties of 3d transition-metal endohedral Ge 12 M (M= Sc–Ni) clusters, Computational and Theoretical Chemistry, 969 (2011) 56-60.
[118] Ş. Katırcıoğlu, Structure and stability of Ge n C m− n clusters, Journal of Molecular Structure: THEOCHEM, 629 (2003) 295-302.
[119] J. Andzelm, N. Russo and D. R. Salahub, Ground and excited states of group IVA diatomics from local-spin-density calculations: Model potentials for Si, Ge, and Sn, The Journal of Chemical Physics, 87 (1987) 6562-6572.
[120] R. W. Schmude Jr and K. A. Gingerich, Thermodynamic investigation of small germanium–tin clusters with a mass spectrometer, The Journal of Chemical Physics, 109 (1998) 3069-3071.
[121] J.-G. Han, P.-F. Zhang, Q.-X. Li, H. Gao, G.-Y. Cao, L.-S. Sheng and Y.-W. Zhang, A theoretical investigation of Ge n Sn (n= 1–4) clusters, Journal of Molecular Structure: THEOCHEM, 624 (2003) 257-265.
[122] M. Ikezawa and T. Nanba, Two-phonon difference absorption spectra in Ge crystals, Journal of the Physical Society of Japan, 45 (1978) 148-152.
[123] J. R. Heath, J. Shiang and A. Alivisatos, Germanium quantum dots: Optical properties and synthesis, The Journal of Chemical Physics, 101 (1994) 1607-1615.
[124] J. Wilcoxon, P. Provencio and G. Samara, Synthesis and optical properties of colloidal germanium nanocrystals, Physical Review B, 64 (2001) 035417.
[125] L. X. Benedict, E. L. Shirley and R. B. Bohn, Theory of optical absorption in diamond, Si, Ge, and GaAs, Physical Review B, 57 (1998) R9385.
[126] D. V. Melnikov and J. R. Chelikowsky, Absorption spectra of germanium nanocrystals, Solid state communications, 127 (2003) 361-365.
[127] H.-C. Weissker, J. Furthmüller and F. Bechstedt, Structure-and spin-dependent excitation energies and lifetimes of Si and Ge nanocrystals from ab initio calculations, Physical Review B, 69 (2004) 115310.
[128] G. Nesher, L. Kronik and J. R. Chelikowsky, Ab initio absorption spectra of Ge nanocrystals, Physical Review B, 71 (2005) 035344.
[129] M. Palummo, G. Onida and R. Del Sole, Optical properties of germanium nanocrystals, physica status solidi (a), 175 (1999) 23-31.
[130] M. Palummo, G. Onida, R. Del Sole, A. Stella, P. Tognini, P. Cheyssac and R. Kofman, Optical Properties of Germanium Quantum Dots, physica status solidi (b), 224 (2001) 247-251.
[131] J. Tauc, Optical properties and electronic structure of amorphous Ge and Si, Materials Research Bulletin, 3 (1968) 37-46.
[132] N. A. Hill, S. Pokrant and A. J. Hill, Optical Properties of Si− Ge Semiconductor Nano-Onions, The Journal of Physical Chemistry B, 103 (1999) 3156-3161.

[133] V. N. Brudnyi and S. N. Grinyaev, Optical absorption spectra of Si with Ge quantum dots, Russian Physics Journal, 53 (2010) 703-705.
[134] V. Brudnyi and S. Grinyaev, Silicon germanium nanostructures: Electronic parameters and optical characteristics, Russian Physics Journal, 47 (2004) 577-582.
[135] E. Schrödinger, Quantisierung als Eigenwertproblem, Annalen der Physik, 384 (1926) 361-376.
[136] M. Born and R. Oppenheimer, Zur Quantentheorie der Molekeln, Annalen der Physik, 389 (1927) 457-484.
[137] P. Hohenberg and W. Kohn, Inhomogeneous electron gas, Physical review, 136 (1964) B864.
[138] R. M. Dreizler and E. K. U. Gross *Density functional theory : an approach to the quantum many-body problem*; Springer-Verlag: Berlin; New York, 1990.
[139] W. Kohn and L. J. Sham, Self-consistent equations including exchange and correlation effects, Physical Review, 140 (1965) A1133.
[140] W. Kohn and L. J. Sham, Self-Consistent Equations Including Exchange and Correlation Effects, Physical review, 140 (1965) A1133-A1138.
[141] D. M. Ceperley and B. J. Alder, Ground State of the Electron Gas by a Stochastic Method, Physical Review Letters, 45 (1980) 566-569.
[142] J. P. Perdew, J. A. Chevary, S. H. Vosko, K. A. Jackson, M. R. Pederson, D. J. Singh and C. Fiolhais, Atoms, molecules, solids, and surfaces: Applications of the generalized gradient approximation for exchange and correlation, Physical Review B, 46 (1992) 6671-6687.
[143] J. P. Perdew and W. Yue, Accurate and simple density functional for the electronic exchange energy: Generalized gradient approximation, Physical Review B, 33 (1986) 8800-8802.
[144] *Modern methods and algorithms of quantum chemistry: Winterschool, 21-25 February 2000, Forschungszentrum Jülich, Germany : proceedings*; John von Neumann Inst. for Computing: Jülich, 2000.
[145] J. C. Phillips and L. Kleinman, New method for calculating wave functions in crystals and molecules, Physical Review, 116 (1959) 287.
[146] W. C. Topp and J. J. Hopfield, Chemically motivated pseudopotential for sodium, Physical Review B, 7 (1973) 1295.
[147] D. Hamann, Schl and M. quot, uter, and C. Chiang, Phys. Rev. Lett, 43 (1979) 1494-1497.
[148] D. Hamann and M. Scluter, Pseudopotentials that work: from H to Pu, Phys. Rev. B, 26 (1982) 4199-4228.
[149] J. C. Slater, Atomic shielding constants, Physical Review, 36 (1930) 57.
[150] M. A. Marques and E. K. Gross, Time-dependent density functional theory, Annu. Rev. Phys. Chem., 55 (2004) 427-455.
[151] E. Runge and E. K. U. Gross, Density-Functional Theory for Time-Dependent Systems, Physical Review Letters, 52 (1984) 997-1000.
[152] A. Castro, M. A. L. Marques and A. Rubio, Propagators for the time-dependent Kohn–Sham equations, The Journal of Chemical Physics, 121 (2004) 3425-3433.

[153] K. Yabana and G. Bertsch, Time-dependent local-density approximation in real time, Physical Review B, 54 (1996) 4484.
[154] A. Castro, H. Appel, M. Oliveira, C. A. Rozzi, X. Andrade, F. Lorenzen, M. A. Marques, E. Gross and A. Rubio, Octopus: a tool for the application of time-dependent density functional theory, physica status solidi (b), 243 (2006) 2465-2488.
[155] A. Castro, M. A. Marques and A. Rubio, Propagators for the time-dependent Kohn–Sham equations, The Journal of Chemical Physics, 121 (2004) 3425-3433.
[156] W. Magnus, On the exponential solution of differential equations for a linear operator, Communications on Pure and Applied Mathematics, 7 (1954) 649-673.
[157] A. Castro, H. Appel, M. Oliveira, C. A. Rozzi, X. Andrade, F. Lorenzen, M. A. L. Marques, E. K. U. Gross and A. Rubio, octopus: a tool for the application of time-dependent density functional theory, physica status solidi (b), 243 (2006) 2465-2488.
[158] P. L. v. Chebyshev *Théorie des mécanismes connus sous le nom de parallélogrammes*; Imprimerie de l'Académie impériale des sciences, 1853.
[159] C. Moler and C. V. Loan, Nineteen Dubious Ways to Compute the Exponential of a Matrix, Twenty-Five Years Later, SIAM Review, 45 (2003) 3-49.
[160] P. Ordejón, E. Artacho and J. M. Soler, Self-consistent order-N density-functional calculations for very large systems, Physical Review B, 53 (1996) R10441-R10444.
[161] J. M. Soler, E. Artacho, J. D. Gale, A. Garcia, J. Junquera, P. Ordejon and D. Sanchez-Portal, The SIESTA method for ab initio order-N materials simulation, in: arXiv e-prints, 2001.
[162] M. C. Payne, M. P. Teter, D. C. Allan, T. A. Arias and J. D. Joannopoulos, Iterative minimization techniques for ab initio total-energy calculations: molecular dynamics and conjugate gradients, Reviews of Modern Physics, 64 (1992) 1045-1097.
[163] J. M. Soler, E. Artacho, J. D. Gale, A. García, J. Junquera, P. Ordejón and D. Sánchez-Portal, The SIESTA method forab initioorder-Nmaterials simulation, Journal of Physics: Condensed Matter, 14 (2002) 2745-2779.
[164] D. R. Hamann, M. Schlüter and C. Chiang, Norm-Conserving Pseudopotentials, Physical Review Letters, 43 (1979) 1494-1497.
[165] N. Troullier and J. L. Martins, Efficient pseudopotentials for plane-wave calculations, Physical Review B, 43 (1991) 1993-2006.
[166] L. Kleinman and D. M. Bylander, Efficacious Form for Model Pseudopotentials, Physical Review Letters, 48 (1982) 1425-1428.
[167] J. C. Slater, Atomic Shielding Constants, Physical Review, 36 (1930) 57-64.
[168] S. F. Boys and A. C. Egerton, Electronic wave functions - I. A general method of calculation for the stationary states of any molecular system, Proceedings of the Royal Society of London. Series A. Mathematical and Physical Sciences, 200 (1950) 542-554.
[169] J. M. Soler, E. Artacho, J. D. Gale, A. García, J. Junquera, P. Ordejón and D. Sánchez-Portal, The SIESTA method for ab initio order-N materials simulation, Journal of Physics: Condensed Matter, 14 (2002) 2745.
[170] M. Frigo and S. G. Johnson Proceedings of the 1998 IEEE International Conference on Acoustics, Speech and Signal Processing, ICASSP '98 (Cat. No.98CH36181), 1998; p 1381-1384 vol.3.

[171] C. L. Lawson, R. J. Hanson, D. R. Kincaid and F. T. Krogh, Basic Linear Algebra Subprograms for Fortran Usage, ACM Trans. Math. Softw., 5 (1979) 308-323.
[172] E. Anderson, Z. Bai, J. Dongarra, A. Greenbaum, A. McKenney, J. D. Croz, S. Hammarling, J. Demmel, C. Bischof and D. Sorensen, LAPACK: a portable linear algebra library for high-performance computers, in: Proceedings of the 1990 ACM/IEEE conference on Supercomputing, IEEE Computer Society Press, New York, New York, USA, 1990, pp. 2-11.
[173] M. Galassi, J. Davies, J. Theiler, B. Gough, G. Jungman, P. Alken, M. Booth, F. Rossi and R. Ulerich *GNU scientific library*; Network Theory Limited, 2002.
[174] M. A. L. Marques, A. Castro, G. F. Bertsch and A. Rubio, octopus: a first-principles tool for excited electron–ion dynamics☆☆E-mail: octopus@tddft.org, Computer Physics Communications, 151 (2003) 60-78.
[175] C. A. Ullrich, Time-dependent density-functional theory beyond the adiabatic approximation: Insights from a two-electron model system, The Journal of Chemical Physics, 125 (2006) 234108.
[176] K. Yabana and G. F. Bertsch, Time-dependent local-density approximation in real time, Physical Review B, 54 (1996) 4484-4487.
[177] P. Ordejón, E. Artacho and J. M. Soler, Self-consistent order-N density-functional calculations for very large systems, Physical Review B, 53 (1996) R10441.
[178] J. P. Perdew and A. Zunger, Self-interaction correction to density-functional approximations for many-electron systems, Physical Review B, 23 (1981) 5048.
[179] J. P. Perdew, K. Burke and M. Ernzerhof, Generalized Gradient Approximation Made Simple, Physical Review Letters, 77 (1996) 3865-3868.
[180] L. Kleinman and D. Bylander, Efficacious form for model pseudopotentials, Physical Review Letters, 48 (1982) 1425.
[181] N. Kapila, I. Garg, V. Jindal and H. Sharma, First principle investigation into structural growth and magnetic properties in Ge n Cr clusters for n= 1–13, Journal of Magnetism and Magnetic Materials, 324 (2012) 2885-2893.
[182] E. Sosa-Hernández and P. Alvarado-Leyva, Magnetic properties of stable structures of small binary FenGem (n+ m≤ 4) clusters, Physica E: Low-dimensional Systems and Nanostructures, 42 (2009) 17-21.
[183] J. Wang and J.-G. Han, A computational investigation of copper-doped germanium and germanium clusters by the density-functional theory, The Journal of Chemical Physics, 123 (2005) 244303.
[184] X.-J. Hou, G. Gopakumar, P. Lievens and M. T. Nguyen, Chromium-Doped Germanium Clusters CrGen (n = 1−5): Geometry, Electronic Structure, and Topology of Chemical Bonding, The Journal of Physical Chemistry A, 111 (2007) 13544-13553.
[185] I. Vasiliev, S. Öğüt and J. R. Chelikowsky, Ab initio calculations for the polarizabilities of small semiconductor clusters, Physical Review Letters, 78 (1997) 4805.
[186] J. Wang and J.-G. Han, The growth behaviors of the Zn-doped different sized germanium clusters: A density functional investigation, Chemical Physics, 342 (2007) 253-259.

[187] A. A. Shvartsburg, B. Liu, Z.-Y. Lu, C.-Z. Wang, M. F. Jarrold and K.-M. Ho, Structures of Germanium Clusters: Where the Growth Patterns of Silicon and Germanium Clusters Diverge, Physical Review Letters, 83 (1999) 2167-2170.
[188] R. G. Parr and R. G. Pearson, Absolute hardness: companion parameter to absolute electronegativity, Journal of the American Chemical Society, 105 (1983) 7512-7516.
[189] R. Parr and W. Yang, Density Functional Methods of Atoms and Molecules, in, Oxford University Press, New York, 1989.
[190] K. Yabana and G. Bertsch, Time-dependent local-density approximation in real time: Application to conjugated molecules, International journal of quantum chemistry, 75 (1999) 55-66.
[191] M. A. Marques, A. Castro and A. Rubio, Assessment of exchange-correlation functionals for the calculation of dynamical properties of small clusters in time-dependent density functional theory, The Journal of Chemical Physics, 115 (2001) 3006-3014.
[192] A. Castro, M. A. Marques, J. A. Alonso, G. F. Bertsch, K. Yabana and A. Rubio, Can optical spectroscopy directly elucidate the ground state of C 20?, The Journal of Chemical Physics, 116 (2002) 1930-1933.
[193] A. Castro, M. A. Marques, J. A. Alonso and A. Rubio, Optical properties of nanostructures from time-dependent density functional theory, Journal of Computational and Theoretical Nanoscience, 1 (2004) 231-255.
[194] S. Botti and M. A. Marques, Identification of fullerene-like CdSe nanoparticles from optical spectroscopy calculations, Physical Review B, 75 (2007) 035311.
[195] G. Malloci, G. Mulas and C. Joblin, Electronic absorption spectra of PAHs up to vacuum UV-Towards a detailed model of interstellar PAH photophysics, Astronomy & Astrophysics, 426 (2004) 105-117.
[196] G. Malloci, G. Mulas, G. Cappellini, V. Fiorentini and I. Porceddu, Theoretical electron affinities of PAHs and electronic absorption spectra of their mono-anions, Astronomy & Astrophysics, 432 (2005) 585-594.
[197] K. G. Dyall, P. R. Taylor, K. Faegri Jr and H. Partridge, All-electron molecular Dirac–Hartree–Fock calculations: The group IV tetrahydrides CH4, SiH4, GeH4, SnH4, and PbH4, The Journal of Chemical Physics, 95 (1991) 2583-2594.
[198] U. Itoh, Y. Toyoshima, H. Onuki, N. Washida and T. Ibuki, Vacuum ultraviolet absorption cross sections of SiH4, GeH4, Si2H6, and Si3H8, The Journal of Chemical Physics, 85 (1986) 4867-4872.
[199] J. E. Vincent, 2001.
[200] M. Mitchell, X. Wang, C. Chin, M. Suto and L. Lee, Quantitative photoabsorption and fluorescence spectroscopy of GeH4 in the vacuum ultraviolet, Journal of Physics B: Atomic and Molecular Physics, 20 (1987) 5451.
[201] C. Y. R. Wu, F. Z. Chen and D. L. Judge, Photoabsorption and photoionization cross sections of gas phase GeH4 and Rydberg structures of GeH4 and SiH4, The Journal of Chemical Physics, 99 (1993) 1530-1536.
[202] A. Tsolakidis and R. M. Martin, Comparison of the optical response of hydrogen-passivated germanium and silicon clusters, Physical Review B, 71 (2005) 125319.

[203] A. L. Efros and A. L. Efros, Interband absorption of light in a semiconductor sphere, Soviet Physics Semiconductors-Ussr, 16 (1982) 772-775.
[204] L. Brus, Zero-dimensional" excitons" in semiconductor clusters, IEEE Journal of Quantum Electronics, 22 (1986) 1909-1914.
[205] A. Görling, Density-functional theory for excited states, Physical Review A, 54 (1996) 3912.
[206] I. M. Kupchak, D. V. Korbutyak, Y. V. Kryuchenko, A. V. Sachenko, I. O. Sokolovskiĭ and O. M. Sreseli, Exciton characteristics and exciton luminescence of silicon quantum dot structures, Semiconductors, 40 (2006) 94-103.
[207] C. D. Jeffries, Electron-hole condensation in semiconductors: Electrons and holes condense into freely moving liquid metallic droplets, a plasma phase with novel properties, Science, 189 (1975) 955-964.